A-4

MS-I

8411-6004-RU000

STUDY OF LUNAR LANDING SENSOR PERFORMANCE FINAL REPORT

Contract No. NAS8-5205

22 SEPTEMBER 1965

Prepared for
GEORGE C. MARSHALL SPACE FLIGHT CENTER
Huntsville, Alabama

TRW SYSTEMS

STUDY OF LUNAR LANDING SENSOR PERFORMANCE FINAL REPORT

22 September 1965

Contract No. NAS8-5205

Prepared for

George C. Marshall Space Flight Center
Huntsville, Alabama

Prepared: C. B. Coulbourn
C. B. Coulbourn Jr.
Project Engineer

Approved:
J. E. Holland, Manager
Guidance Sensors Department

J. Heilfron, Director
Guidance Laboratory

TRW SYSTEMS
ONE SPACE PARK • REDONDO BEACH, CALIFORNIA

CONTENTS

CONTENTS (continued)

ILLUSTRATIONS

ILLUSTRATIONS (continued)

TABLES

1. INTRODUCTION

This report, in conjunction with three interim reports and one special report, constitutes the final report of "The Lunar Landing Sensor Performance Study," NASA Contract NAS8-5205. The four associated reports are:

(1) "Study of Lunar Landing Sensor Performance Interim Report No. 1," dated 21 June 1963.

(2) "Study of Lunar Landing Sensor Performance Interim Report No. 2," dated 31 October, 1963.

(3) "Study of Lunar Landing Sensor Performance Interim Report No. 3," dated 31 July, 1964.

(4) "X-Band Solid-State Signal Source Special Report," dated 15 January 1965.

This report describes the results of the analytical and experimental work performed under Modification 8 of the contract. The objective of this work was to advance the knowledge of lunar landing sensors, particularly those employing dithered PRF modulation for ranging, so that future system development could be accomplished with greater assurance that an optimum approach was used, and with greater assurance that the circuit techniques employed were feasible. Although this work is directed toward lunar landing, the results are general for cases where altitude measurements from 380 nmi to touchdown are required.

The various systems tests were performed using an extended range altimeter feasibility model which was available at TRW Systems Group. This system had been developed originally under Company-sponsored research programs, and under earlier modifications of this contract. The operation of the system is described in Interim Report No. 1. The necessary subsystem feasibility tests were also performed, using for the most part subsystems that had been developed either under earlier modifications of this contract or under Company-sponsored research programs.

The work performed under this modification of the contract is a logical extension of work performed under earlier modifications. The work performed prior to the beginning of the Modification 8 phase included an evaluation of separate beacon and non-beacon assisted lunar landing sensors; fabrication and delivery of a 100-mw solid-state signal source; analytical and experimental work on the development of an extended range altimeter employing a dithered PRF ranging modulation technique; and the development of a 1-watt solid-state signal source. The follow-on work reported herein contains three tasks: (1) the study of a unified descent sensor capable of operating with or without a beacon, (2) the further investigation of the square-wave modulation of varactor sources, and (3) the experimental evaluation of the extended range altimeter operating with a simulated spread spectrum lunar return signal.

With regard to the report layout, the first two sections are the Introduction and Summary, the latter section summarizing the tasks performed under Modification 8 and presenting some of the more pertinent data. Section 3 describes the analysis performed for the various sensor systems and their antennas. Block diagrams and tradeoff design features are presented in detail. Section 4 contains a description of the tests performed in connection with varactor gating, and provides extensive test data. This data permits evaluation of varactor multiplier switching for either modulation or static "On-Off" control. Section 5 documents the results of the evaluation of the extended range altimeter operating in the presence of a simulated lunar return. From the data presented, predictions can be made regarding altimeter accuracies that can be obtained under varying operating conditions. The final section presents a discussion of the conclusions to be drawn from the present project, and recommends certain areas for further study. An appendix is included which presents detailed design data for various types of antennas that are most suitable for unified lunar sensors. This aspect of the unified sensor system is described in extensive detail because the antenna poses such a severe limitation for satisfactory unified sensor performance.

The following personnel at TRW Systems Group performed the work described in this report:

Mr. D. N. Jacob	Unified Sensor System Study
Mr. A. E. Ratkevich	Unified Sensor Antenna Study
Mr. R. N. Fenton	Analysis of the Lunar Return Signal
Mr. J. Habra, assisted by Mr. N. Harvey Mr. B. Gililland	Experimental Work for Varactor Switching and Extended Range Altimeter Evaluation

2. SUMMARY

Three subtasks, each intimately associated with lunar landing sensors employing a dithered PRF modulation technique, were pursued to fulfill this contract. The subtasks, analytical and/or experimental in nature, are as follows:

- Perform studies of a unified lunar descent sensor.
- Investigate the switching characteristics of varactor power sources.
- Evaluate the extended range altimeter performance when its received signal is a simulated spread spectrum lunar return.

2.1 STUDY OF UNIFIED LUNAR DESCENT SENSORS

The study of the unified lunar landing sensors concentrated on three types of sensors: viz, (1) an extended range altimeter, (2) a short range altimeter/velocity sensor, and (3) a beacon tracking radar. The performance characteristics assumed for each of the sensors are the same as those established during an earlier phase of the LLS Study. These characteristics are given on pages 6 and 7 of the "Study of Lunar Landing Sensor Performance Interim Report No. 1," dated 21 June 1963

A transmitting frequency of about 10 gc appears to be optimum for each of the systems except the beacon tracker, but including the lunar-based beacon. This frequency is high enough so that it will result in small range and velocity errors for altimetry, and small angle tracking errors for beacon tracking. It also results in lower transmitter efficiency, and in greater receiver noise temperature than lower frequencies. This tradeoff appears justifiable for the applications evaluated.

A much lower transmitting frequency of about 300 to 600 Mc appears best for the beacon tracker. The advantages of this lower frequency are, in addition to higher transmitter efficiency and lower receiver noise, that the transmitted beam will be broad enough so that the lunar-based beacon need have only its receiver turned on prior to acquisition. The low

frequency will also permit a simpler beacon acquisition scheme because of a lower associated doppler spread. Of course, angle data would be obtained from the beacon to radar uplink, the frequency of which would be X-band.

Dithered PRF modulation, initially adopted during earlier phases of this program, has continually improved its stature relative to the techniques of pulse modulation, swept CW modulation, phase modulation, frequency shift keying, and pseudo-random noise modulation. Dithered PRF modulation appears perfectly suited to narrowband, low-peak power solid-state signal sources, and it permits high values of transmitter-receiver isolation to be obtained without the necessity of utilizing dual antennas. Dithered PRF modulation range data is available in digital form, requiring only a low frequency counter to process it. Finally, the use of dithered PRF modulation permits the receiver to be turned off 50 percent of the time, thereby resulting, theoretically, in a 3-db reduction in thermal noise level.

Unified transmitter/receiver systems comprising an extended range altimeter/beacon tracker combination, a short-range altimeter/beacon tracker, and a short-range altimeter/interferometer beacon tracker all appear feasible. In each of the systems a common transmitter is used to generate the X-band signal and the 300- to 600-Mc signal. This is accomplished by, effectively, tapping off the lower frequency from the proper point in the transmitter multiplier chain. The PRF modulation scheme being used by each of the sensors also permits the incorporation of common circuits for the unified sensors.

It appears feasible to use a single antenna for the extended range altimetry and beacon tracking functions, and at only slight expense in performance. The cost in performance would result from the UHF radar to beacon downlink antenna being superimposed on the X-band uplink antenna, and from the fact that some compromise in the best antenna type for each function would be necessary for an optimized unified antenna. Combining the low altitude altimeter/velocity sensor antenna with any other antenna appears questionable considering the tradeoffs required.

Tables 2-I and 2-II present an evaluation summary of antennas of the types most suitable for use with the various lunar landing sensors. The more important characteristics of each antenna are rated on a comparative basis, as based upon the intended usage.

Table 2-I. Beacon Tracker Antenna Evaluation Summary

Antenna Type	Package	Temperature Sensitivity	Overall Performance
Motor Driven Feed-Reflector Conical Scan	Average	Average	Average
Array Cluster Electronic Conical Scan	Good	Good	Good
Array Cluster Electronic Sequential Lobing	Good	Good	Average
Feed-Reflector Amplitude Monopulse	Average	Average	Good
Array Phase Monopulse	Good	Good	Good
Interferometer Search and Angle Track	Good	Average	Poor

Table 2-II. Altimeter/Velocity Sensor Antenna Evaluation Summary

Antenna Type	Package	Temperature Sensitivity	Overall Performance
Multibeam, Dual Reflector	Poor	Average	Good
Multibeam Transmit Array, Single Beam Receivers	Good	Good	Good
Two-Beam Dual Switching Array	Good	Good	Average

2.2 INVESTIGATION OF MODULATED VARACTOR POWER SOURCES

The procedure used in evaluating the switching capabilities of varactor multipliers was, first, to modify two multiplier chains so they could be suitably switched, second, perform a series of bench tests to obtain preliminary data, and third, measure the transmitter to receiver isolation afforded by the switched varactor multiplier chains utilized in the extended range altimeter. One of the multiplier chains modified was a times-16 X-band transmitter consisting of four cascaded doublers and capable of producing 100 mw. The second was a times-4 multiplier consisting of two cascaded doublers and capable of producing 1 watt at X-band. Each of the multiplier chains was similar to units which had been delivered to MSFC under this contract.

During the bench tests, preliminary isolation measurements and complete switching characteristic data were obtained. The isolation measurements were considered preliminary because the available instrumentation was not sufficient to measure the higher values of isolation involved. The switching characteristic data related the shape of the modulated RF signal envelope to that of the modulating signal. A summary of this data is presented in Table 2-III.

Table 2-III. Switching Characteristics of an X-Band Varactor Multiplier Modulated with a 100 KC Signal

Parameter	Value, nsec
Modulator Pulse Turn-On Time	120
RF Envelope Turn-On Time	26
Modulator Turn-Off Time	120
RF Pulse Turn-Off Time	20
Delay Time	90
Storage Time	20

In Table 2-III, the delay time is the time between the 50 percent point of the modulating waveform leading edge and the 50 percent point of the RF envelope waveform leading edge. Conversely, the storage time is the time between the 50 percent point of the trailing edges of the modulation waveform and the RF envelope waveform.

During the system tests, with gated times-16 X-band multipliers utilized as the transmitter and local oscillator of the extended range altimeter, it was practical to obtain conclusive data describing the isolation characteristics. This data was taken for the case when a dc bias was used to switch the RF signal off, and for cases when varying frequency square-wave modulation was used to modulate the transmitter and local oscillator multiplier chains. Of course, when square-wave modulation was added, it was phased so that the altimeter transmitter and receiver were turned on alternately, so that the isolation obtained represented the receiver transmitter isolation to be achieved by varactor gating. Table 2-IV presents a summary of the "On" to "Off" ratios, in db, for different modulating frequencies. The decrease in "On" to "Off" ratio when the PRF increases primarily results from the sidebands of the modulated local oscillator intermixing to generate a signal falling within the IF passband of 65 Mc.

Table 2-IV. X-Band Varactor Multiplier Isolation Characteristics

Pulse Repetition Frequency	RF "On" to "Off" Ratio
0	$\geq$ 144 db
300 cps	140 db
3 kc	118 db
30 kc	96 db
300 kc	74 db
1 Mc	60 db

2.3 EVALUATION OF THE EXTENDED RANGE ALTIMETER WITH A SIMULATED LUNAR RETURN

The analysis of the terrain return signal of the extended range altimeter from a lunar surface reveals that spectrum spreading of the reflected energy will occur. This was primarily determined by differential doppler considerations of the scatterers in the area illuminated by the beam of the antenna. For an orbital velocity of 5260 ft/sec the spreading occupies a 7-kc bandwidth for a beamwidth of 1/15 rad and a transmitted frequency of 10 gc.

A good laboratory simulation of the terrain return signal is shown to be narrowband thermal noise. Bandwidth control of this noise signal can be used to accommodate different velocities throughout the trajectory.

For a 100-nmi altitude, it is estimated that the power returned to the receiver will be 137 db below the transmitted power and will vary as the inverse square of range instead of the more conventional inverse fourth power of range, because the "target" fills the narrow antenna beam.

The noise generator, or terrain return simulator developed for system testing processed low frequency, uniform spectrum, white noise into a PRF gated X-band signal with a 400-cps and/or 5-kc noise bandwidth. Thus, orbital velocity and near touchdown effects could be evaluated by the two bandwidth extremes.

The altimeter system including the variable bandwidth terrain return signal simulator was assembled complete with PRF loop, adjustable power level, and adjustable range delay. Included also was a controllable amount of PRF dither at a 30-cps rate.

Twelve data points were calculated from system PRF measurements for each of the various combinations of signal power, spectral spreading and dither magnitude. Each of these 12 data points represented a 10-sec average. Deviations from the mean PRF were calculated and reveal that spectral spreading worsens ranging accuracy from about 1/3 percent with no spreading less than 1 percent with 5-kc spreading, assuming a dither of 5 percent or greater.

3. STUDY OF UNIFIED LUNAR DESCENT SENSORS

3.1 INTRODUCTION

The objective of the study of unified descent sensors was to investigate an extended range altimeter, a beacon tracking radar, and a short range altimeter/velocity tracker to determine the feasibility of combining them into a single packaged unit. To form a basis for an opinion regarding feasibility, a detailed study and establishment of certain basic parameters were required for each of the systems. Because of the extensive work previously performed with the electronics systems, major effort was directed toward antenna considerations.

During the study, it was assumed that the lunar descent sensors would be used for a spacecraft effecting a soft landing either from a direct cis-lunar trajectory or from a lunar orbit. A beacon would be located appropriately on the lunar surface and would ordinarily be used during landing. If it were to fail, however, or an abort maneuver were required, the non-beacon tracking sensors would be used. The basic intent of the unified system then would be to provide added capability and added reliability without the extra weight and power requirements of purely redundant systems.

The specific performance characteristics assumed for the three different sensors are the same as those established during an earlier phase of the contract. These characteristics are listed on Pages 6 and 7 of the "Study of Lunar Landing Sensor Performance, Interim Report No. 1," dated 21 June 1963.

The first half of this section presents the results of an investigation of the electronics section of the three lunar sensors. The second half of this section presents a discussion of applicable lunar landing sensor antenna configurations, with emphasis on beacon tracking antennas and on low-range altimeter/velocity sensor antennas. Extended range altimeter antennas are not discussed in detail because an antenna of this type would ordinarily be straightforward in design, not being required either to angle track or to transmit and receive at widely separated frequencies. Extensive appendices describing the various antenna designs in detail are included to supplement the discussion of this section.

3.2 TRANSMITTER/RECEIVER

3.2.1 Introduction

This subsection contains the results of investigation into the feasibility of designing a beacon tracking system, and a short and extended range altimeter system using the same electronics and range processing circuits. In devising such a unified system, it was necessary to determine and reaffirm the optimum transmitting frequencies and to evaluate them with regard to accuracy and range requirements. The unified system resulting from this investigation appears comparatively simple, lightweight, reliable, and accurate, although the analysis of all the features and functions is still somewhat preliminary in scope.

The receiver-transmitter that appears most suitable for a unified beacon tracker and altimeter-velocity sensor employs a dithered PRF tracking scheme originally adopted during the extended range altimeter study performed under earlier phases of this contract. Through the use of a recently devised high-frequency PRF generator, the tracking range can be extended down to a few feet for both the altimeter and beacon tracker. The PRF generator has a self-adjusting feature which permits it to maintain a constant loop gain at all ranges without the need for any automatic dither adjustment or internal loop adjustments. This feature results in a highly stable tracking loop.

The new dithered PRF generator utilizes a voltage-controlled oscillator covering a two-to-one frequency range, a series of divide-by-two circuits, and auxiliary sweeping and switching circuits. To obtain a variation in PRF, the VCO is swept slowly from one extreme to the other, quickly reset, and then swept again over the same two-to-one range. Subsequent to each frequency sweep, as the VCO is being reset, a divide-by-two circuit is either added to or removed from the circuit, depending upon whether the VCO is being swept upward or downward. Automatic switching is used so that when the VCO reaches its limit on either the high- or low-frequency side, the divider switches by two, and the VCO is nearly instantaneously swept to the other side of the scale. The discontinuity that is caused by the switching can be kept to a short duration so as not to affect the tracking performance. This PRF technique is readily adapted to the use of microminiature techniques.

Dithered PRF tracking is particularly appealing at short ranges because a wideband tracking receiver is not required subsequent to the PRF gating. Also the gating can be performed even prior to the first mixer. Diode gating of a few nanosec or less, representing a foot or less in accuracy, is also readily available at the present time. Preliminary measurements of ranges of less than 10 ft with an accuracy of one foot or less have been obtained in the laboratory.

The use of PRF tracking permits a simple digital range readout by using the PRF to switch a counter, counting at a fixed frequency, "On" and "Off." Early in the program, it had appeared that the dither frequency would have to be turned "Off" while the PRF was being measured to determine ranges in order to avoid PRF variations, but this requirement appears unnecessary if the PRF can be divided down to a frequency somewhere between 10 and 100 times the dither frequency. By this technique, the frequency variation due to the dither can be averaged out or reduced to a low value. The count thus obtained by using the PRF as the timing signals of the counter results in a direct digital reading of range that can be used for both the altimeter and the beacon tracker.

One modification appears necessary, however, in going from extended-range altimeter operation to short-range altimeter operation because of an isolation problem. At extended ranges, one antenna can be used and isolation obtained by the use of a delay between the receiver and transmitter "On" times. However, at short ranges some difficulty has been experienced with the short switching time requirement. Further development might solve this difficulty, but at present, good short-range altimetry has been achieved only by the use of two antennas – one for reception and one for transmission.

A 50-percent duty cycle is required for non-assisted altimetry to obtain the required isolation, but this does not appear particularly necessary for a beacon tracker. Here, a 90-percent or more (transmitter "On" time) duty cycle could be used because of the isolation possible with frequency diplexing. (However, gating the IF to reduce the thermal noise by up to 3 db would improve the merits of the 50-percent duty cycle system.)

Some modification of the altimeter dithered PRF scheme appears necessary to adapt it to a beacon tracker. A dithered PRF return from the beacon appeared at first to be difficult to obtain, in contrast to the case of the altimeter where a signal nearly identical to that transmitted was returned from the ground. However, this difficulty was finally resolved by resorting to the technique of dithering the PRF in one direction only, i.e., on the tracker to beacon link or vice versa. By so doing, it appeared that satisfactory tracking could be achieved at both the beacon and the radar.

The PRF tracking loop transfer function of the beacon is somewhat different from that of the radar or altimeter in that the equations describing the radar and altimeter tracking loops are dependent upon the range. The beacon PRF tracking loop, on the other hand, is essentially independent of range and might be regarded as a phase-locked loop rather than a frequency-lock loop as in the beacon tracking radar or altimeter.

A phase-tracking loop requires a different type of PRF generator design than that used with the frequency-tracking loop for maintaining a constant tracking loop gain with range or PRF variations. This PRF generator design is quite simple in that only a voltage-controlled oscillator, or its equivalent, is required. The PRF variation will be directly proportional to the controlling voltage at all ranges, a characteristic also required for the dither generation. This characteristic is required because the loop gain does not vary with range in the beacon. Therefore, the use of dividers in the beacon PRF generator is not desirable for this application.

The dither needs to be applied only in the beacon and not in the radar while operating in the beacon-track mode. The dither reference signal would be sent to the beacon from the radar by the use of carrier-phase modulation.

It is also desirable to keep the beacon PRF tracking-loop frequency response relatively high compared to that of the radar to avoid adverse effects that otherwise would be obtained by having the beacon introduce additional tracking delays in the radar tracking loop.

A block diagram of the radar, or altimeter, tracking loop is shown in Figure 3-1. The phase of the outgoing PRF is made to track the phase of the returning PRF. A voltage proportional to the phase difference between the outgoing PRF and the returning PRF is obtained and is used to control the PRF generator through two integrating amplifiers. A differential phase error, $\Delta\phi$ rad = $\frac{\Delta PRF}{PRF}(\pi)$, is directly proportional to a differential PRF frequency error, ΔPRF, and therefore the loop is considered to be a frequency-locked loop. Conversly, for a phase-locked loop such as used in the beacon PRF tracker, the differential phase error is proportional to the integral of the differential frequency error. The differential phase error is also proportional to range changes, delayed by a time proportional to the range. This space time delay is $T_d = \frac{2(\text{range to beacon})}{C} = 0.00466$ sec at 380 nmi and is negligible compared to the tracking loop time response, so that it can be ignored.

3.2.2 Optimum Carrier Frequency

The choice of the transmitted and received carrier frequencies requires the consideration of many related factors. For altimetry and for beacon angle tracking, a high frequency is desirable because of the increased accuracy obtainable in altitude velocity sensing and in beacon angle tracking. However, a higher frequency results in a lower efficiency, and a greater receiver noise temperature, particularly for receivers operating at frequencies higher than 10 Gc and employing crystal mixers. For frequencies below 1 Gc, transistor amplifiers become practical for replacing first mixers to further reduce receiver noise. At 400 Mc, for example, a noise temperature of 5 db less than that achievable at X-band is possible. Also low noise temperatures can be achieved with masers, parametric amplifiers, traveling wave tubes and backward-wave amplifiers, but they require additional circuitry and complexity so that they are not presently preferred for many long-term space missions.

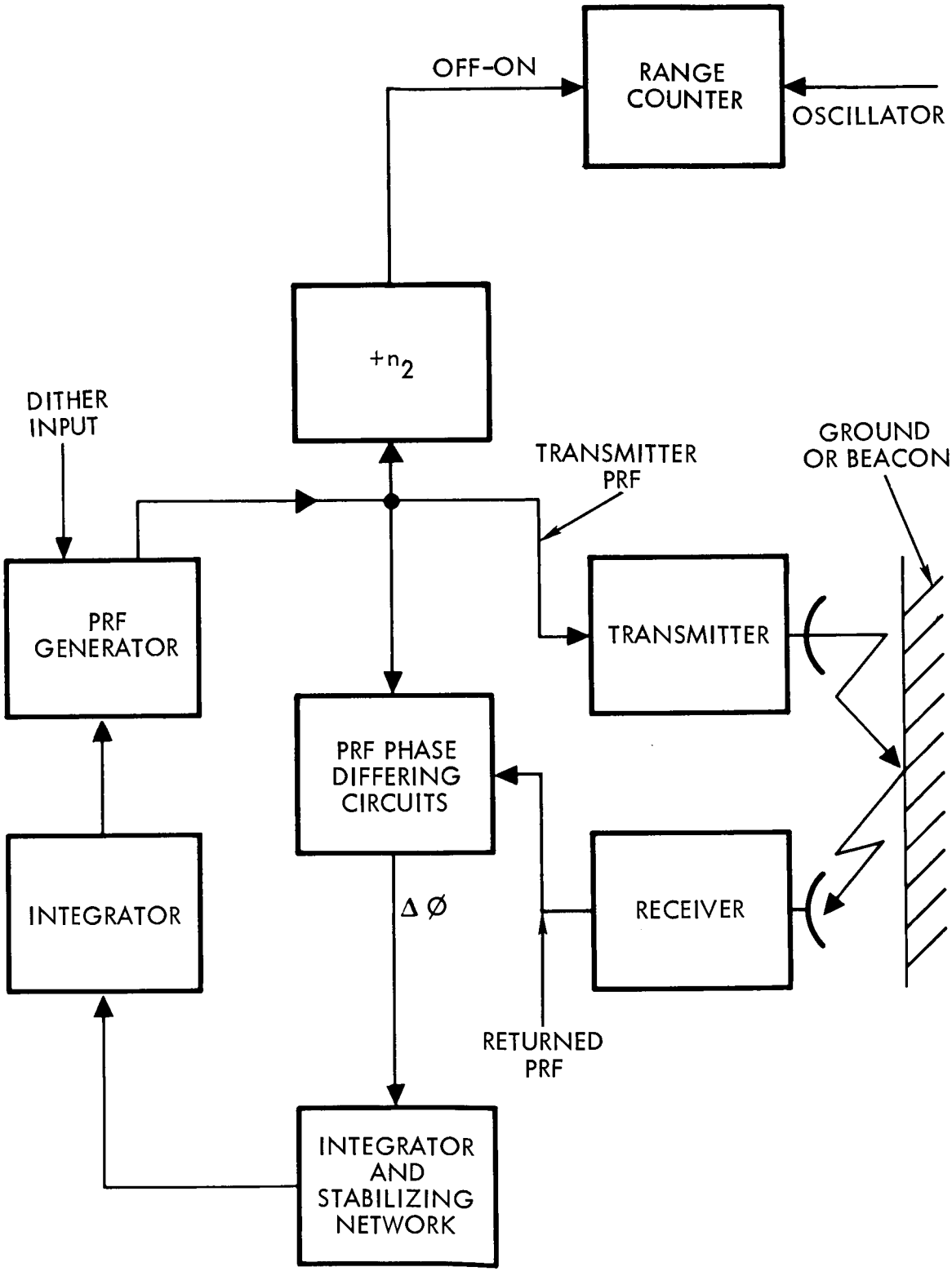

Figure 3-1. Functional Configuration for Radar or Altimeter PRF Tracking

An X-band frequency of about 10 Gc appears to be the highest frequency practical for altimetry or rendezvous. Such a frequency gives small range and velocity errors for altimetry and small-angle tracking errors for beacon tracking.

A lower frequency between 300 and 600 Mc appears to offer advantages for the beacon tracking radar. One advantage of low-frequency transmission to the beacon is that the transmitted beam can be broad so that the beacon need initially have only its receiver turned "On," thus saving power. Beacon lock-on will also be simpler because of a lower doppler frequency shift at the lower transmitted frequency. When the beacon achieves lock-on, it could turn its X-band transmitters "On," and the radar, which would be searching in frequency, could detect the beacon and stop its search. The radar antenna could be a dual broad-beam, low-frequency type for transmission and a narrowbeam high-frequency type with an angle track capability for reception at X-band.

The use of the lower frequency from radar to beacon would also assure a higher S/N ratio at the beacon because,first, higher power could be transmitted at the lower frequency and, second, the receiver would have a lower noise temperature at the lower frequency. The loss of antenna gain at the radar when transmitting the lower frequency could be compensated for by a greater antenna area at the beacon. If, however, the frequency were made too low, much lower than 300 Mc for an antenna of 2 ft, the advantages of the low frequency would diminish due to the limited antenna size. As has been noted, a frequency lower than X-band for altimetry is not desirable because the errors in the measurement of altitude and velocity would increase. However, for the beacon mode, the requirement for X-band operation to obtain high-angle measurement accuracy at the radar is not so pronounced.

The angle rate error due to thermal noise can be shown to vary for a fixed receiving antenna size as:

$$\dot{\theta}_{\substack{(\text{rms}) \\ \text{thermal}}} \approx \frac{1}{F} \sqrt{\frac{T_e}{P_t}} \quad \text{(units)}$$

or inversely proportional to frequency and to the square root of the transmitted power, and directly proportional to the square root of the noise temperature.

Thus, if the frequency of a radar having an antenna of constant size were decreased, there would be a resulting increase in angle error due to thermal noise. However, the lower noise temperature and higher power possible with a solid-state power source would tend to compensate for this angle error. For example, if an X-band frequency were reduced 16 times, the angle noise would increase by about 24 db; however, it could be reasonably decreased by about 12 db by increasing the transmitted power and it would also decrease, typically, by 5 db because of a lower receiver noise temperature. The net result would be only a 7-db increase in angle noise due to the lower frequency operation.

There are, however, other problems at lower operating frequencies such as multipath errors and errors due to a varying field with antenna position, each of which would further affect the error in angle tracking. It also appears that there is some advantage in keeping the radar-received frequency and the altimeter frequency nearly the same to make use of identical receiver units in a unified system. The exact requirements for angle tracking accuracy, however, would undoubtedly vary for different missions. Thus, the actual angle accuracy requirements should certainly affect the final decision concerning the operating frequency.

3.2.3 Ranging Modulation

A number of modulation techniques might be suitable for use with the combined sensors, each having certain advantages and disadvantages. The technique chosen, however, is one employing dithered PRF modulation. This technique was selected during the first phase of the contract, and has subsequently proven more desirable that first anticipated. Tests now indicate that dithered PRF tracking is satisfactory down to extremely low altitudes, less than 10 ft, without a change in ranging technique required. Also, a newly developed PRF generator, well suited to integrated circuit techniques, allows PRF generation by simple techniques and tends to compensate for any effect that range changes have on the tracking loop gain. Also, means have been developed to keep the amount of dither modulation at the correct value over all possible values of PRF.

The use of diode switching at short ranges has proven desirable, experimentally, for obtaining high-ranging accuracy, while varactor switching at greater ranges has proven a simple means for obtaining increased isolation between the transmitter and receiver. At the greater ranges, a single antenna is normally sufficient for transmission and reception as the added isolation afforded by two antennas is not required. An added advantage of the dithered PRF modulation scheme is that high accuracy range data in digital form is readily available with only a fairly low frequency counter being required for processing the data.

A factor which would further improve the status of dithered PRF modulation relative to other techniques is the improvement in receiver sensitivity to be obtained by gating the IF amplifier. It appears possible, theoretically, though not confirmed experimentally, that the receiver IF can be gated with a 50 percent duty cycle to effect a reduction in thermal noise of 3 db. This would mean that the carrier power would be down only 3 db from the unmodulated carrier, rather than 6 db as would be the case if switching were accomplished in the RF portion of the receiver.

Other modulation ranging schemes that have been considered are short pulse modulation, a swept cw signal homodyne technique, ranging phase modulation on a cw signal, cw frequency shift keying, and pseudo-random noise modulation.

- o Short Pulse Modulation. A pulse system requires a very high modulation voltage to obtain reasonable transmitter power and range. Ranging at short distances is difficult unless exceedingly short pulses are used; these could be switched to long pulses at extended ranges. Also, range-rate must be obtained by differentiating the ranging signal. The range rate thus obtained does not represent the true ground doppler, particularly if the ground area being viewed is changing topographically. Also, direct digital readout requires an extremely high frequency counter for obtaining high accuracy range measurements of the order of a few feet. Otherwise accurate short range digital readings must be converted from analog-data readings.

- o Swept CW Signal. A swept-cw signal requires high frequency deviation to obtain high accuracy range data. Such wide frequency deviation is not too readily obtained in a reliable all solid-state system using frequency multiplication. Also, direct ground doppler or velocity readout is not readily available. Further, varactor multiplier chains tend to be noisy, which can result in difficulties in measuring range.

- o Phase Modulation on a CW Signal. This method of modulation has found some use in all solid-state systems operating over relatively small altitudes. Extending this system to greater altitudes might present problems, particularly with a single-antenna system.

- o CW Frequency Shift Keying. Frequency shift-keying, where transmitter and local oscillator are jumped between two frequencies, should work well at extended ranges. However, at short ranges where high accuracy is required, difficulty will be experienced due to phase-shifts in typically narrowband multiplier chains.

- o Pseudo-Random Noise Modulation. Pseudo-random noise ranging modulation for an altimeter would probably present problems in obtaining the required transmitter-receiver isolation, and also in the relatively long time delay between initial carrier lock-on and the availability of range data.

3.2.4 Loop Time Constant Considerations

3.2.4.1 Altimeter Tracking Loops

To receive the return echo when the transmitter is not transmitting, a near 50-percent duty cycle or less is required, and a 180-deg phase shift between the outgoing pulse and returning pulse is required. The method of obtaining the 180-deg phase shift requires that the PRF be varied at a rate equal to

$$\frac{Vc}{R} \text{ (PRF) cycles/sec}^2$$

where

Vc is the closing velocity

R is the range to the ground.

Because the PRF is used as a direct measurement of range, it will contribute on a direct percentage basis to the range error if it should vary from this value.

The value of $\frac{Vc}{R}$ can generally be assumed to remain constant over the operating range and, if this is the case, then the variation of

PRF/sec due to range closure will vary directly as the PRF. The question that now might arise is: "What will be the allowable error due to this PRF change and what is the required value of tracking-loop gain or bandwidth that is required to track this variation?"

A block diagram of the transfer functions for the altimeter dithered PRF tracking loop is shown in Figure 3-2. The PRF is directly proportional to the output voltage of the second electronic integrator, divided by a factor n. A variation in the PRF or range will result directly in an equivalent PRF phase tracking error. The phase-tracking error is the difference in phase between the incoming and outgoing PRF and results in a dithered frequency error whose phase and amplitude is proportional to the sense and magnitude of the PRF or range error. The dither frequency is detected, giving an output dc voltage whose sense and amplitude are proportional to the PRF error. The output detected dc voltage is used to drive the first electronic integrator through the appropriate filter and stabilizing networks. Two electronic integrators are used in the loop to obtain zero steady-state frequency error when tracking the required change in the PRF due to range closure.

During PRF lock-on, a transient error will be present. This PRF transient error should be restricted to a value of 20 percent of the maximum allowable tracking error in the absence of thermal noise by designing the loop gain to be sufficiently high. As can be shown, this value of transient error will allow tracking at the minimum S/N ratio with the maximum possible time before tracking loop loss of lock-on. The maximum allowable tracking error will be a function of the percentage that the PRF is dithered. The maximum dither obtainable is ±90 deg. A smaller percentage of dither can be used and might be desirable in some cases to reduce the possible range errors due to nonlinearity of the dithering networks. Therefore, ±45 deg of dither will be assumed for the present. The allowable PRF transient error assuming 20 percent of this will be ±9 deg or a ±5 percent variation in PRF.

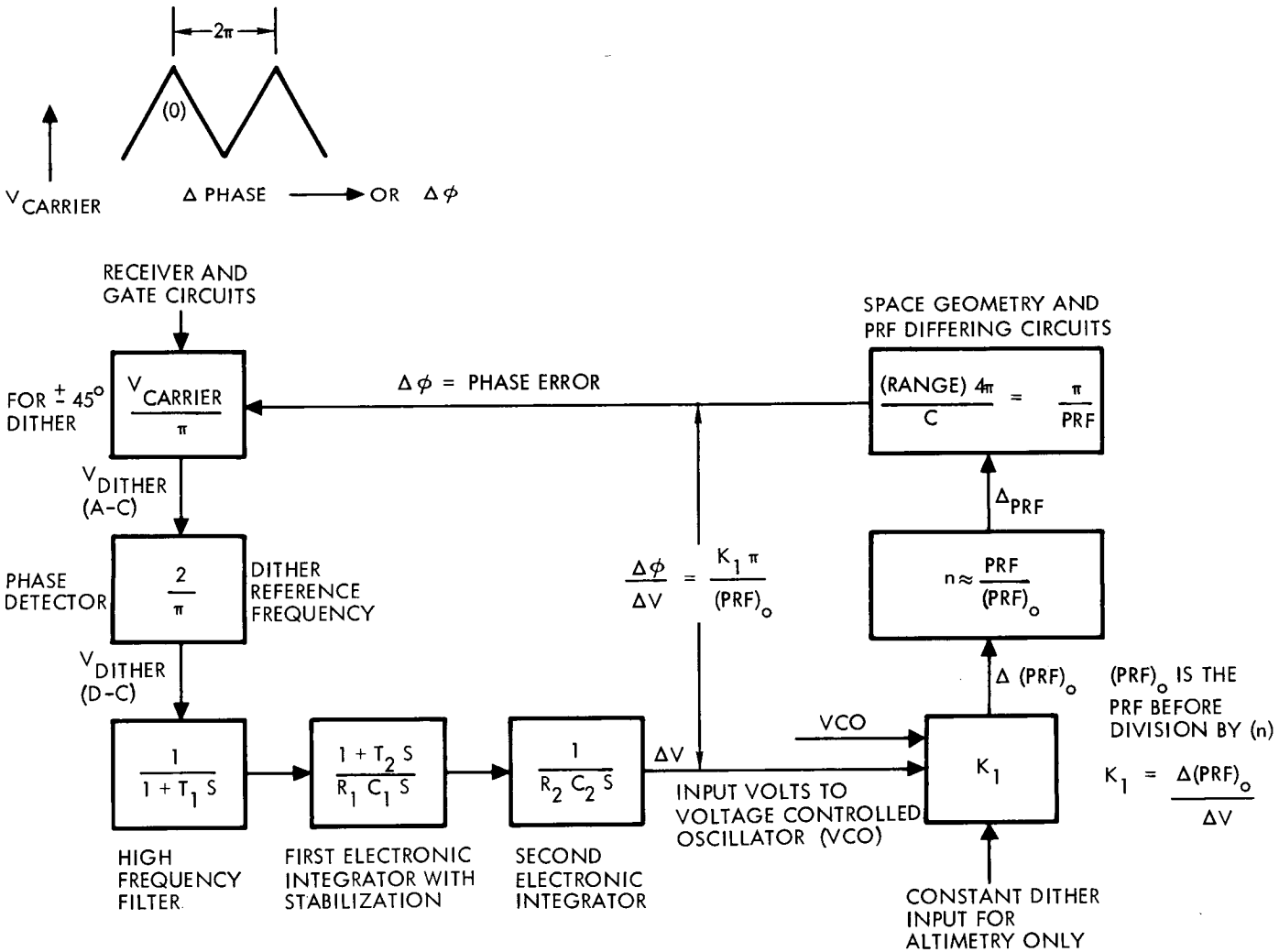

NOTE: (1) $(PRF)_o$ IS DESIGNED TO VARY ONLY BY A RATIO OF 2 TO 1.

(2) $V_{CARRIER}$ = CONSTANT DUE TO RECEIVER'S AGC.

(3) LOOP GAIN VARIES ONLY 2 TO 1 WITH RANGE.

Figure 3-2. Transfer Functions for Radar or Altimeter PRF Tracking Loop

The loop gain for a two-integrator frequency locked loop can be shown to be ω_n, where ω_n is the natural loop frequency expressed in rad/sec. The term ω_n is also approximately equal to the inverse of the loop time constant and can also be assumed to be approximately equal to the tracking loop equivalent white-noise bandpass expressed in cps.

The transient response of the loop is shown in Figure 3-3 in terms of ω_n for a step input in PRF frequency such as would be initially be obtained during lock-on. The cross-hatched area is equal to the maximum error of the PRF, (ΔPRF), that will be obtained for a step input of $\left(\frac{\Delta PRF}{sec}\right)_{step}$

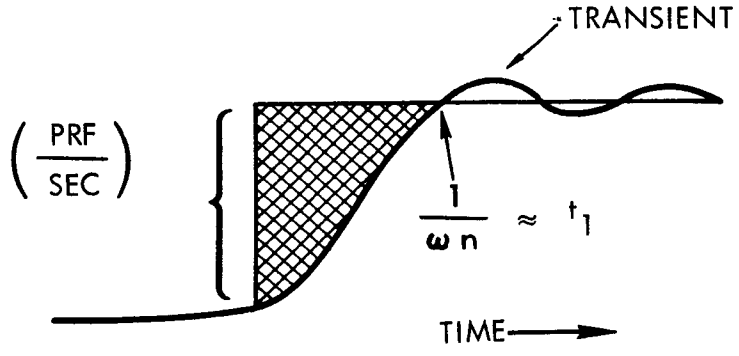

Figure 3-3. Loop Transient Response

To find the required value of ω_n that will restrict the initial lock-on transient, due to $\frac{\Delta PRF}{sec}$ caused by the velocity V_c, to 5 percent of the PRF, it is necessary to determine the transient response of the loop to a step change of $\left(\Delta\frac{PRF}{sec}\right)$. The expression for the transient error is

$$(\Delta PRF)_{\text{error transient}} \approx \left(\Delta\frac{PRF}{sec}\right)_{step} \times t_1\left(\frac{1}{2}\right)$$

Substituting $\omega_n = \frac{1}{t_1}$ in the above equation, one obtains

$$\omega_n = \frac{\left(\frac{\Delta PRF}{sec}\right)_{step}\left(\frac{1}{2}\right)}{(\Delta PRF)_{error\ transient}} \quad cps$$

If $(\Delta PRF)_{error\ transient} = 0.05\ (PRF)$,

and $\left(\frac{\Delta PRF}{sec}\right)_{step} = \left(\frac{V_c}{R}\right)(PRF)$, then ω_n is found to be:

$$\omega_n = \frac{\frac{V_c}{R}(PRF)}{0.05\ PRF}\ \frac{1}{2} = \frac{V_c}{0.1\ R}\ cps$$

3.2.4.1.1 Altimeter PRF Tracking Loop Time Constant

For a value of $V_c = {}^{*}8200$ ft/sec and for a maximum value of R of *380 nmi.

$$\omega_n = \frac{8200\ ft/sec}{(0.1)\ 380\ nmi} = 0.036\ cps$$

and $T = \frac{1}{\omega_n} = 28$ sec.

It thus appears that limiting transient errors due to initial lock-on to 5 percent of the PRF will require a tracking loop time response equal to or less than 28 sec for the altimeter PRF tracker. A 28-sec tracking-loop time constant appears to be too long for a practical system and a somewhat reduced time constant should be used. This would result in even less transient error, although the minimum tracking S/N in thermal noise would be increased.

* See page 7, "Study of Lunar Landing Sensor Performance, Interim Report No. 1," prepared by TRW Systems under NASA Contract NAS8-5205.

3.2.4.1.2 Altimeter Carrier Tracking Loop Time Constant. An investigation of the maximum ground clutter spread that might be expected at maximum range has indicated that a frequency discriminator bandwidth of about 10 kc would be desirable for tracking the carrier. This requirement would necessitate a maximum transient or steady state tracking error of about one fifth this value or 2 kc to insure optimum performance in the thermal noise region.

The altimeter carrier tracking loop is essentially similar to the PRF tracking loop and consists of a two-integrator frequency locked loop. The approximate formula previously derived for the PRF tracking transient error is applicable here with ΔPRF/sec made equal to the maximum anticipated altitude acceleration of 30 ft/sec^2. Expressed in cycles/sec^2 at X-band, the value of the acceleration, g, becomes:

$$g = \frac{30 \text{ ft/sec}^2}{\lambda/2} = 600 \text{ cycles/sec}^2$$

If frequency error ΔPRF, or in this case ΔF, is equated to 2000 cps, then

$$\omega_n = \frac{g}{2\Delta F} = \frac{600 \text{ c/sec}^2}{2\ (2000)} = 0.15 \text{ cps}$$

and t_1 = 6.6 sec (the value of the loop time constant).

3.2.4.2 Radar Tracking Loops

3.2.4.2.1 Radar PRF Tracking Loop. The radar PRF tracking loop requirements are the same as those for the altimeter with regard to loop gain and tracking transients, and will likewise necessitate a tracking loop time constant of 28 sec or less for a closing velocity V_c, = 8200 ft/sec and a range, R = 380 nmi. However, because the radar carrier tracking loop will be phase locked instead of frequency locked as in the altimeter, coherent detection of the PRF-dithered signal by a quadrature carrier phase detector can be used. Coherent phase detection can substantially reduce the thermal noise effects and should allow tracking the PRF at a lower S/N ratio than is possible in the altimeter.

3.2.4.2.2 Radar Carrier Tracking Loop. The type of tracking loop that will be used here, as previously noted, is a phase-locked loop at X-band. A phase-locked loop is desirable because it will allow more precision in tracking the carrier doppler. The minimum S/N tracking capability for a phase- and frequency-locked loop are, in general comparable, although this will vary somewhat due to system parameters.

If the signal should have considerable phase noise on it, this might necessitate a higher equivalent tracking loop bandwidth for the phase-locked loop, thereby degrading its minimum S/N tracking capability somewhat. Care must therefore be exercised to ensure the lowest possible phase noise on the echo signal coming both from the beacon and from the local oscillator signal used in the radar.

The tracking loop bandwidth required for a phase-locked loop to track a target of known acceleration, g, with a phase error $\Delta\phi$, expressed in cycles is well known and is equivalent to

$$W_n = \sqrt{\frac{g}{\phi_{cycles}}}$$

The value of g is 30 ft/sec^2 = 600 cps/sec^2 at X-band and is the same value as for the altimeter. ϕ_{deg} = 18 deg, or 1/5 of 90 deg, 90 deg being considered the maximum linear phase error obtainable out of a limiter-type phase detector. Hence

$$W_n = \frac{600 \text{ c/sec}^2}{\frac{18}{360}} = \sqrt{600\ (20)} = 110 \text{ cps}$$

This might be, as has been noted, too small a value for ω_n due to possible signal and LO phase errors.

Laboratory tests at TRW have indicated phase errors at X-band of 6 deg rms for loop gains of ω_n = 1000. This value, undoubtedly, can be reduced by additional development.

3.2.4.3 Beacon Tracking Loops

The beacon tracking loops are phase-locked types for both the carrier and PRF. The factor determining loop bandwidths is the radar-beacon acceleration for the carrier loop and for the PRF tracking loop. The equivalent acceleration for the PRF tracking loop is

$$\frac{\Delta PRF}{sec} = \frac{V_c}{R} (PRF) \text{ cycles/sec}^2$$

In the beacon carrier loop, as in the radar carrier tracking loop, a phase error of 18 deg can be allowed. However, in the PRF tracking loop there will be a fixed phase error required for tracking the changing PRF; however, this phase error must be kept small because it results directly in a range error.

A block diagram of the beacon PRF tracking loop is shown in Figure 3-4. As may be seen, only one electronic integrator is used in the loop. Additional integration is inherent in the VCO, resulting in phase variations proportional to the integral of frequency. An equivalent third integrator or integral network can be added for further reducing phase error, but it is not shown in the block diagram.

The open loop transfer function is essentially

$$\frac{\omega_n^2}{S^2} \frac{(1 + T_2 S)}{(1 + T_1 S)}$$

As noted previously, the PRF loop gain is maintained constant automatically for varying values of PRF.

The phase error resulting for a rate of change of input frequency of

$$\frac{V_c}{R} (PRF) = \Delta PRF/sec \approx 1/4 \text{ cycles/sec}^2$$

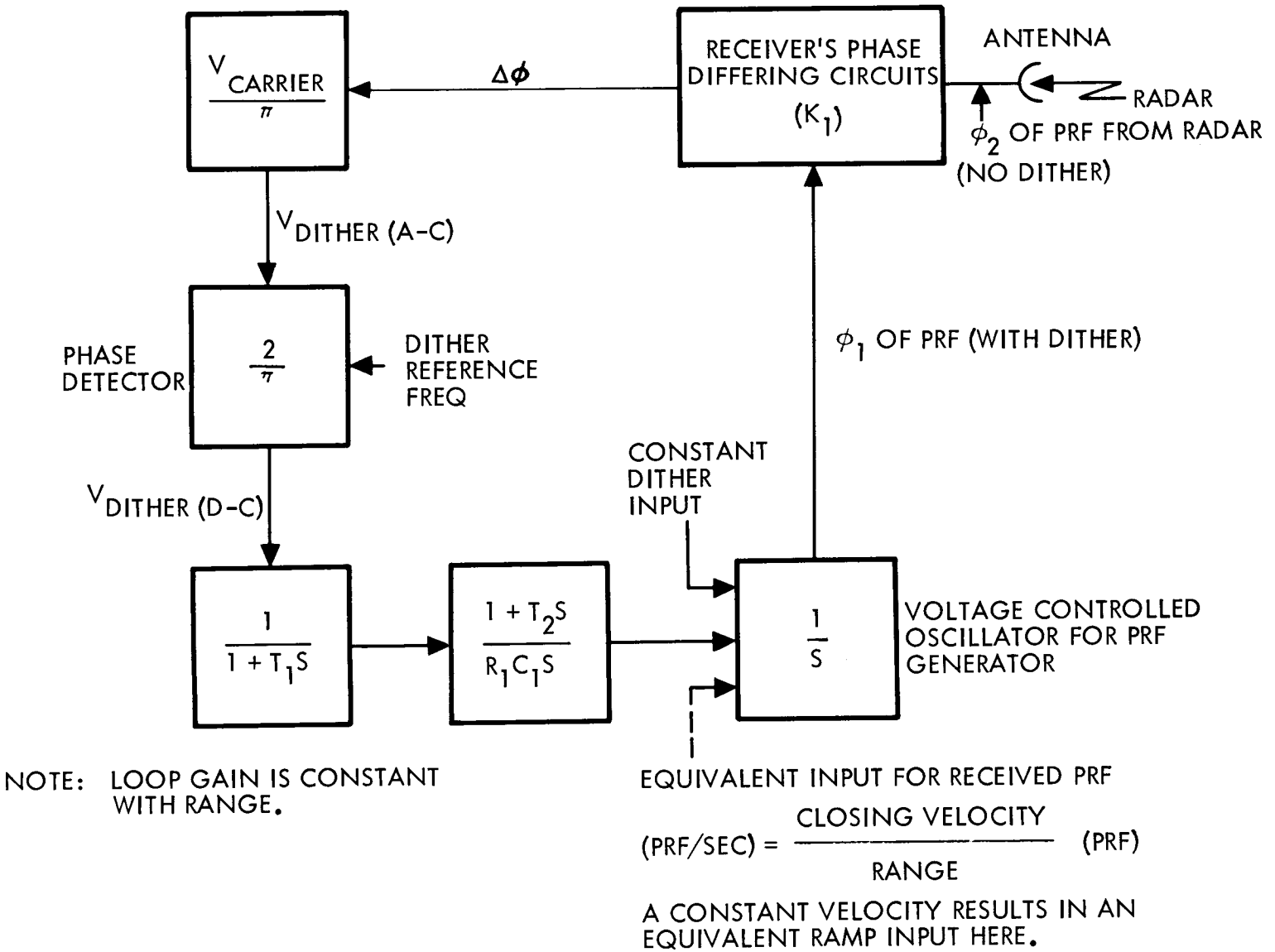

Figure 3-4. Transfer Function Block Diagram for Beacon Tracking Loop

where V_c = 8200 ft/sec

R = 380 nmi

and PRF = 70 cps

is

$$\theta_{\text{cycles}} = \frac{\Delta \text{PRF/sec}}{\omega_n^2} = \frac{1/4 \text{ cycles/sec}^2}{\omega_n^2}$$

3.2.4.3.1 Beacon PRF Tracking Loop Gain. If the PRF tracking loop phase error is kept to 0.9 deg or $\frac{0.9}{360}$ of a cycle due to the PRF change because of the closing velocity, then

$$\omega_n = \sqrt{\frac{\Delta \text{PRF/sec}}{\theta \text{ cycles}}} = \sqrt{\frac{1/4 \text{ cps/sec}}{0.9/360}} \approx 10$$

However, the $\frac{\Delta \text{PRF}}{\text{sec}}$ input will vary directly as the PRF when the ratio of V_c/R is constant. In this case, the phase tracking error will increase with decrease of range. Therefore, a third integral network appears desirable and also a high gain tracking loop is desirable to keep the phase error low as the range changes. After the range has decreased by roughly 100 times and the PRF is 7 kc, it appears desirable to switch to another PRF generator which will allow the attainment of even a higher loop gain or ω_n to further reduce phase error. Such a change in the PRF tracking loop gain in the beacon might be required twice between the ranges of 380 nmi and 10 ft.

3.2.4.3.2 Beacon Carrier Tracking Loop. The value of loop gain required to track the carrier in a phase-locked loop may be determined as in the above calculations. In this case, an acceleration tracking capability of

$$30 \text{ ft/sec}^2 \approx 19 \text{ cycles/sec}^2$$

is required where the carrier frequency is 310 mc. For a phase error of 18 deg, a value of ω_n of 19.5 is required, i.e.,

$$\omega_n = \sqrt{\frac{19 \text{ cycles/sec}^2}{18/360}} = 19.5$$

3.2.4.4 Summary of Tracking Loop Time Constants

Table 3-I presents a summary of the requisite loop-time constants.

3.2.5 Unified Extended Range Altimeter/Beacon Tracker

Figure 3-5 is a block diagram that shows how the dithered PRF modulation scheme may be synthesized to provide a unified long-range altimeter and beacon tracking radar. The altimeter uses a single antenna for transmission and reception. A separate dual frequency antenna is shown for beacon tracking, although in this case the same antenna could be used for both beacon tracking and altimetry if certain penalties in performance could be tolerated.

The altimeter system is referred to as being a "long-range" type because of the use of the use of a single high-gain antenna. If a separate transmitting and receiving antenna were used, the system could be made to operate at short ranges. Separate antennas would provide the required isolation between the transmitter and receiver at low altitudes. At long ranges a single antenna is sufficient because the time delay allowable between the initiation of transmitter turn-off and of receiver turn-on may be made long enough to permit satisfactory isolation. That is, the time is available for the transmitter signal to be sufficiently attenuated when the receiver is turned on, so that any leakage signal will be much less than the ground returned signal.

At short ranges this is not possible, because the PRF is sufficiently high so that the required time delay is comparable to the pulse "on" time. The requisite time delay cannot be shortened because the relatively high Q's of varactor signal source limit the switching speeds. Tests with varactor-gated multipliers have indicated only an 8.5-db decay every 4.5 nanosec. Thus, in 23 nanosec the RF power would be reduced by only 44 db. Now the ratio of the received power to the transmitted power at a range of 62 ft is about 68 db, assuming a 1-ft antenna diameter and a coefficient of ground reflection of -17 db. Thus, it is apparent that even a 23-nanosec time delay between the transmitter turn-off and the receiver turn-on times is not sufficient to reduce the leakage power below the return ground echo.

Table 3-I. Summary of Tracking Loop Time Constants

	Δ PRF/sec or $\left[\frac{V_c}{R}(PRF)\right]$	(g) max CPS/sec	IF Error Allowed	Phase Error Allowed	Δ PRF Error Allowed	Tracking Loop Gain (W_n)
Altimeter PRF	1/4 cycle/sec^2 V_c = 8200 ft/s R = 380 nmi				0.05 PRF (transient)	$W_n = 1/28 = 0.036$
Altimeter Carrier (X-Band)		30 ft/sec^2 (600 cps/sec)	2000 cps (~1/5 Frequency discriminator bandwidth)			$W_n = 1/6.6 = 0.15$
Radar PRF	1/4 cycle/sec^2 V_c = 8200 ft/s R = 380 nmi				0.05 PRF (transient)	$W_n = 1/28 = 0.036$
Radar Carrier (X-Band)		30 ft/sec^2 (600 cps/sec)		18 deg		$W_n = 110$ (Phase error on LO and carrier might require $W_n > 100$)
Beacon PRF	$\frac{\Delta PRF}{sec}$ = 1/4 cycle/sec^2 V_c = 8200 ft/sec R = 380 nmi				0.005 PRF (0.5 percent range error)	$W_n = 10$
Beacon Carrier (310 mc)		30 ft/sec^2 (20 cps/sec)		18 deg		$W_n = 19.4$ (Phase error on LO and carrier might require $W_n > 19$)

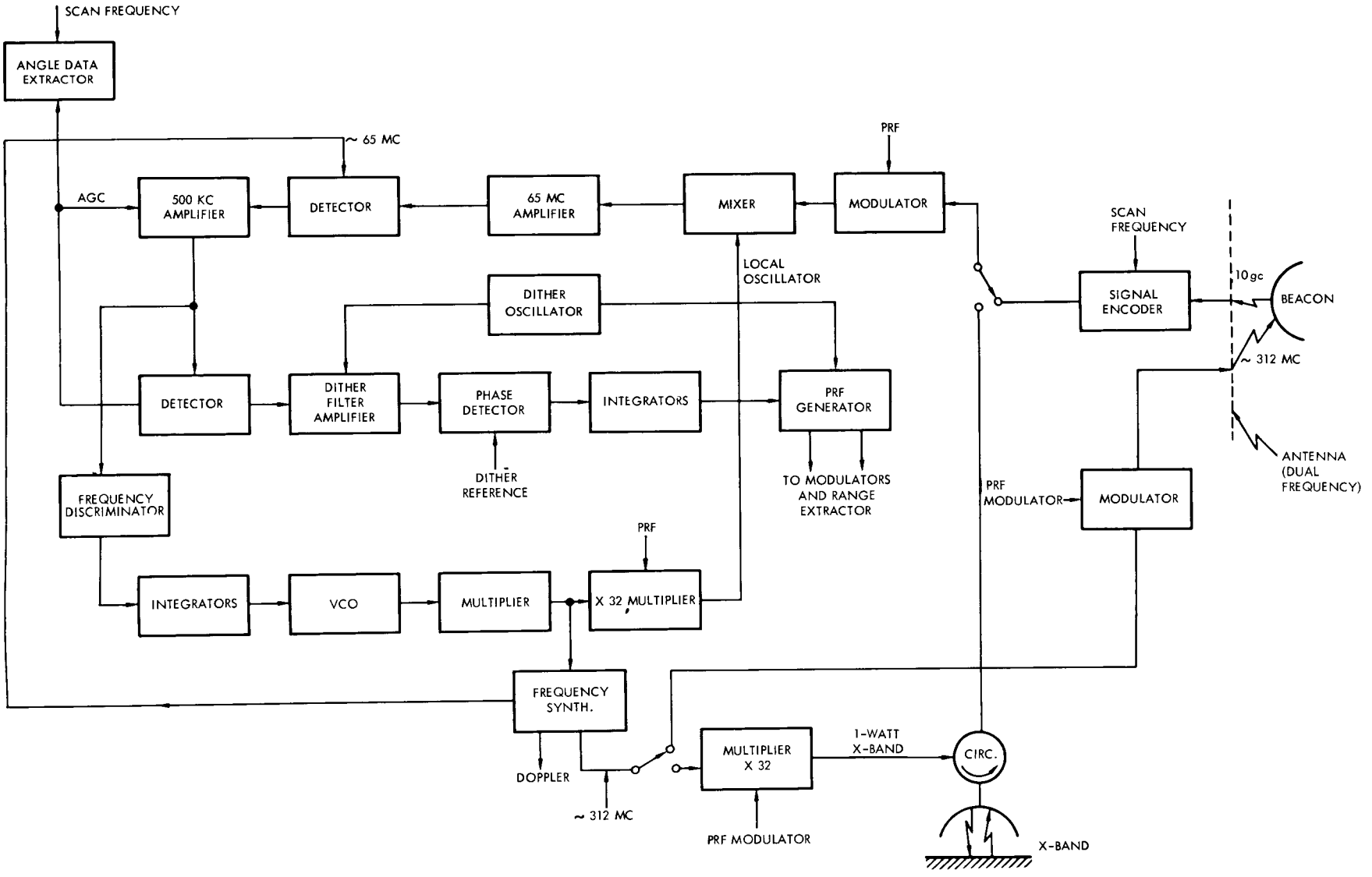

Figure 3-5. Unified Long-Range Altimeter and Beacon Tracking Radar

However, this is no problem at extended ranges because sufficient time for decay is available. The leakage should also be at least 10 to 20 db below the returned signal.

The system shown in Figure 3-5 also incorporates gating of the local oscillator varactor multiplier chain in the altimeter mode to obtain the high isolation required at extended ranges.

For the beacon mode, diode switch gating of the transmitted and received signal is also used. The isolation required in the beacon mode is obtained by the diplexing action of the single dual frequency antenna. Filters could be added if more isolation were required. The beacon signal is tracked in angle by the use of a signal encoder, such as that used in monopulse radars or in lobe switching. This feature is discussed further in Subsection 3.3.

The carrier frequency is tracked by utilizing a frequency discriminator to control the local oscillator frequency. A frequency synthesizer using a separate oscillator is used to generate the transmitter frequency. The frequency synthesizer also reduces doppler data by mixing a frequency from the LO multiplier chain with the appropriate synthesizer signal. The altitude or range, as the case may be, is obtained by the use of dithered PRF tracking. Range can be extracted by using the PRF to turn on and off an electronic counter. The counter reading would then indicate range directly.

A cursory estimate of the physical characteristics and power requirements of this system indicates a weight of 12.7 lb, a volume of 0.2 cu ft, and a prime power requirement of 78 watts. For purposes of the estimate, it was assumed that off-the-shelf micromodules were used where possible, and that an all solid-state signal source providing one watt at X-band was used as the transmitter. This RF power level would permit operation over the specified range.

An estimate of the MTBF of this unified system, based upon the use of electronic parts with a standard reliability level, operating at 40 percent of rated value in an aerospace vehicle equipment temperature of $50^{\circ}C$, is 19,900 hr. For purposes of definition, these parts would be selected through a standard parts program, defined in the TRW Systems Reliability Manual, dated 12 July 1965, as follows:

The standard parts program characteristics and requirements include the following usual military procedures in addition to adequate applications engineering:

(1) Definition of parts characteristics in specifications, controlled procurement, and quality control.

(2) Choice of proven parts and listing in preferred parts lists.

(3) Qualification testing of each type (but not each lot) to applicable environments.

It is evident that this unified sensor system displays definite advantages, with regard to size, weight, power requirements, and reliability, over two separate sensors performing the same functions. As is apparent from the block diagram, these advantages are a direct result of subsystems common to each mode of operation being used almost exclusively. Only a section of the transmitter and certain signal processing circuits are not common. The unified sensor would be expected to have essentially the same functional characteristics and display the same dependence on environment as would an independent system performing only one of the two major functions of the unified sensor.

Figure 3-6 shows a block diagram of the transponder to be used as the beacon with this and the other systems to be discussed later. Lock-on circuitry is not shown, but because of the low carrier frequency received, 312 mc, carrier doppler shift is fairly low and the carrier tracking loop bandwidth can be made wide enough for lock-on without search. The range modulation is not turned on until after carrier lock-on is accomplished. Also in the beacon track mode, dither is only applied to the PRF at the beacon.

The received 312-mc signal is amplified after gating in a low-noise figure amplifier. The signal is further amplified and automatic gain controlled in a 65-mc IF amplifier after mixing. Mixing is done in such a way that coherency of the retransmitted X-band signal is maintained with the 312-mc received signal. The carrier is tracked in a phase-locked loop.

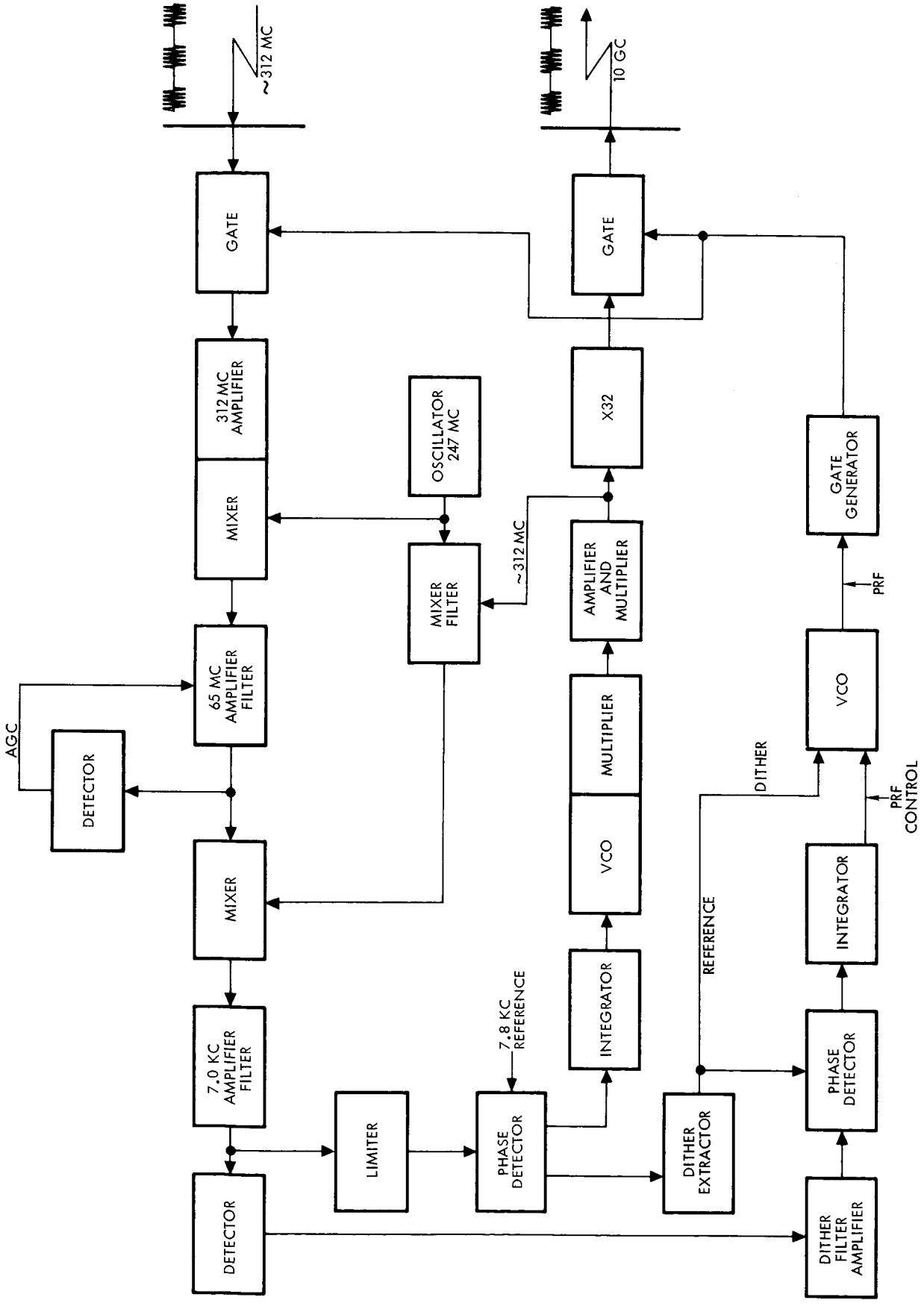

Figure 3-6. Beacon for Unified System

Range tracking in the beacon is accomplished by detecting the dither frequency after it has been added with the gating signal, and adjusting the PRF to obtain zero dither frequency at the fundamental dither frequency. The dither frequency used in the beacon is obtained from the radar/altimeter unit by carrier phase modulation being processed by circuits not shown in the block diagram. (See Figure 3-6).

A mechanical layout of the beacon transponder is shown in Figure 3-7. Microminiaturization or integrated circuits are assumed used throughout. The transponder weight is estimated to be 6 lb. Reliability is very high because of the use of solid-state and integrated circuit techniques.

3.2.6 Unified Short-Range Altimeter/Beacon Tracker

Figure 3-8 shows the configuration of a combined short-range altimeter with multibeam velocity tracking and beacon tracking radar. Separate antennas are used with beam switching or rotation and are discussed in a subsequent section. The gain for this type of antenna arrangement is low and will not permit the long range performance that a single beam and single antenna system will. Diode switching is used to increase the time accuracy over that obtained with varactor switching. High modulation accuracy is required at the short ranges.

Range and frequency tracking are achieved in a manner similar to that discussed in Paragraph 3.2.5 except that three frequency tracking loops with the appropriate switching are necessary for the multiple beams. The beams are switched in the antenna by ferrite switches. Switching is performed at a rate sufficiently fast so that the frequency tracking loops continuously track the carrier return. The VCO drift between samples is considered negligible. The signal for PRF tracking is obtained from only one beam, resulting in an eclipsing power loss obtained when the received signal is from one of the other altimeter beams. Initial carrier lock-on circuits for the three beams are not shown.

A cursory estimate of the power requirements and physical characteristics of the unified short-range altimeter and beacon tracking radar indicated a weight of 12.3 lb, a volume of 0.23 cu ft, and a prime power requirement of 19 watts. For purposes of the estimate, it was assumed

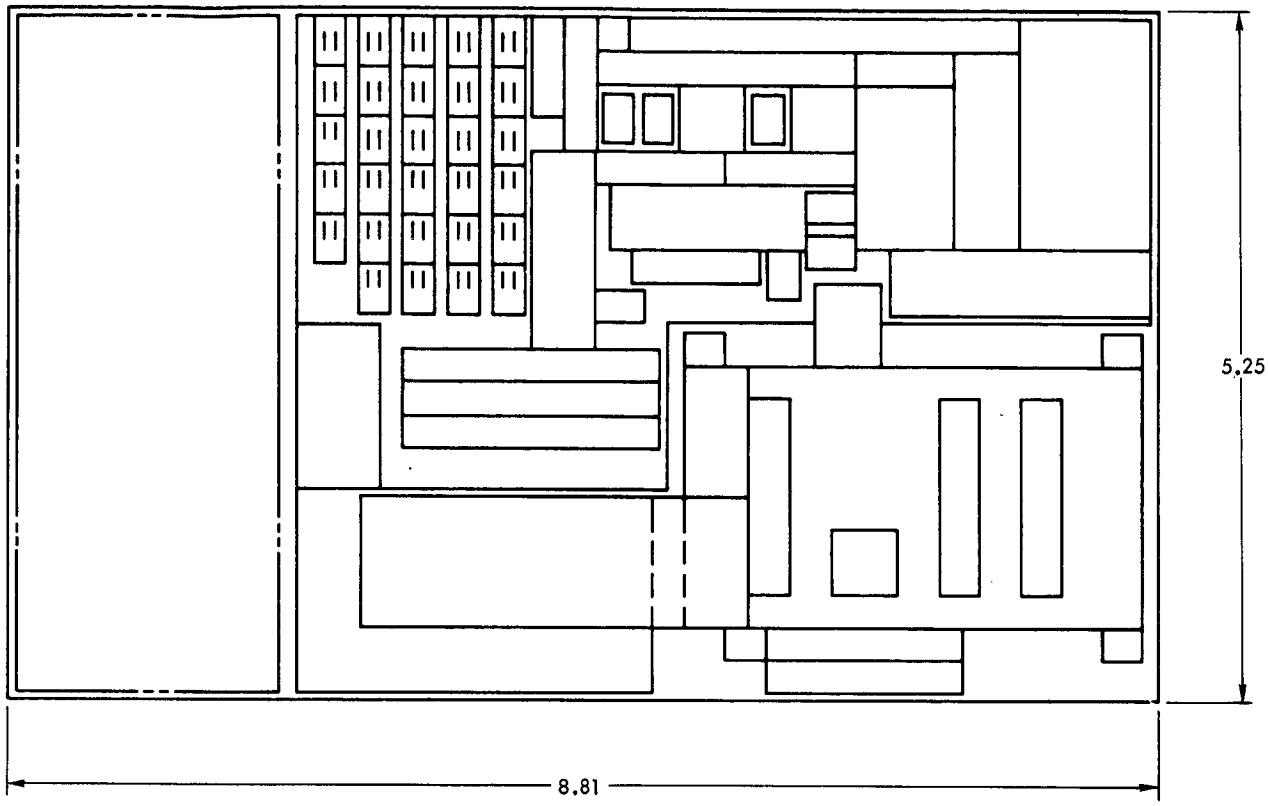

TOP VIEW

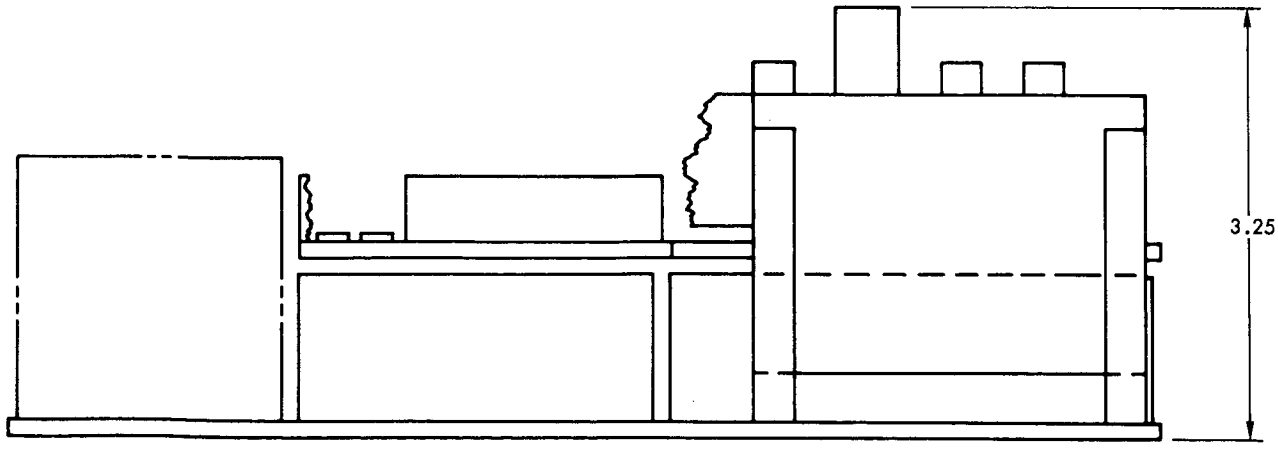

SIDE VIEW

Figure 3-7. Beacon Transponder Layout

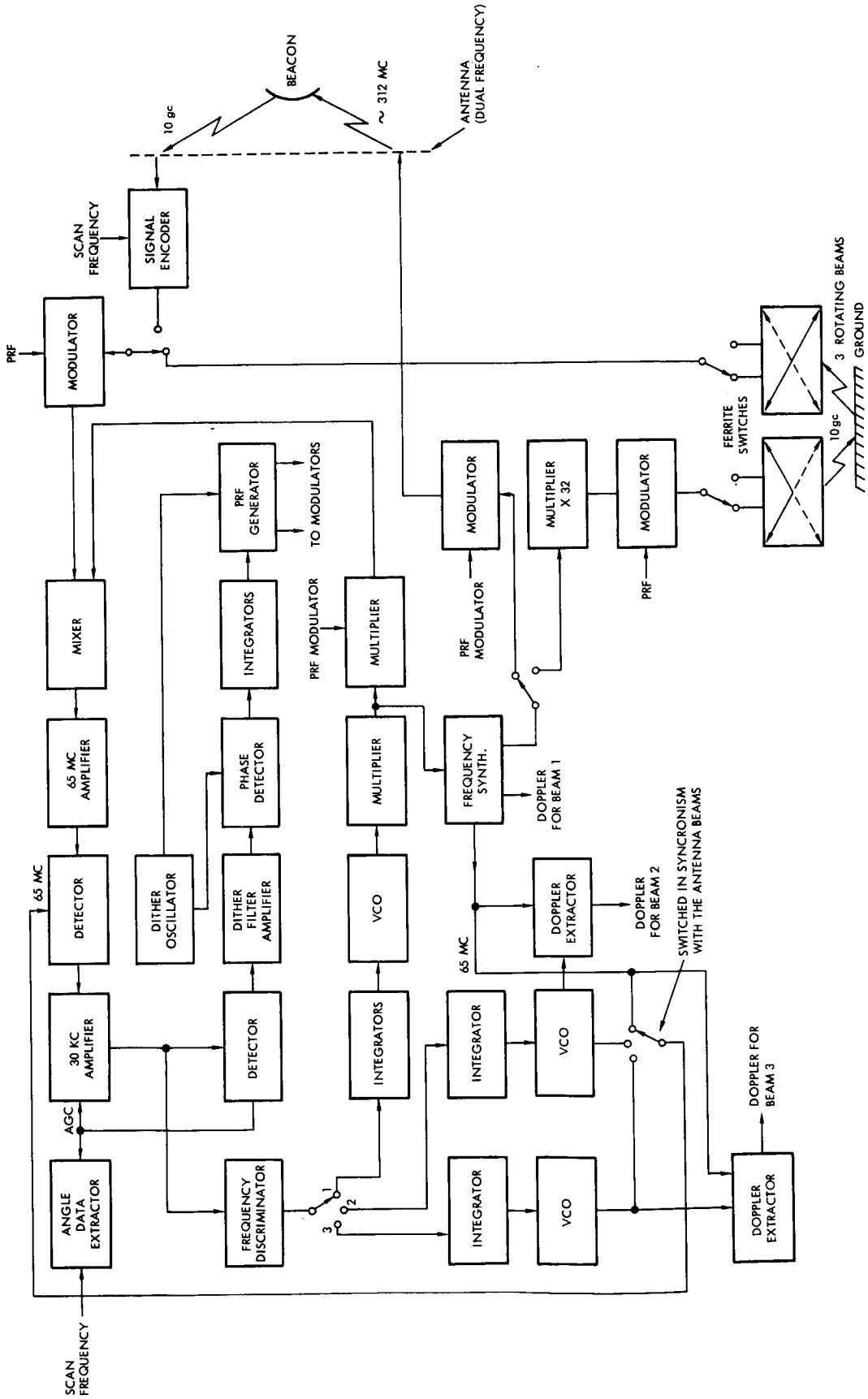

Figure 3-8. Unified Short-Range Altimeter and Beacon Tracking Radar

that off-the-shelf micromodules were used where possible, and that an all solid-state signal source providing 100 mw at X-band was used as the transmitter.

An estimate of the MTBF for this system, assuming the same electrical component restraints as for those used with the unified extended range altimeter and beacon tracker, is 20,000 hr.

A unified system of this type would include very few subsystems in addition to that which normally would be used in a low range altimeter/velocity sensor. The additional circuits required by the unified system would include a frequency synthesizer and some signal processing circuitry. This means that the unified sensor size, weight, power, and reliability are comparable to a low range altimeter/velocity sensor alone. The unified sensor would also be expected to have the same dependency on environment conditions as would either of the sensors functioning alone.

3.2.7 Unified Short-Range Altimeter/Interferometer Beacon Tracker

Figure 3-9 is a block diagram of an interferometer beacon tracking radar and a short-range altimeter. An injected reference signal separated in frequency from the returned 10-gc beacon signal by 30 kc is injected into the front end of the receiver to aid in canceling out phase shifts in the receiver circuits. The detected 30-kc signals, after appropriate amplification and limiting, are used to control the on and off gates of the counter. The counter then measures or indicates the beacon angle in digital form, which is equivalent to the phase shift in the vertical or horizontal channels. Switching between antenna channels is obtained with high-speed ferrite switches. Ranging is obtained by the use of dithered PRF tracking both for the altimeter and the beacon. At low altitudes, the PRF will be high enough to ensure that the PRF modulation harmonics are not locked onto during carrier tracking. For the beacon, PRF modulation is not used until after carrier lock-on has been achieved.

An interferometer system, while having reduced range capabilities, has certain advantages when a broad angle coverage is desired without the use of gimbals. The use of an X-band carrier frequency also reduces the effect of angle tracking error due to multiple ground returns that might be present if the lower frequency interferometer system were used.

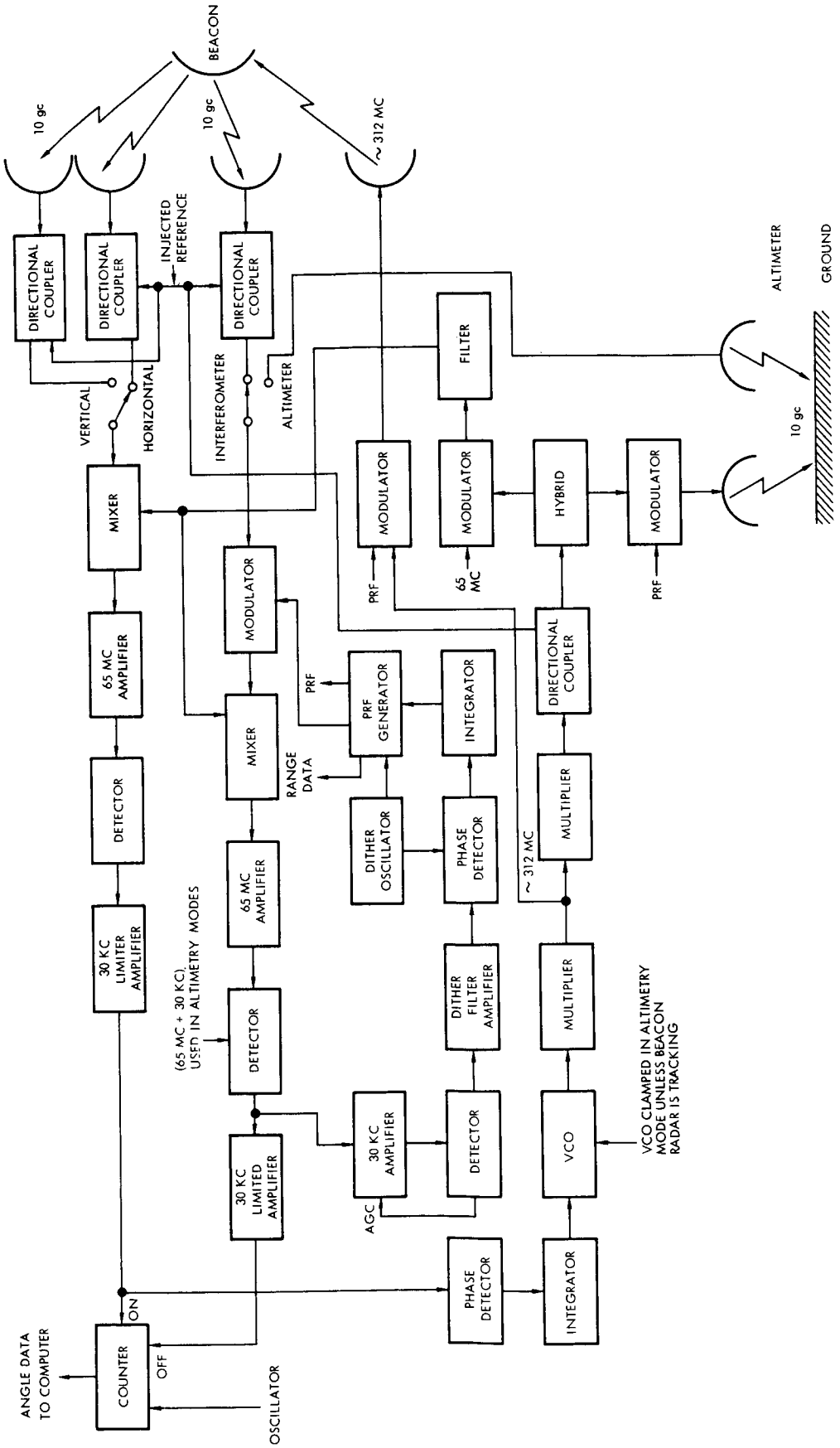

Figure 3-9. Interferometer Beacon Tracking Radar and Short-Range Altimeter

A cursory estimate of the weight, size, and power requirements for the unified interferometer beacon tracking radar and short range altimeter yielded results of 9.8 lb, 0.84 cu ft, and 16 watts, respectively, exclusive of the counter and antenna. It was assumed that this unit was microminiaturized to the extent possible using off-the-shelf components, as were the other two unified systems.

An estimate of the MTBF for this system, assuming the same electrical component restraints as for those used with the unified extended range altimeter and beacon tracker, is 24,500 hr.

As is apparent from the block diagram, this unified system is in essence an interferometer beacon tracking radar, with part of the interferometer circuits being used for a short range altimetry function. Thus, only slight additional circuitry is required for a unified sensor over what normally would be required for an interferometer beacon tracker alone. The additional circuitry requirements are for a high frequency transmitter section, some PRF processing networks, and some signal processing networks. As a result, the size, weight, power, and reliability of a unified system would be very similar to the corresponding parameters of an interferometer beacon tracking radar alone. The unified system would also be expected to have essentially the same operational characteristics and dependence upon environmental parameters as would either of the functional systems operating alone.

3.3 ANTENNAS

3.3.1 Introduction

In this section, applicable antenna types for the lunar landing sensors (LLS) are evaluated with the objective of presenting their advantages and disadvantages, of specifying their performance parameters, and of arriving at a trade-off performance summary. Where pertinent, the dithered PRF ranging modulation technique is assumed used. With this technique, it is necessary that separate transmit and receive atennas be used for low attitude operation in the non-beacon case. In general, however, the antenna performance evaluation applies to any RF modulation technique, rather than only dithered PRF.

Design analysis details of applicable antenna types not described in the reference literature are provided in the appendices. The antenna types include velocity sensor multi-beam resonant arrays, array cluster conical scan, and high resolution, wide angle, electronic search and track planar interferometers. In addition, a number of design details for phase and amplitude monopulse antenna types are presented to demonstrate the performance tradeoffs that must be made with respect to gain, sum beam sidelobes, and error angle slope.

Since the radiating antenna must have an unshielded face that is subject to either the cold shadow, the IR radiation from the hot daytime moon surface or the unattenuated direct sun radiation, the antenna thermal sensitivity is considered to be especially pertinent in LLS applications. Therefore, a subsection devoted to thermal considerations is provided.

3.3.2 Mission Requirements

The generalized LLS mission requirements encompass direct or orbital descent towards a soft lunar landing with or without the use of a beacon on the lunar surface. Where a beacon is available on the lunar surface, the landing may be at the beacon or down-range from the beacon.

In the beacon-assist mode, a search and angle track antenna is required. The functional requirements of the beacon tracking radar are an angle search capability, acquisition capability, and angle, angle rate, range, and range rate tracking capability. The corresponding beacon tracking radar antenna performance requirements are an angle search capability (gimbaled or electronic); the presence of sufficiently low side lobes to avoid false acquisition or degrading gain and error angle detection slope; and the contribution of minimum angle and angle rate tracking errors. The antenna system weight and power requirements are also of prime importance in a space mission. When acquisition is to be at the start of burn in the direct approach, or while in lunar orbit near the horizon (with respect to the beacon) in the orbital approach, the maximum lock on range capability is assumed to be in the order of 380 n.m.

In the non-beacon-assist mode, two antenna types are required: (1) a single beam antenna for the extended range altimeter, and (2) a multibeam antenna (3 or 4 beams) for the low altitude altimeter/velocity sensor. The extended range altimeter antenna requires gimbaling in the orbital approach and can be body-mounted in the direct approach. The maximum ranging requirements are 100 n.m. for the 100 n.m. orbital approach and 380 n.m. for ranging at the start of burn in the direct approach . The performance requirements of the antenna necessitate maximum gain for maximum range and minimum two-way beamwidth for minimum lunar terrain doppler spread.

The altimeter/velocity sensor multi-beam antenna can be body-mounted in the direct approach and either gimbaled or capable of being latched at either of two positions in the orbital approach. When latching is used, computer correction for the constant pitch rate of 0.12 deg/sec at altitudes above 1000 ft will be necessary. The altimeter/velocity sensor is required to measure altitude, altitude rate, and forward and lateral velocity. The associated antenna must have the characteristics of maximum gain, minimum two-way beam width for minimum doppler spread, low side lobes to minimize velocity errors due to crosstalk and low angle terrain return, and minimum beam angle errors to minimize velocity errors. The maximum operational altitude for either the direct or orbital approach is in the order of 5 n.m.

Table 3-II summarizes the applicable sensor performance requirements. The parameters shown are for the non-orbital direct radial approach and the Hohmann trajectory orbital approach. The parameters for other approaches from orbit should fall between these two extremes. In a combined mode, when lunar landing is to be effected with both beacon assist and non-beacon assist sensors, the extended range altimeter and beacon tracking radar antennas can be combined. For direct approach in the altimeter mode, the gimbaled antenna would be latched to a fixed position. Although, conceptually, a combined extended range altimeter, beacon tracker, and altimeter/velocity sensor antenna is feasible with a reflector type antenna; the resultant performance degradation, compared to a separate altimeter/velocity sensor antenna, does not appear to justify such a three-fold antenna utilization. However, one advantage would be gimbaled altimeter/velocity sensor antenna, thereby eliminating the requirement for computer correction of the varying pitch angle in the orbital descent approach.

Table 3-II. Related Sensor/Antenna Performance Requirements

Sensor Type	Beacon Tracker		Extended Range Altimeter		Altimeter/Velocity Sensor	
Descent	Orbital	Direct	Orbital	Direct	Orbital	Direct
Range, km	0 to 700	0 to 700	-	-	-	-
Altitude, km	-	-	1.8 to 220	1.8 to 800	0 to 10	0 to 10
Range/Altitude Accuracy (3σ)	*0.5 % + 1 m	0.5% + 1m	0.5%	0.5%	1% ±1 m	1% ±1 m
Altitude Rate, m/sec	-	-	60 max (80 km altitude)	0 to 2500	0 to 120	0 to 250
Horizontal Velocity, m/sec	-	-	1600 (orbital)	0	0 to 550	0
Altitude Rate Accuracy (3σ)	-	-	-	-	2% ±0.5 m/sec	2% ±0.5 m/sec
Horizontal Velocity Accuracy (3σ)	-	-	-	-	1% ±0.5 m/sec	1% ±0.5 m/sec
Angle Track Accuracy (3σ)	0.3 deg	0.3 deg	-	-	-	-
Angle Track Rate Accuracy (3σ)	0.03 deg/sec	0.03 deg/sec	-	-	-	-
Antenna Beam Coverage	gimbaled 60-deg yaw 120-deg pitch	gimbaled 60-deg yaw 120-deg pitch	gimbaled 60-deg yaw 120-deg pitch	fixed	**latch positions 0 and 40 deg	fixed

* 0.05-percent accuracy is required for orbit determination while in orbit.

** Latch angle change at 1000-ft altitude; at altitudes greater than 1000 ft require computer correction for 0.12 deg/sec pitch angle change.

3.3.3 Beacon Tracking Radar Antennas

3.3.3.1 General Discussion

A search and track antenna system requires either mechanical gimbaling or electronic beam steering for search; and either sequential lobing, conical scan, or simultaneous lobing (monopulse) for angle tracking. Electronic beam steering over a wide solid angle can be implemented by controlling the phase of individual elements of either a high gain, many element, planar-phased array, or a low gain, planar interferometer with a minimum of five elements for wide angle ambiguity resolution. Simultaneous lobing can be realized by either an amplitude monopulse or phase monopulse antenna.

For a beacon assisted lunar landing mission, the following considerations apply with regard to a comparative evaluation of various types of antennas:

(1) The target is cooperative so that the choice of a null tracking technique need not consider a susceptibility to skin tracking types of errors such as target amplitude and angle scintillations. However, for those descent modes where the look angle is near grazing elevation angles, lunar multi-path scintillations can occur; and where a solid propellant is used for powered descent, scattering scintillations by the exhaust particles may also occur.

(2) Since beacon power may be utilized to compensate for a low-gain beacon tracker antenna, the high resolution, wide angle, ambiguity resolving, electronic search and angle track interferometer deserves consideration.

(3) A dithered PRF ranging technique is used, beacon-to-tracker transmission is at X-band, and tracker-to-beacon transmission is at VHF. Since the beacon tracker transmits at VHF and receives at X-band, different transmit and receive antennas are necessary. The VHF transmission is at high power and low gain. The antenna might be a half-wave element (circular polarized or linear) and interlaced with the X-band tracking antenna. Ranging by the dithered PRF technique requires a maximum pulse rise-time of 10 to 20 nanosec. The corresponding antenna bandwidth requirements are about 50 to 100 Mc or 0.5 to 1 percent at X-band. These bandwidth requirements can be satisfied by both reflector or array type antennas.

(4) The antenna will be exposed to an extreme thermal environment. Antenna thermal sensitivity is therefore considered to be the limiting environmental factor.

(5) To meet the angle and angle rate accuracy requirements, a 2-ft antenna for X-band is assumed for quantitative evaluation purposes. Since search and acquisition is at long ranges (380 nmi), a priori information regarding seeker to target look angles is available; and since the angle rate during angle track is not large (8 deg/sec or less), the antenna mass-angle rate product will be small. Therefore, the utilization of an inertialess, electronic beam steering technique is of questionable advantage unless a savings in weight and power consumption can also be effected.

For example, a 2-foot by 2-foot X-band phased array for beam steering and angle tracking over a 120^{o} pitch by 60^{o} yaw sector would require n elements and n phase shifters, where

$$n = \frac{2\,\text{ft} \times 2\,\text{ft}}{K_{1\lambda} \times K_{2\lambda}} = \frac{20\,\lambda \times 20\,\lambda}{K_1 K_2\,\lambda^2} = \frac{400}{K_1 K_2} = 740$$

K_1, the element spacing in wavelengths in the pitch plane, would be equal to about 0.6 for a ±60-deg scan. K_2, the element spacing in wavelengths in the yaw plane, would equal about 0.9 for a ±30-deg scan. The weight of the usual parallel feed, 0 to 360 deg RF phase shifter would be a minimum of 0.25 lb, thereby resulting in a total weight of 185 lb. This extreme weight, as well as extreme drive complexity, design complexity, and RF phase-shifter thermal control and compensation requirements, negate any further consideration of a high-gain, electronic beam steering array antenna. In contrast, a 5-element, low-gain interferometer can provide inertialess beam steering with a savings in weight and power relative to a gimbaled beam steering antenna. This antenna type will be evaluated in more detail.

3.3.3.2 Antenna Design and Performance Factors

For beacon tracking, the antenna performance factors that directly affect overall sensor performance are gain, error angle slope, and antenna null tracking errors. Antenna null tracking errors are dependent upon the error angle slope, bias effects (such as beacon-to-tracker multipath), and environmental effects (thermal extremes in particular). Antenna gain is dependent upon the aperture dimensions, the side lobe specifications, and the number of design controls available for optimizing aperture distribution for maximum gain with a given side lobe specification. Antenna error angle slope is dependent upon the null tracker type, the antenna beamwidth for an amplitude comparison null tracker, and the effective aperture separation for a phase comparison null tracker.

These interrelating factors are reviewed for each antenna type in the Appendices. The assumed aperture dimensions are either a 2-ft diameter reflector or a 2-ft by 2-ft array aperture. For mathematical convenience, a wavelength $\lambda = 1/10$ ft for a frequency = 9.84 gc will be used. Since the maximum side lobe specification affects gain, beamwidth, error angle slope, and design complexity of any antenna type, the side lobe design objective warrants some discussion. For the beacon-assist lunar landing sensor, the principal purpose of a sidelobe specification is to minimize the probability of false side lobe acquisition or detection thresholding.

It is assumed that a peak detector or some other device will be available to discriminate between the main lobe and the side lobes for the short range, strong signal case if loss of target occurs due to a sudden maneuver or temporary signal drop. For example, the probability of target loss is expected to be greater at the 1000 ft altitude where a large and rapid pitch angle change occurs with one descent trajectory. At this range, also, the available signal above receiver noise is 68 db stronger than the signal above noise at the maximum 380 n.m. range for a landing at the beacon. In this situation, a main lobe or side lobe discriminating device is obviously necessary to ensure a satisfactory reacquisition.

At maximum range, the side lobe only needs to be low enough so it does not appreciably increase the probability of false thresholding if a threshold detector is used. A side lobe level of 20 to 25 db below the main beam should be sufficient for this purpose.

First side-lobe specifications lower than -25 db should be avoided, unless specifically found necessary, because of the difficulty of meeting them. These difficulties arise from feed-support structure obstructions on a feed-reflector antenna, and from feed interaction effects in an amplitude monopulse or sequential lobing reflector (especially in the E plane). The consequences of attaining lower side lobes is error angle slope degradation, especially in a phase monopulse array, a conical scan array, or a sequential lobing array.

3.3.3.3 Antenna Performance Analysis

A detailed discussion and performance analysis of the applicable beacon track antenna types is given in Appendix A. The antenna types evaluated are a motor-driven, feed-reflector conical scan, array cluster electronic conical scan, array cluster electronic sequential lobing, feed-reflector amplitude monopulse, array phase monopulse, and interferometer electronic search and angle track. In support of Appendix A, Appendix B evaluates the phase monopulse array error angle slope-sum beam side lobe tradeoffs. Appendix C evaluates the amplitude monopulse feed-reflector performance limitations on the basis of the orthogonality principle and on the lack of separate sum and difference arm aperture illumination control for circular polarized angle track. Appendix D derives the design equations of a high resolution, wide angle, ambiguity resolving planar interferometer. Appendix G reviews the various error angle slope definitions for the purpose of obtaining a common comparative slope factor, K, for the various antenna types. Appendix H reviews the comparative sensitivities of an X-band and a VHF radar to beacon downlink.

3.3.4 Non-Beacon Assist Lunar Landing Sensor Antennas

3.3.4.1 General Discussion

For a non-beacon-assist lunar landing, the two antenna types required are a single beam antenna for the extended range altimeter and a multiple-beam antenna having three or four beams for the low altitude altimeter velocity sensor. As discussed in Paragraph 3.3.2, the extended

range altimeter beam may be obtained from the beacon tracker beam (sum beam for a monopulse tracker) when a combined mode lunar landing mission is desired. For a single mode lunar landing mission, a low weight single beam parabolic antenna, with or without gimbaling, depending upon the type of lunar approach, would most likely be preferred. The purpose of this section is to evaluate the more complex multibeam antenna for the low altitude altimeter velocity sensor antenna.

The following considerations apply to a comparative evaluation of altimeter velocity sensor antenna types:

(1) Altitude and velocity information is required to touchdown. Near simultaneous, within 20 nanosec for an antenna 10 ft above the landing pads, transmission and reception is therefore necessary. To avoid the complexity, reliability problems, and disadvantages of a very short pulse-rapid TR switching altimeter velocity sensor type, separate transmit and receive antennas are necessary during the near touchdown phase. When separate transmit and receive antennas are used over the full 0 to 5 nmi altitude range, the lowering of isolation switching requirements in the order of 50 to 70 db, depending on the antenna type, provides an added reliability factor to the dithered PRF technique. Also, any CW velocity sensor requires separate transmit and receive antennas at all altitudes for practical, low-noise implementation.

(2) Since the lunar terrain target is essentially of infinite extent, both a high two-way antenna gain and a narrow two-way beamwidth are the most pertinent antenna performance factors. A minimum two-way beamwidth optimizes lunar return coherence, minimizes the doppler spread, and minimizes velocity errors due to terrain bias effects.

(3) To optimize the sensor sensitivity for a given package size, a common aperture would be desired for the three velocity sensor beams and the single altimeter beam. With time sharing, the single altimeter beam may be common with one of the three velocity sensor beams.

(4) As reviewed in Appendix E, beam orientation symmetry with respect to the three velocity vectors results in minimum velocity errors with landing craft pitch and roll. Since the common aperture altimeter beam should be normal, or near normal, during the near touchdown landing phase, a conflict with respect to velocity sensor beam orientation symmetry occurs when the altimeter beam is common and time shared with one of the velocity sensor beams. For this case, a compromise final landing position orientation is discussed in Appendix E.

(5) To meet the velocity sensor accuracy specifications (Table 3-I), the antenna performance requirements would be: 1 mr beam pointing accuracy, -35 to -40 db two-way side lobes and -30 db cross-talk lobes. The side lobe levels of main concern are those normal to the lunar surface where the error doppler return is at an enhanced signal level due to shorter range and increased terrain reflectivity. A two-way level of -35 to -40 db is satisfied by transmit and receive antenna side-lobe levels of -17.5 to -20 db. A -30-db cross-talk lobe is the most difficult lobing specification to satisfy since it is essentially a one-way receiver side-lobe level, i.e., a receiver side lobe from beam 1 in the direction of the maximum of transmitter beam 2.

3.3.4.5 Antenna Design and Performance Factors

A 3- or 4-beam transmitter antenna and a 3- or 4-beam receiver antenna operating at $\lambda = 1/10$ and designed for a 4 sq ft radiating area is assumed for the comparative model. The beam tilt objectives are assumed to be about 20 deg.

A symmetrical multi-pencil beam antenna, whose beam tilt is frequency and temperature insensitive, might be implemented using a dielectric lens, a parabolic or circular curvature reflector, or a resonant array. Although a dielectric lens could be designed for efficient performance at relatively large beam tilts off normal, it is not considered practical for spaceborne applications for a number of reasons. A natural dielectric lens is excessively heavy and its performance stability under spaceborne temperature extremes is questionable. A loading foam dielectric lens is acceptably light in weight but is more lossy; and the same doubt applies to its performance under spaceborne temperature extremes.

In addition, since a loaded foam dielectric, or ceramic, necessarily has a large volume of air cells, a foam lens coating problem is to be anticipated to prevent spaceborne pressure leakage and outgassing with a consequent change of lens performance.

A circular curvature reflector is primarily used for large beam tilts where, to keep the side lobes from becoming excessively high, different sections of the circular surface are used for different beam tilt angles, each section being decreased as beam tilt increases. For the present case where the beams are tilted only 3 to 4 beamwidths, the parabolic surface would be expected to perform as well.

The antenna types to be considered in more detail are then the parabolic reflector and the resonant array.

3.3.4.3 Antenna Performance Analysis

A detailed discussion and performance analysis of applicable types of altimeter velocity sensor antennas is given in Appendix A. The three antenna types evaluated are illustrated in Figure 3-10. For the packaging dimensions shown, the resultant radiating area is approximately 4 sq ft for each antenna type. The packaging area of the multibeam dual reflector is approximately 0.6 sq ft greater than the array packaging area. The packaging depth of the multibeam reflector will be about 2.5 times greater than the 4-beam transmitter multibeam array type. The 2-beam switching array is seen to provide the minimum package depth.

In support of Appendix A, Appendix E discusses the preferred altimeter velocity sensor beam orientations for the LLS mission, and Appendix F provides an analysis of the multibeam array antenna types. Figure F-1 presents the velocity sensor doppler equations in terms of the array beam coordinate system.

3.3.5 Unified Beacon Tracker/Altimeter/Velocity Sensor Antenna

The following considerations apply towards the concept of a combined antenna providing the necessary beaming for beacon angle and range tracking, extended range altimetry, and low-altitude altimetry and velocity sensing.

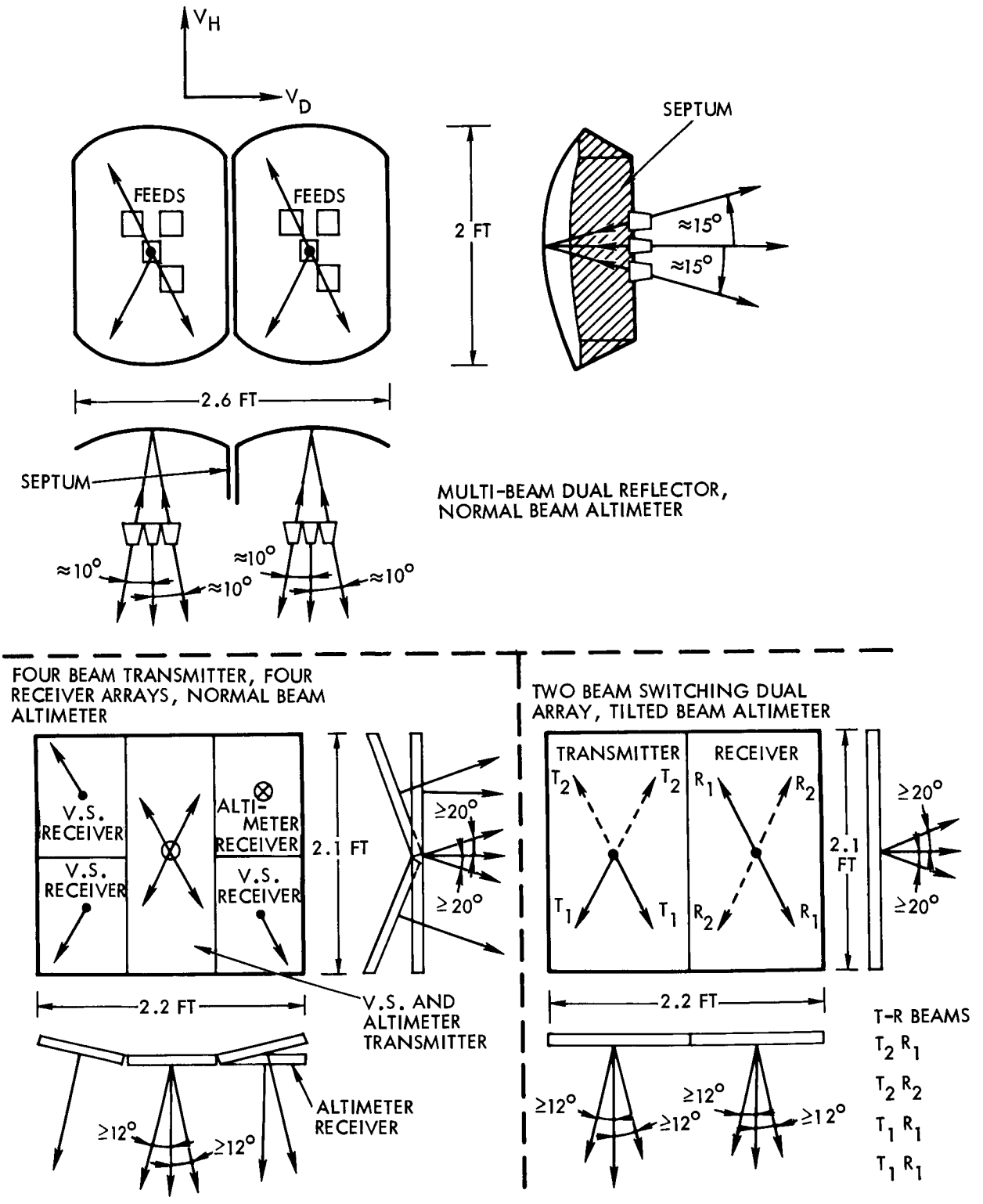

Figure 3-10. Alternate Altimeter/Velocity Sensor Antenna Configurations

(1) Separate transmit and receive antennas are necessary during the near touchdown phase of altitude and velocity sensing. In addition, reliable low-noise operation at all altitudes, from 0 to 5 n.m., favors separate transmit and receive antennas where the dithered PRF or FM-CW altimetry technique is used or where the ICW or CW velocity sensing radar is used.

(2) The multibeam array for velocity sensing is not adaptable to also provide the necessary beaming for angle tracking.

(3) The dual multi-beam reflector antenna type (Figure 3-9) for the altimeter velocity sensor can, conceptually, be modified towards also providing the necessary beaming for beacon angle and range tracking and for extended range altimetry.

Modification of the dual multi-beam reflector of Figure 3-9 might be effected by gimbal mounting for angle tracking, and by splitting the on-axis normal beam horn (altimeter beam horn) into two horns, H_u and H_d. By a suitable arrangement of combining hybrids, an up-down ($H_u - H_d$) amplitude monopulse difference beam and a left-right (reflector 1 - reflector 2) phase monopulse difference beam is formed. The sum beam would be a combination of up-down amplitude addition ($H_u + H_d$) and left-right phase addition (reflector 1 + reflector 2). With the addition of two switches, the low altitude altimeter beam would use the sum of the two horns ($H_u + H_d$) from reflector 1 for transmit and the sum of the two corresponding horns from reflector 2 for receive. With a third switch, the extended range altimeter beam would be made common with the angle-track sum beam.

The consequences of such a combined mode dual reflector antenna system are a gimbal-mounted antenna that is larger, deeper, and heavier than the single reflector or array angle track antenna. In addition, the 3 switch RF package would be appreciably more complex than the array packages for separate antenna systems. Although the radiating area is greater than for the separate angle track antennas, the performances would be comparable or favor the separate antenna case due to the need for compromise of the feed aperture illuminations between the amplitude and phase monopulse beaming.

The advantages are a gimbal-mounted, pitch and roll servo compensated, altimeter/velocity sensor antenna and a common antenna base for packaging the unified ICW radar modules.

Since the qualitative disadvantages presently outweigh the advantages, a quantitative performance evaluation of a unified antenna system has not been made in this study.

3.3.6 Antenna Thermal Analysis

The two types of antennas analyzed thermally were a parabolic dish reflector and a flat array antenna. Both types of antennas normally have associated electronics packages and gimballing motors that dissipate heat during their operating modes. However, the electronics package, assumed located directly on the back of the antenna, would be thermally insulated from the antenna itself. Also, the dish-type antenna normally has a signal generating element at the focal point of its parabolic dish which must be considered because this element and its associated electronics are isolated and therefore more subject to thermal extremes than the dish itself.

The environments that an antenna of the type under consideration may experience are varied, therefore only the environments that produce temperature extremes are considered.

The coldest temperature that an antenna could experience would be during the earth-lunar transit periods when the antenna would be shadowed by its vehicle. The hottest steady-state condition would be with the antenna facing the lunar surface directly and with the sun impinging on the back of it. However, it is possible that the beacon tracking antennas could have the sun impinging on its front side during the approach to the lunar descent area when the antenna would be locked to the beacon located on the lunar surface. If the antenna were to reach its steady-state temperature during this period, it would be 248°F. However, the antenna is not expected to be in this position long enough to reach equilibrium conditons.

The temperatures that the antenna would reach during the aforementioned environments are given in Table 3-III. The temperature extremes of the signal generating focal element were calculated based on a view factor of 0.05 between the focal element and the dish. The focal element temperature extremes are also given in Table 3-III.

To maintain temperatures within reasonable limits, the front face of the antenna, i.e., the one that faces the moon during operation, should be painted with a black paint such as black Cat-a-lac which has an α/ϵ of 1.1, and the back side painted with a silver paint such as "Rinshed-Mason Q36Z803" which has an α/ϵ of 0.94. Because of the uncertainties of the orientation of the antenna to its vehicle and of the vehicle properties, it was assumed that there was no thermal coupling between the antenna and the vehicle. Also, it was assumed that during the earth-lunar transit the vehicle upon which the antenna is mounted would be maneuvered so that the antenna would not be shadowed for any long period of time. If the antenna were to be shadowed for a long period of time, it would require approximately 100 to 150 watts of heater power to maintain the same temperature as obtained during cyclic heating.

Table 3-III. Reflector Temperature Environment

	Array or reflector antenna temperature, ^{o}F	Reflector focal element temperature, ^{o}F
Earth-lunar transit with cyclic heating	-118	-206
Earth-lunar transit with no heating (shadow)	-384	-400
Lunar descent looking at moon	120	18
Lunar descent with sun on the front face	248	50

An alternate method of limiting the temperature extremes would be to paint the exposed surfaces with alternate strips of black and white paint. This would be done to achieve the necessary α/ϵ ratio for sufficient

antenna temperature control. However, this method might introduce undesirable local lateral temperature gradients within the antenna. Because the temperature gradient from one face of the antenna to the other would probably be practically non-existent, the necessary α/ε ratio would probably best be obtained by painting both sides solid colors.

The firing of the lunar descent engine would not be expected to affect the antenna or any of the associated equipment as long as the engine were liquid fueled; however, if the engine were a metallic loaded solid propellant motor, the heating from the solid particle plume would be significant and would have to be accounted for in a more detailed analysis.

The analysis of the different types of antennas considered in this study was of a preliminary nature, however, some conclusion can be drawn concerning the thermal coatings (such as the black and silver combination) that should be used to keep the antenna temperature extremes within reasonable limits.

By comparing the two types of antennas from a thermal standpoint, the dish-type appears to be the least desirable of the two. The focal signal generating unit associated with this type antenna would be exposed to severe thermal environments and would require a considerable amount of thermal control equipment such as heaters, insulation, etc., to maintain the element within a satisfactory temperature range.

3.3.7 Tradeoff Summary

Tables 3-IV, 3-V and 3-VI summarize the comparative performance factors of the beacon tracker and altimeter/velocity sensor antennas. Quantitative evaluation was based on a wavelength $\lambda = 1/10$ ft, an angle tracker reflector diameter of 2 feet or an array dimension of 2 ft by 2 ft, and the altimeter/velocity sensor antenna types illustrated in Figure 3-9. The dimensions shown are the estimated package dimensions to provide equal radiating areas (4 sq ft) for both the multibeam reflector and multibeam array antenna types. Appendices A through G present the design concepts and the analysis details used in arriving at the summary presented in Tables 3-IV, 3-V, and 3-VI. Appendix H reviews the sensitivity factor derivations.

The amplitude monopulse angle tracker was discussed in detail in Appendix A. 4 to clarify the critical factors (satisfaction of the orthogonality principal and the need for separable control of the sum and difference arm illuminations) that need to be considered before a reliable performance estimate could be made. As shown in Table 3-V, an angle track sensitivity loss of 2. 9 db, due to state of the art design limitations, was estimated when circular polarized angle tracking is specified. In view of this sensitivity loss, it would appear desirable to consider application of a more reliable linearly polarized amplitude monopulse reflector or phase monopulse array with a CP beacon transponder. The 3-db signal loss incurred with linear reception of a CP signal is compensated for by the increased sensitivity of these linearly polarized angle trackers.

Although the electronic search and angle track interferometer discussed in Appendix A. 6 has a respectable angle track sensitivity because of its high-error angle slope, it is still far removed from being applicable because the gain is much too low for ranging signal requirements. An increase in beacon gain and/or transmitted power in the order of 25 db would be necessary. However, the inertialess, low-weight interferometer does show promise for short range applications. On the basis of the performance data in Table 3-IV and 3-V, the phase monopulse array or the amplitude monopulse reflector (linear or CP) is the best choice for the LLS mission beacon tracker.

The altimeter/velocity sensor summary in Table 3-VI shows the multi-beam dual reflector to provide greater sensitivity at the expense of a much more bulky package and potential temperature instability unless weighty feed support structures are used. Where the cross talk lobe specification must be lower than 25 db, the four-beam transmit array with four separate single beam receive arrays would be favored. When minimum bias errors and maximum heading velocity accuracy is desired, either of the array types would be preferable. The switching array, although the least sensitive (for the case of a maximum 6 db time sharing loss), possesses the advantages of minimum heading velocity beam width and a single receiver arm. The compact packaging and the consequent natural temperature stability of the array antenna types would favor their application in the LLS mission.

The use of a VHF rather than an X-band, radar-to-beacon down-link provides an increased sensitivity at the expense of an increased likelihood of multipath down-link ranging errors due to the wider transmission beamwidth. However, the greater VHF sensitivity of from 19 to 34 db can be traded off for a directive beacon receiver antenna to decrease these multi-path effects. Appendix H presents a review of the comparative VHF and X-band down-link sensitivites.

Table 3-IV. Beacon Tracker Antenna Qualitative Comparison

	Packaging	Temperature Sensitivity	Performance Advantages and Disadvantages
Motor driven feed-reflector conical scan	Deep, awkward VHF element design and packaging.	Motor thermal cooling problem, requires extra structure for temperature stability.	Adaptable to CP; comparatively low angle track sensitivity.
Array cluster electronic conical scan	Compact rigid, shallow package. Non-obstructing VHF slot elements.	RF phase shifters require thermal control.	Not adaptable to CP, low sensitivity, complex phase control.
Array cluster electronic sequential lobing	Compact rigid, shallow package. Non-obstructing VHF slot elements.	RF phase shifters require thermal control.	Not adaptable to CP, lowest sensitivity, simple phase control.
Feed-reflector amplitude monopulse	Deepest package, awkward VHF element design and packaging.	Requires extra structural support for temperature stability.	Adaptable to CP, side lobe problem, highest sensivity for linear polarization.
Array phase monopulse	Compact rigid, shallow package, non-obstructing VHF slot elements.	Temperature stable package.	Not adaptable to CP, must tradeoff sensitivity for low side lobes.
Interferometer electronic search and angle track	Compact rigid and shallow package, minimum weight and power due to absence of gimbal assembly.	Needs special baseline material to minimize errors due to thermal expansions.	Adaptable to CP, lowest gain, highest error angle slope.

Table 3-V. Beacon Tracker Antenna Quantitative Comparison

	Gain		Maximum Side Lobe	Servo Loop Error Angle Slope, K, mv/mr per V	RF Systematic Error Sensitivity (per mr Error Angle)	Angle Track Sensitivity $S = K\sqrt{G}$
	Search	Track				
Feed-Reflector Conical Scan	33 db	30 db	-20 to -25 db	22.15	0.4 db	S_o - 6.3 db
Array Cluster Conical Scan	34.5*	31.7*	-20 to -25 db	22.15	0.4 db (or 2.7° phase error)	S_o - 4.6 db
Array Cluster Sequential Lobing	34.5*	31.7*	-20 to -25 db	14.1	0.4 db (or 2.7° phase error)	S_o - 8.5 db
Feed Reflector Amplitude Monopluse, CP:	33	33	-20 db	23.04	0.8 db	S_o - 2.9 db
Linear:	33	33	-20 db	32.2	0.5 db	S_o (Reference)
Array Phase Monopulse	35	35	-20 to -23 db	22.84	2.63°	S_o - 1 db
Interferometer Electronic Search and Angle Track ($\theta = \pm 60^\circ$ in El and $\pm 30^\circ$ in A_z)	3 to 8 db over θ		used for ambiguity resolution	125.7 cos θ (mr/mr)	7.2° cos θ	Max: S_o -13.2 db Min: S_o -18.2 db

* Includes 0.5 db phase shifter insertion loss

Table 3-VI. Altimeter/Velocity Sensor Antenna Comparison***

	Multi-beam Dual Reflector	Multi-beam Transmit Array, Single Beam Receivers	Two-Beam Dual Switching Array
Packaging	Awkward, deep, heavy due to feed support structure	Compact, shallow, rigid, needs minimum support structure	Compact, shallow, rigid, needs minimum structure
Temperature Stability	Support structure design critical to avoid angle errors	Naturally temperature stable package	Naturally temperature stable package
Two-Way Gain			
Velocity Sensor	58.8 db	56.7 db	56.8 db*
Altimeter	61 db	55.4 db	56.8 db*
Two-Way Beamwidth			
Velocity Sensor			
Lateral, B_l	4.5°	6.65°	4.66°
Fore-aft, B_f	3°	2.73°	2.33°
Altimeter			
Lateral, B_l	4.5°	6.36°	4.66°
Fore-aft, B_f	2.6°	2.69°	2.33°
Maximum Two-Way Side Lobe			
Velocity Sensor	-35 to -36 db	-35 to -40 db	-35 to -40 db
Altimeter	-40 db	-40 db	-35 to -40 db
Cross Talk Lobe	-25 db	-30 db	-25 db
Echo Power Sensitivity, S_E			
Velocity Sensor	+35 db	+34.1 db	+32 db*
Altimeter	+36.5 db	+32.3 db	+32 db*
$(S_E = G_T G_R B_l B_f)$			
Signal to Noise Sensitivity, S_N			
Velocity Sensor	+47.7 db	+47.3 db	+45.9 db*
Altimeter	+49.9 db	+47.1 db	+45.9 db*
$(S_N = G_T G_R B_l^{**})$			

*For the effective gain case assuming a 6 db time share loss
**For the case of receiver bandwidth matched to the doppler spread.
***See Table 8-I, Appendix I, for more detailed qualitative comparisons

4. INVESTIGATION OF MODULATED VARACTOR POWER SOURCES

4.1 INTRODUCTION

The capability of switching varactor multipliers is very important to the dithered PRF modulation ranging technique, as indeed it is for other techniques utilizing either ICW or pulse modulation. Varactor switching permits isolations of greater than 120 db to be attained with virtually no penalty in either "on-time power loss," or increased modulation drive requirements. Normally, the modulation drive requirements are less than those required for an RF-diode switch providing 20 db or so isolation.

Because of the promise shown by varactor multiplier switching, an investigation of the techniques involved has been a study objective of the Lunar Landing Sensor Performance Study, NAS 8-5205. A report on the initial results of this study is included in the "Study of Lunar Landing Sensor Performance Interim Report No. 3," dated 31 July 1964, prepared under this same contract. The concluding results are presented in this section.

The varactor multiplier switching tests are described in the order in which they are performed, i.e., the tests performed on the bench are discussed first, and those performed with the feasibility model of the altimeter system are discussed subsequently. The description of the bench tests includes general data regarding multiplier switching that might be of interest for a system other than a radar or altimeter employing dithered PRF modulation. The data include insertion loss vs bias level, and wave shapes of the modulating waves and of the modulated RF-signal envelope. These latter data define rise times, storage times, delay times, and fall times to be expected under different conditions.

The tests performed with the test varactor multipliers installed in the altimeter indicated that the altimeter could satisfactorily operate over altitudes of from 100 nmi to 62 ft, corresponding to a change in PRF of 400 cps to 4 Mc. The tests also permitted further evaluation of the switching capabilities of varactors, both regarding dc, or static switching, and modulated, or dynamic switching. This latter measurement is

normally difficult to make because it entails measuring the "On" to "Off" ratio of a square wave modulated X-band signal, to a value of 100 db or more.

4.2 BENCH TESTS

Although the primary purpose of the bench tests was to appropriately adjust and/or modify the test varactor multipliers for switching, much interesting data was assembled. Tests performed on the bench included measurements of "On/Off" ratios, turn-on time, turn-off time, delay time, and storage time. The tests were performed on each of two varactor multiplier chains: a low power times-16, X-band unit capable of providing 100 mw; and a high power times-4, X-band unit capable of providing 1 watt. Both of the multipliers are similar to ones delivered to MSFC under this contract in the past.

A block diagram of a typical test setup used is shown in Figure 4-1. DC "On/Off" ratios were measured by using one of two versions of the "substitution technique." A reference reading would be taken on an Empire Devices Noise and Field Intensity Meter, NF105, then the signal removed, and a second signal from an HP620A Signal Generator applied in its place and adjusted to reattain the reference. The CW power level could then be determined directly from the signal generator. A separate receiver was used to heterodyne the signal down to a frequency compatible with the NF105 in the cases where the multiplier output signal frequency was too high. After the "On" power and "Off" leakage were each measured in this manner, the "On" to "Off" ratio was calculated.

In the second version of the "substitution technique," a reference would be set at the "leakage power" level, the power increased to its maximum value, and attenuation inserted to return the receiver indicator to the reference position. The ratio between power levels would then equal the attenuator readings. For very large dynamic ranges, the two techniques could be used together in a cascaded fashion. Though not highly accurate, they provide the requisite accuracies required for the tests.

It should be noted that for many of the isolation measurements, instrumentation sensitivities appeared to be the limiting factor rather than the varactor multiplier performance. This was indicated by the fact that

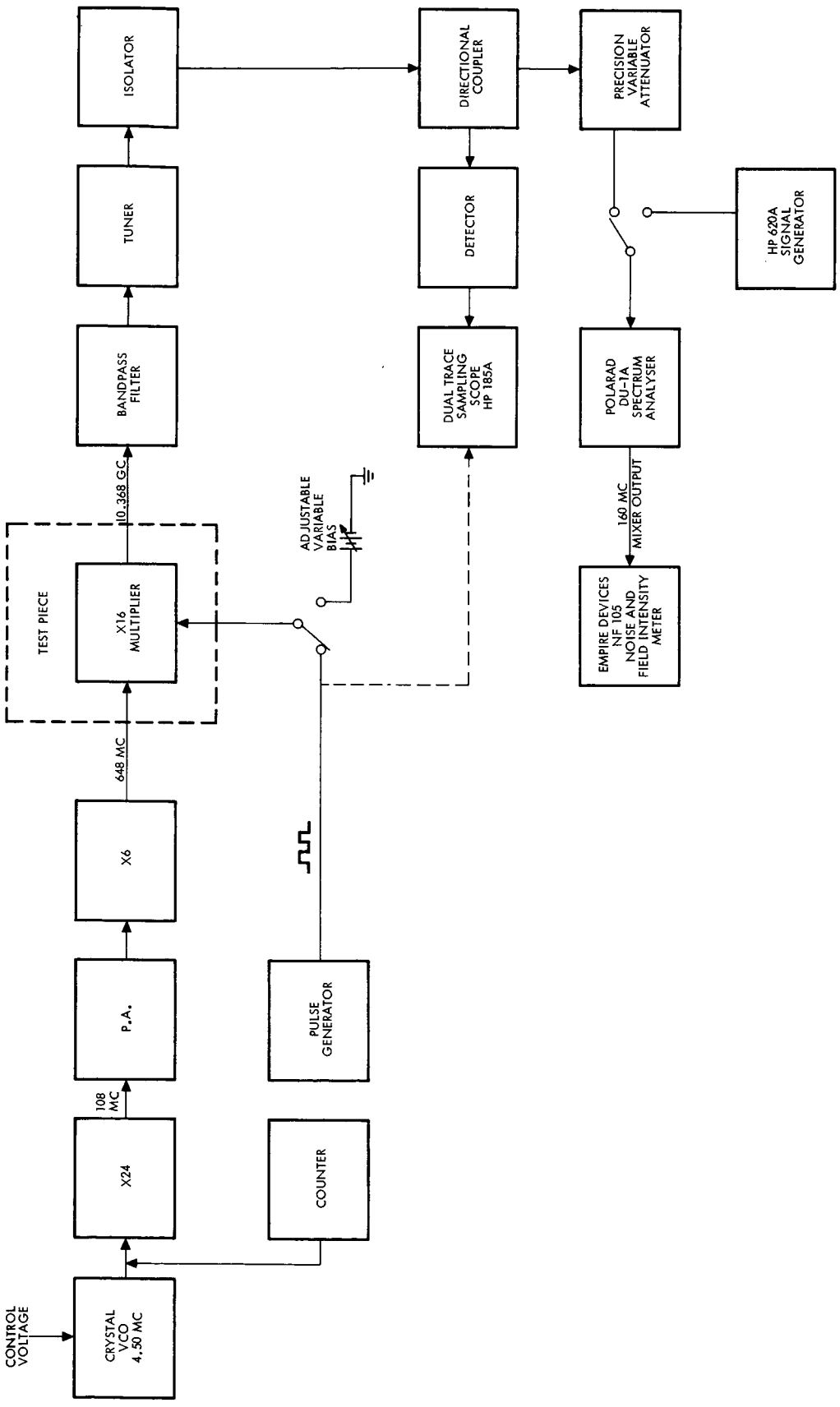

Figure 4-1. Times-16 Multiplier Isolation and Switching Test Instrumentation Block Diagram

sensitivities were encountered well before the maximum rated forward varactor current was drawn. Normally, varactors turn off harder as their forward current is increased.

4.2.1 Times-16 100-mw Multiplier Chain

The 100-mw all solid-state multiplier chain tested is identical to the extended-range altimeter transmitter chain. It consists of a crystal-controlled VCO driving a times-24 transistor multiplier, a times-6 multiplier, and a times-16 (four doubler) multiplier chain. External bias was provided to each varactor of the times-16 multiplier, thus making it possible to square wave modulate each doubler, either singly or together. A variable frequency pulse generator, Rutherford Model B-16, was used to provide the square wave modulation signal. A detector and a dual trace sampling oscilloscope permitted simultaneous monitoring of the varactor gate and detected X-band modulation envelope. As a result, rise times, fall times, and delay and storage times could be satisfactorily measured.

Data taken while gating the first doubler of the times-16 multiplier is shown in Table 4-I. For interest, isolation measurements were first taken at the output of the doubler being gated, then successive doublers added and their isolation measurements taken. It should be noted that the descriptor, "first doubler", refers to the 650 to 1300 Mc doubler, the "second doubler" refers to the 1300 to 2600 Mc doubler, etc.

Table 4-I. Static "On/Off" Power Ratios with the First Doubler Gated

Final Doubler Stage	Output Frequency (gc)	"On/Off" Ratio (db)
First doubler	1.3	70
Second doubler	2.6	≥ 101
Third doubler	5.2	53
Fourth doubler	10.4	$\geq$ 99

The results of this test do not appear entirely logical in that, upon addition of the third doubler, the isolation decreases — a phenomenon probably resulting from some sort of resonance. The addition of the second and fourth doubler does, however, cause the isolation to increase as would be expected. The varactor was only partially forward biased. It could have been driven harder, but the minimum sensitivity point of the test equipment had been reached; thus, no further indication of improvement could be obtained.

The dc switching, or gating, characteristics of the solid-state transmitters are shown in Figure 4-2. For this test, the transmitter was completely assembled as shown in the block diagram of Figure 4-1. Three different biases throughout the multiplier chain were then adjusted in turn to effect the gating action at X-band.

The curve reference, "X-6, 108 Mc," means that the bias of the tripler section in the times-6 multiplier, with an input frequency of 108 Mc, was controlled to achieve the gating curve shown. Likewise, "X-6, 324 Mc" refers to the frequency doubler section of the times-6 multiplier, having an input frequency of 324 Mc, and "X-16, 648 Mc" refers to the first doubler section, with an input frequency of 648 Mc, of the times-16 multiplier.

It is apparent from these curves that the best RF-switching characteristics are obtained by switching lower-frequency stages. Though this characteristic could certainly be utilized to advantage where fairly slow switching times are required, it is to be shown that turn-on times, delay times, etc., degrade appreciably when the lower stages are switched. As was noted before the test, instrumentation limits the detection of powers of less than about -100 dbm, so that the ultimate isolation cannot be determined.

The switching characteristics of the X-band transmitter chain are shown in Figures 4-3 through 4-6 and the pertinent switching parameters are summarized in Tables 4-II and 4-III. The pictures and tables permit comparisons to be made regarding the X-band modulation envelope characteristics when the switching modulation is applied at different points within the chain. The data also shows the results of increasing the modulation frequency from 10 kc to 1 Mc, when the modulation signal is applied to the 648- to 1296-Mc frequency doubler.

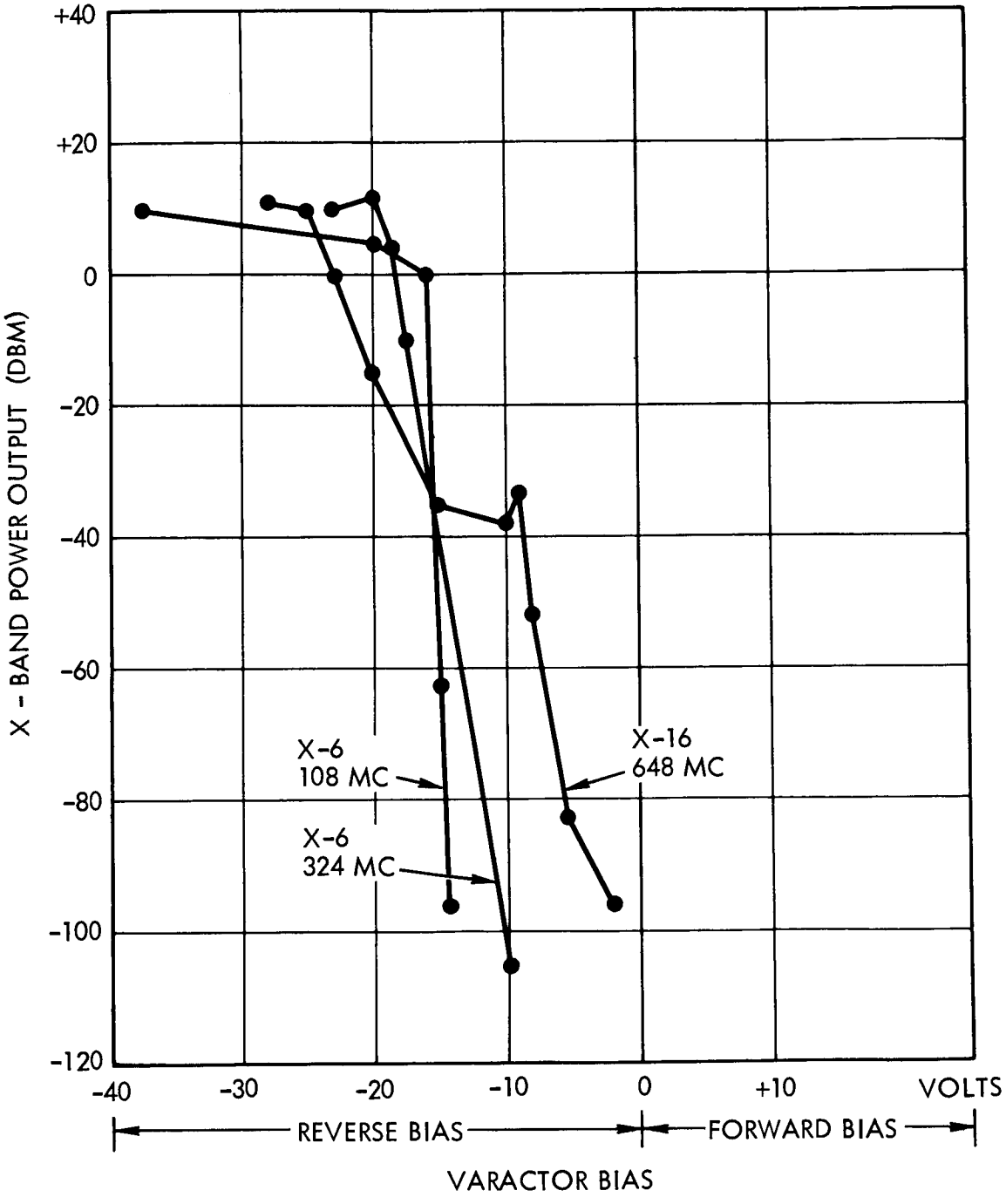

Figure 4-2. Transmitter Chain Switching Characteristics

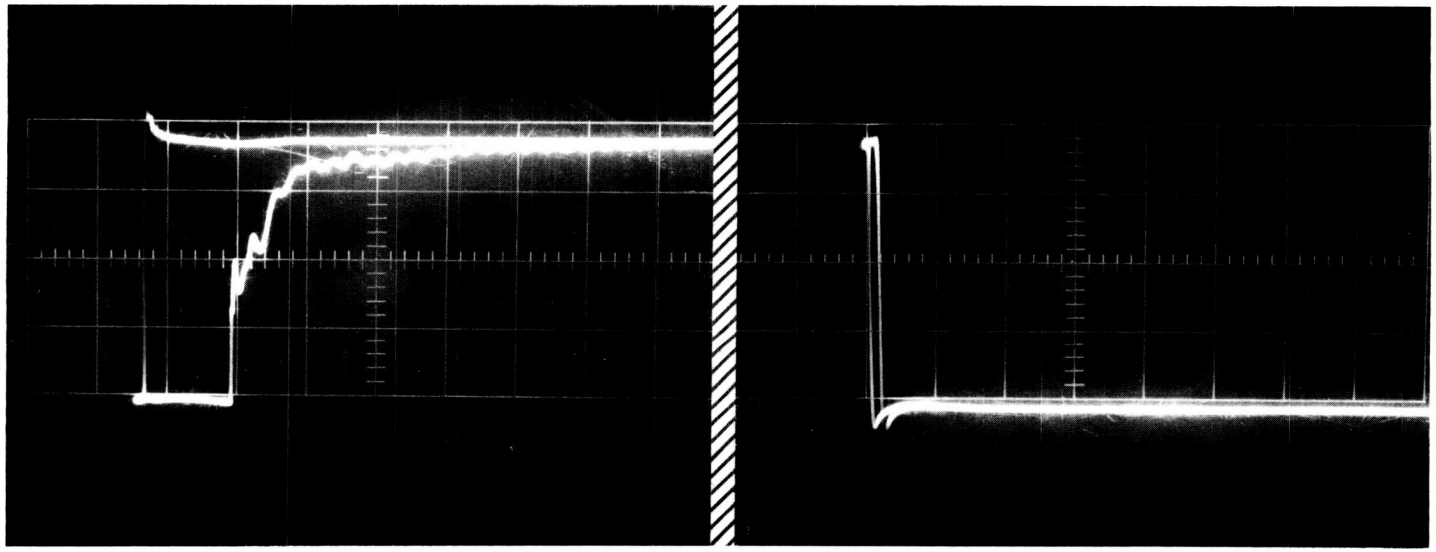

Horizontal Scan Rate = 1000 nsec/cm

PRF = 10 Kc

Figure 4-3a. X-Band Modulation Envelope (Modulation Applied at the 108-Mc Power Amplifier)

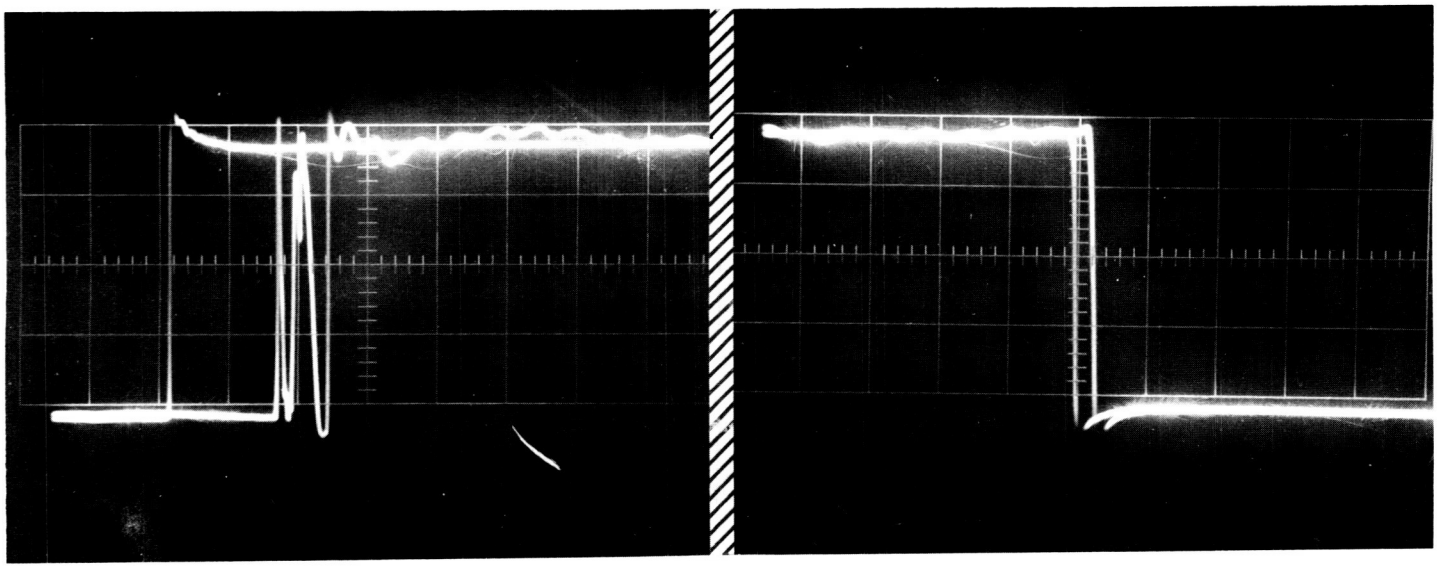

Horizontal Scan Rate = 500 nsec/cm

PRF = 100 Kc

Figure 4-3b. X-Band Modulation Envelope (Modulation Applied at the 108-Mc Power Amplifier)

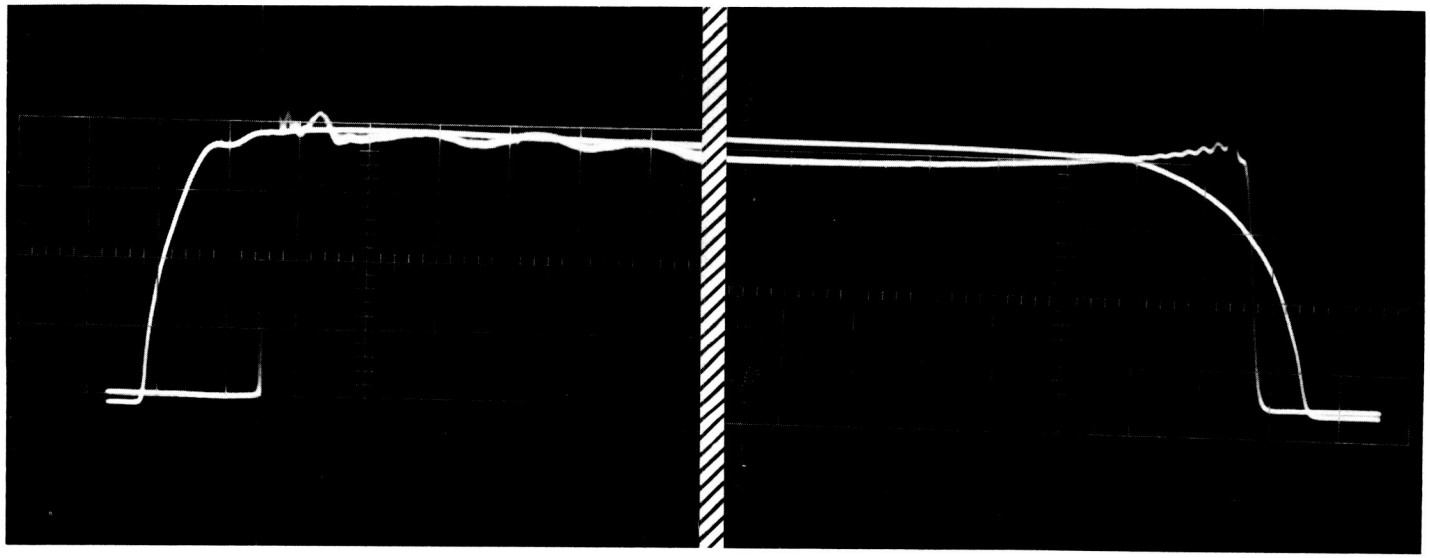

Horizontal Scan Rate = 200 nsec/cm

PRF = 10 kc

Figure 4-4. X-Band Modulation Envelope (Modulation Applied to the 108- to 324-Mc Tripler)

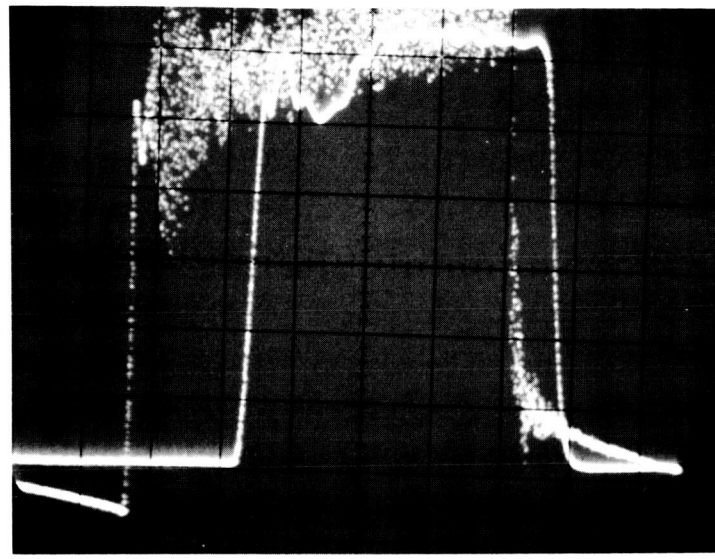

Horizontal Scan Rate = 100 nsec/cm

PRF = 1 Mc

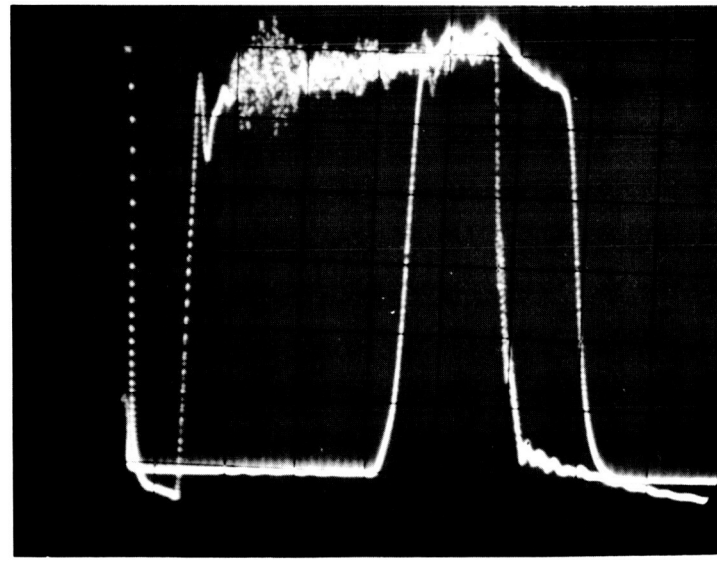

Horizontal Scan Rate = 50 nsec/cm

PRF = 2.5 Mc

Figure 4-5. X-Band Modulation Envelope (Modulation Applied at the 324- to 648-Mc Doubler)

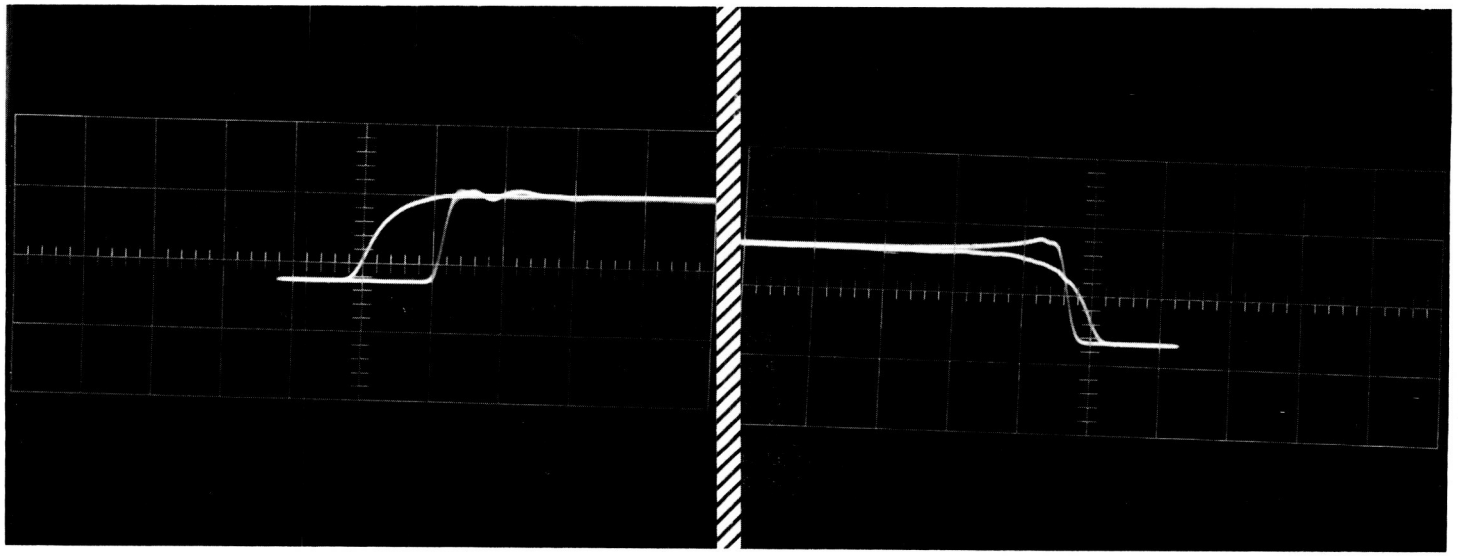

Horizontal Scan Speed = 100 nsec/cm

PRF = 10 kc

Figure 4-6a. X-Band Modulation Envelope (Modulation Applied at the 648- to 1296-Mc Doubler)

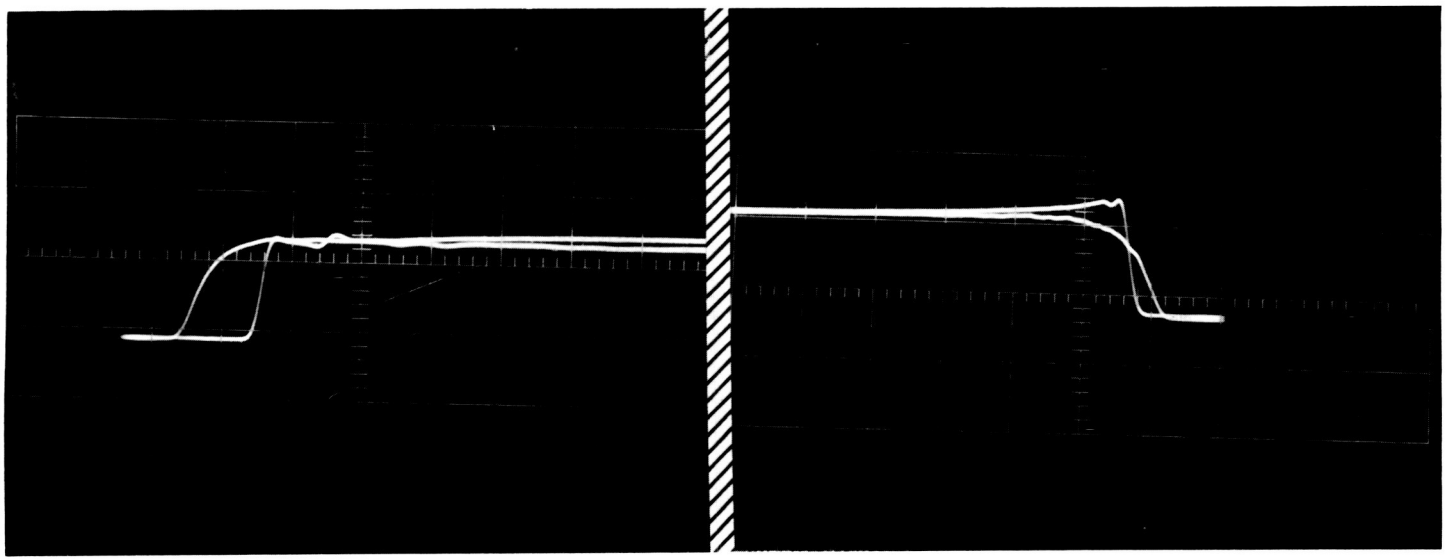

Horizontal Scan Speed = 100 nsec/cm

PRF = 100 kc

Figure 4-6b. X-Band Modulation Envelope (Modulation Applied at the 648- to 1296-Mc Doubler)

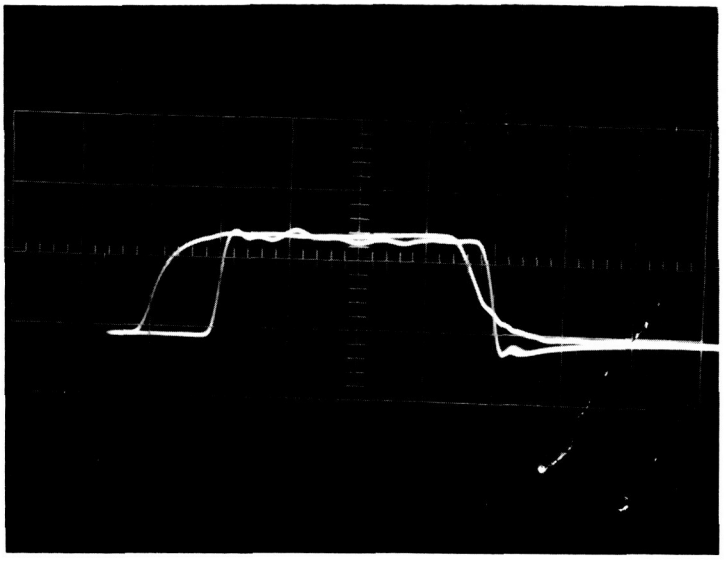

Horizontal Scan Speed = 100 nsec/cm

PRF = 1 Mc

Figure 4-6c. X-Band Modulation Envelope (Modulation Applied at the 648- to 1296-mc Doubler)

Each of the photographs in Figures 4-3 through 4-6 contain the modulating signal waveshape and the detected RF modulation envelope waveshape. Each of the waveshape pairs have the proper time relationship, so to distinguish between any two waveshapes, one must realize that the modulation turns on first.

The rapid "On/Off" fluctuations of the modulation envelope in Figure 4-3b probably results from normal pulse ringing amplified by the nonlinear properties of the successive varactors. In this case, the modulation signal is being applied to a transistor stage which obviously rings appreciably. Figure 4-3a displays the same ringing, but here it is not as pronounced.

By referring to Table 4-II, it is apparent that the time delay between turn-on of the RF signal is appreciably higher when the modulation is applied nearer the beginning of the multiplier chain, i.e., at the lower frequencies. This characteristic has been apparent in all tests performed,

Table 4-II. Summary of 10-kc Modulation Characteristics with Bias Applied at Different Points

	108 Mc Power Amplifier (nsec)	108-324 Mc Tripler (nsec)	324-648 Mc Doubler (nsec)	648-1296 Mc Doubler (nsec)
T_{pulse} ON	16	150	20	120
T_{env} ON	1200	12	30	24
T_{pulse} OFF	24	200	80	120
T_{env} OFF	24	24	28	24
Td	1300	300	180	100
Ts	136	40	60	5

Table 4-III. Summary of Modulation Characteristics at Different Modulation Frequencies (Modulation Applied to the 648- to 1296-Mc Doubler)

PRF	10 kc (nsec)	100 kc (nsec)	1 Mc (nsec)
T_{pulse} ON	120	120	100
T_{env} ON	24	26	24
T_{pulse} OFF	120	120	120
T_{env} OFF	24	20	20
Td	100	90	90
Ts	5	20	20

and presents an obvious limitation with regard to applying high modulation frequencies at the lower frequency stages for the purpose of obtaining optimum "On/Off" ratios. As a result of this series of tests, only the high frequency multiplier stages are modulated during their operation in the extended range altimeter.

Table 4-II also shows that the RF envelope rise times are nearly the same, regardless of where the modulation signal is applied, and regardless of the turn-on time of the driving wave. It appears that this characteristic results from the fact that the nonlinear property of the varactors tend to reshape the pulse, i.e., successive multiplier stages tend not to turn on until the RF drive is very near a precise level. This would explain the lack of sensitivity to slow rise time driving pulses, and also explain why the pulse shape would not be degraded by transmission through a series of, effectively, synchronously tuned high-Q circuits. In effect, then, the varactors would tend to decrease the modulated signal turn-on at the expense of pulse delay time. This might prove to be a very useful technique for waveshaping.

4.2.2 High-Power S- to X-band Frequency Multiplier Tests

Essentially the same series of bench tests were performed on the transmitter chain. These included static, or dc, "On/Off" isolation tests, and tests of any degradation of the modulation signal waveshape. All of the test results were very encouraging.

The S- to X-band frequency multiplier consists of two doublers that are identical to the final two doublers in the 1-watt, X-band, solid-state signal source. During the tests, they were driven by an Alfred Model 5-6868 TWT amplifier and at a power level of 2.6 watts, giving a CW output of about 0.5 watt. The TWT amplifier was driven by an HP616A signal generator.

Bias connectors were added to each frequency doubler so that different biasing arrangements could be evaluated. It should be noted that, with some additional refinement of the bias connections, the CW-output power could be readily increased to 1 watt; this was not done for economy reasons.

Figures 4-7, 4-8, and 4-9 show the dc-switching characteristics of the 2.6- to 5.2-gc frequency doubler, the 5.2- to 10.4-gc frequency doubler, and the two doublers operating together. It is apparent from the curves that only moderate isolation can be obtained by modulating the final doubler in a chain, whether it be the S to C, or the C to X-band unit. Very good "On/Off" isolation, however, can be obtained by modulating the next-to-last doubler stage, most probably better than could be measured with the bench-test setup. From the curves, it is interesting to note that the bias level for maximum power output is relatively noncritical for all of the operating arrangements. Strong RF turn-off does not occur until the bias, normally at -10 v or so, approaches zero.

Table 4-IV summarizes the characteristics of the RF-modulation envelope as a function of modulation frequency. The multiplier arrangement to provide this data is the same as shown in Figure 4-10. It is apparent that the delay times are low, as would be expected when modulating a stage at the output of a multiplier chain. The rise times of the RF-modulation envelope track the rise times of the modulation waveforms fairly well at modulating frequencies of 10 and 100 kc; however, there is a degradation of 18 nanosec at 1 Mc.

The data in Table 4-V is very interesting in that it shows the effect that detuning the multipliers has upon the modulation properties of the chain. Modulation waveform data was taken with the RF carrier at its nominal value and at values above and below nominal, at which the output power dropped 3 db. Essentially, no change in the modulation properties occurred when the frequency was shifted.

4.3 SYSTEMS TESTS

4.3.1 Static Tests

A static test was performed with switchable multiplier chains installed in the extended range altimeter and functioning as transmitter and local oscillator. By the term "static test" is meant a test to determine the "On" to "Off" ratio of each multiplier chain (in this case, when it is installed in the extended range altimeter).

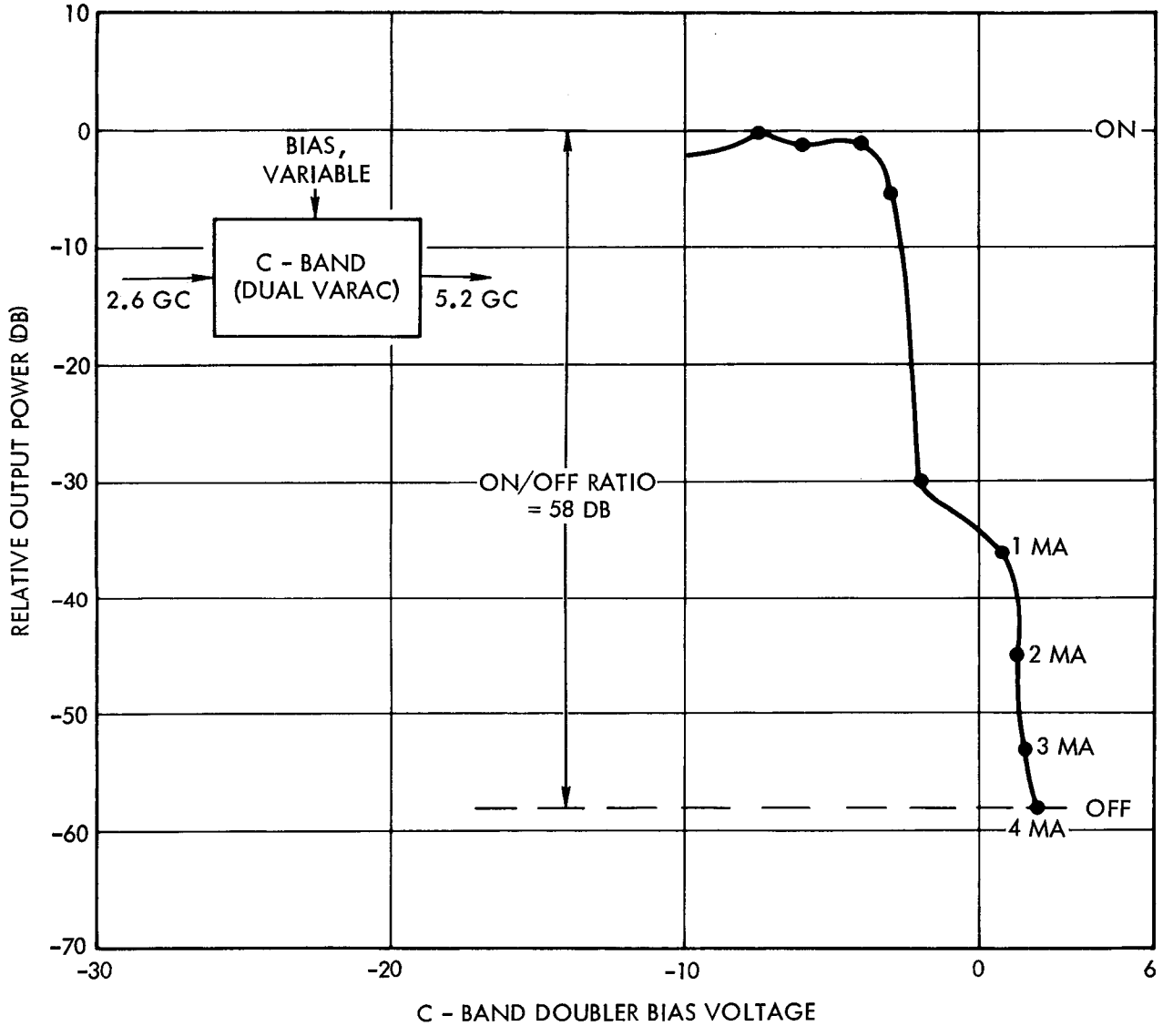

Figure 4-7. Dual Varactor C-Band Doubler Relative Output Power versus Varactor Bias

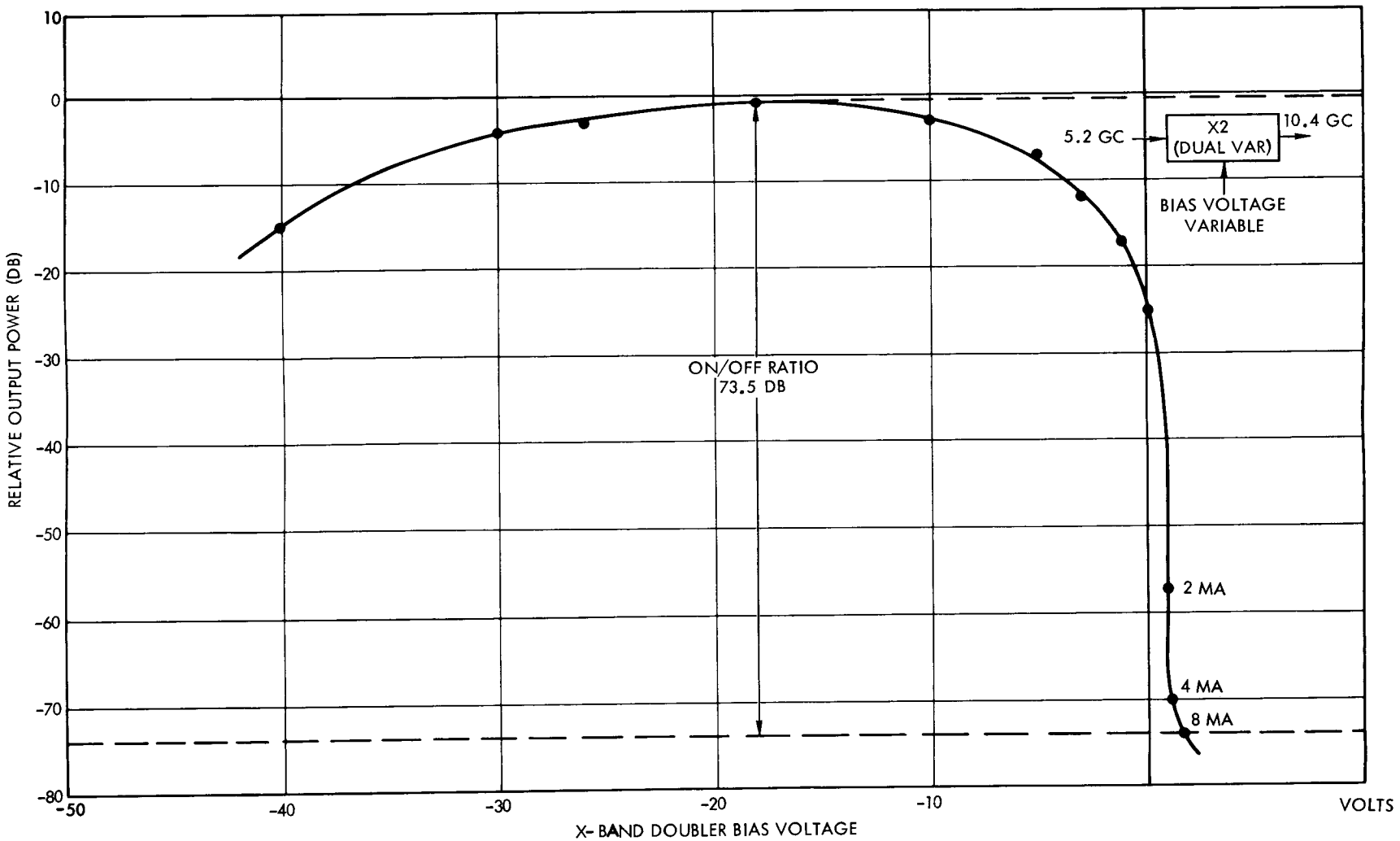

Figure 4-8. Dual Varactor X-Band Doubler Relative Output Power versus Varactor Bias

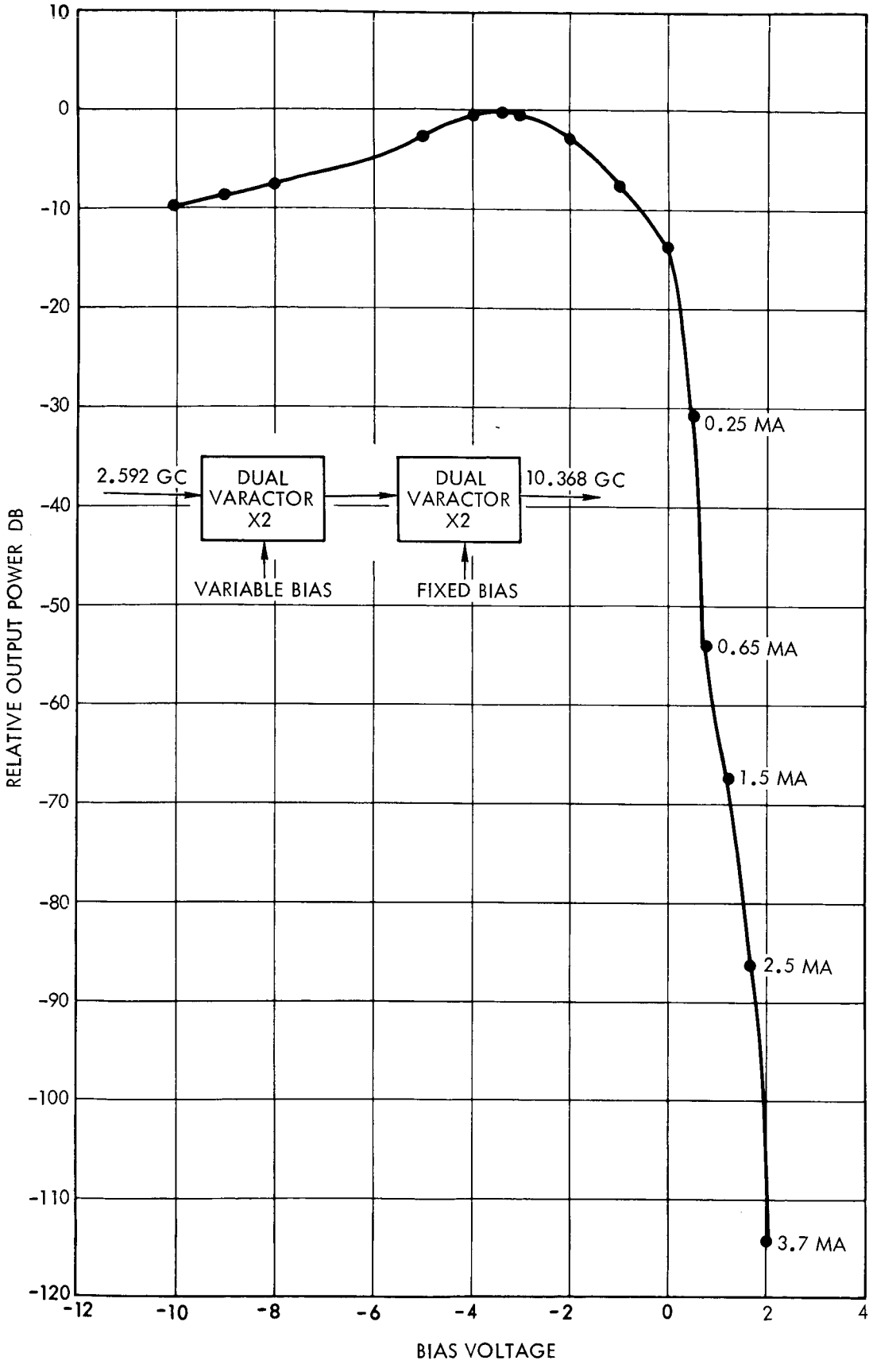

Figure 4-9. Dual Varactor X-Band Quadrupler Relative Output Power versus Varactor Bias

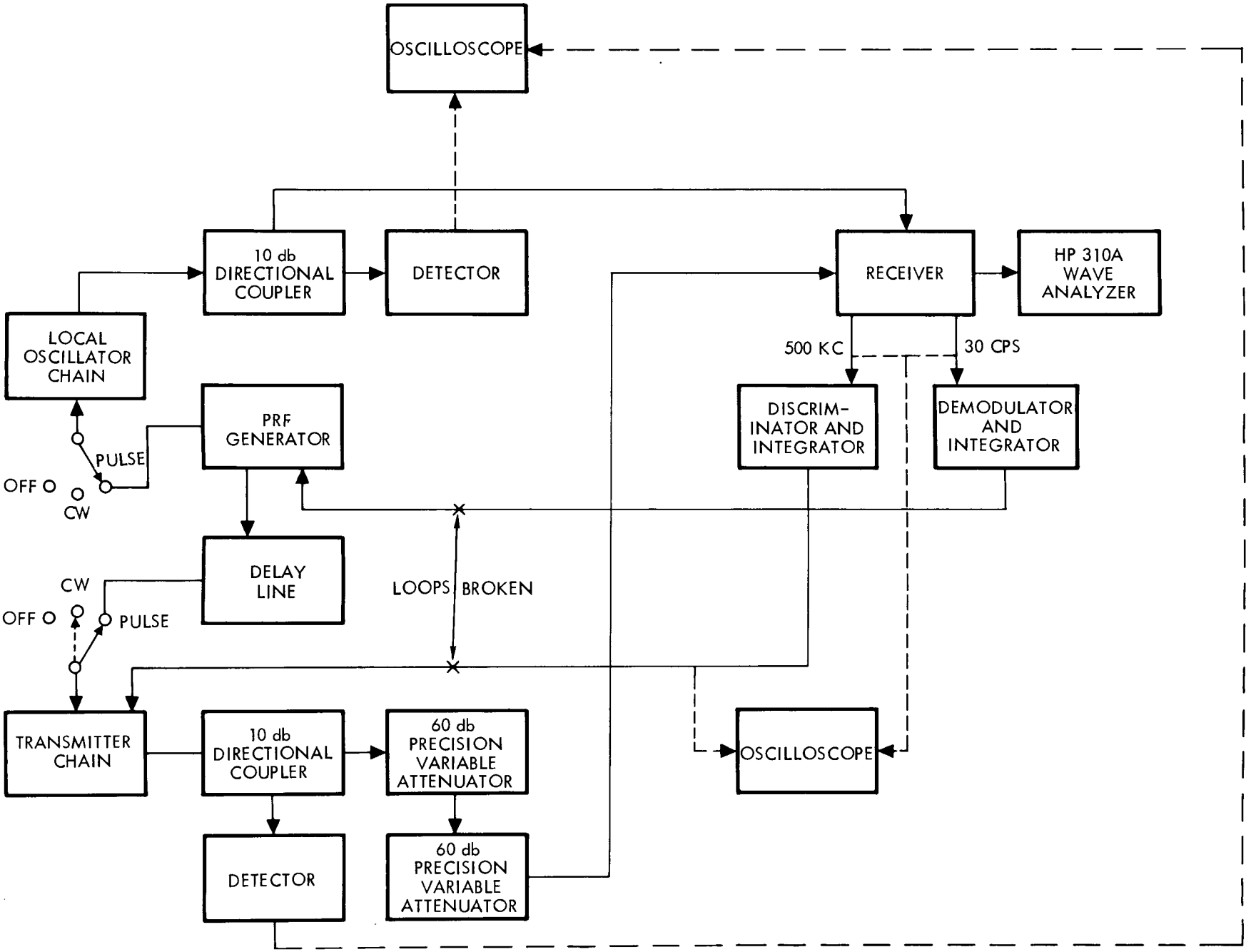

Figure 4-10. Dynamic Isolation Measurement Test Setup

Table 4-IV. C- and X-Band Dual Varactor Multiplier Switching Characteristics Versus Modulation Frequency

PRF	10 kc (nsec)	100 kc (nsec)	1 Mc (nsec)
T_{pulse} ON	7	28	30
T_{env} ON	8	34	48
T_{pulse} OFF	4	32	34
T_{env} OFF	7	38	44
T_d	10	1	6
T_s	10	1	4

Table 4-V. C- and X-Band Dual Varactor Multiplier Switching Characteristics Versus Carrier Frequency

	f_{Lo} (-3 db) (nsec)	f_o (nsec)	f_{Hi} (-3 db) (nsec)
T_{pulse} ON	11	10	9
T_{env} ON	8	10	11
T_{pulse} OFF	11	11	11
T_{env} OFF	8	12	7
T_d	7	10	14
T_s	12	10	10

Multiplier chains incorporating quad-doubler times-16 X-band multipliers were used as both the transmitter and local oscillator during the static and dynamic tests. In the past, a low-power times-16 X-band multiplier, utilizing dual-quadruplers, had been used. However, the switching characteristics of this unit had been proven inferior to the stacked doubler unit, so it was abandoned rather than improved.

Gating was attained by controlling the bias of the first doubler of the times-16 multiplier of each chain. Both transmitter and local oscillator chains could be made to operate CW or pulse, or they could be turned "Off." In this test, the transmitter was connected directly to the receiver through a precision variable attenuator. To measure the static isolation, the local oscillator was operated in the CW mode. The transmitter was gated "Off" by applying forward bias on the varactor, and a reference at the wave analyzer set. Next, the transmitter was gated "On" by applying the correct reverse bias to the varactor. The variable attenuator was then adjusted to give the same reference at the wave analyzer. The difference in attenuator readings was 144 db, the measure of receiver-transmitter isolation to be expected when the receiver and transmitter are operated in a time-sharing ICW mode as they would be during normal operation.

The detector used to indicate a reference point during all system isolation measurements was an HP 310A wave analyzer connected to the output of the 500-Kc IF amplifier. A minimum noise bandwidth of 200 cps was selected for all measurements to maximize the sensitivity of the isolation measurements. Using a more narrow noise bandwidth would have made the measurements very critical, since the IF signal would have been difficult to maintain within this bandwidth.

The isolation was obtained with a varactor forward bias current of 0.5 ma. Greater isolation could probably have been obtained if the varactor had been driven further into its forward bias region. Even so, the system isolation obtained is appreciably greater than the isolation obtained during the bench tests. This is accredited to the higher system sensitivity of the extended-range altimeter. The system receiver noise figure is

still thought to be the limiting factor in measuring still higher isolations. It was checked and found to be excessively high, and attributed to the high noise figure, ≈ 20 db, of the receiver orthomode mixer. About 10 db more isolation, ≈ 154 db, probably could be obtained if the receiver noise figure were improved by 10 db.

4.3.2 Dynamic Test

Dynamic isolation is defined as the isolation actually achievable under operating conditions, that is, with the transmitter and receiver pulsed alternately "On" and "Off." Ideally, the dynamic isolation should equal the static isolation discussed in the preceding section, if turn-on and turn-off times are sufficiently rapid, and if sidebands produced during gating do not intermix to produce a frequency falling within the IF band. As may be seen later, both of these events occur in varying degrees.

Dynamic isolation was measured earlier for a PRF varying from 300 cps to 40 kc, and reported in the Third Interim Report of the Lunar Landing Sensor Performance Study. The PRF range was subsequently extended to the Mc region by the development of a new wideband PRF generator. The dynamic isolation measurements reported on in this section are for the original PRF's, as well as for the extended range of PRF's.

The PRF generator incorporates a continually varying voltage-controlled oscillator which is used to drive a series of divide-by-two networks. The output from the divider networks is split, and one of the two signals inverted. Delay, or dead time, is next added so that a delay is incurred subsequent to the turn-off of a pulse at one output, and before the turn-on of a pulse at the second output. Finally, each of the outputs is matched to the impedance presented by the switched varactor. In operation, the oscillator is swept back and forth over a two-to-one frequency range (slowly in one direction and very fast in the other) and doublers are automatically switched in or out of the circuit to provide the frequency desired.

The operation of the wideband PRF generator was refined enough so that satisfactory results for the dynamic isolation tests could be obtained; however, the matching has not yet been perfected sufficiently to permit operation with PRF's much in excess of 1 Mc. With the slower rise and fall times, additional dead time between transmitter "Off" time and receiver "On" time was required to assure that the transmitter was fully off before the receiver turned on. When the dead time surpassed the "On" times. sensitivity rapidly decreased, and an effective upper PRF limit was reached.

Before the performance of the dynamic transmitter-receiver isolation tests, the extended range altimeter was interconnected for normal operation except that the PRF and carrier tracking loops were broken as shown in the test setup block diagram (Figure 4-10). A wave analyzer was connected to the output of the 500-kc IF amplifier, and attenuators connected between the transmitter and receiver also as shown in the block diagram. Oscilloscopes were used to monitor the system operation.

To make an isolation measurement, all of the isolation between the transmitter and receiver was removed, and a reference set at the wave analyzer. During this time, the transmitter and receiver were each being square-wave modulated with signals 180 deg out of phase, as in the normal operating mode, so that any received signal was, ideally, leakage. Second, 100 db or so of attenuation was added between the transmitter and receiver, and the transmitter set to operate in a CW mode, with its average power now equal to the same value that its peak power was during the PRF mode. While operating in this manner, the attenuator was further adjusted until the reference was reattained on the wave analyzer. The attenuator reading then represented the isolation attained by switching.

Checks indicated that very little extraneous RF leakage from the transmitter to the receiver was experienced. Although considerable care was exercised in shielding the potential radiating components, the largest degree of effective shielding was derived through the frequency diversification inherent in the system. One of the tests performed to check leakage was to note whether the attenuator still properly controlled the transmit signal leakage when this leakage was set near the wave analyzer reference level. Obviously, it would not if most of the signal were bypassing it.

Figure 4-11 shows a plot of the dynamic isolation versus PRF. As may be seen, the isolation decreases from a value of about 140 db at 300 cps to 60 db at 1 Mc. This degradation is due principally to sidebands of the chopped local oscillator signal mixing with the carrier to produce a signal falling within the IF bandwidth. For example, at 1 Mc, the 65th harmonic of the chopped LO signal could mix with its carrier to produce a 65-Mc IF signal. Because high isolation is required at the greater ranges where the PRF values are low, this appears to offer no system limitation, unless a high PRF was used in an ambiguous mode to achieve greater accuracy.

It should be noted that the attenuation values shown in Figure 4-11 are exclusive of that provided by a circulator or dual antennas. For a matched antenna system, a circulator would provide 20 db or more additional isolation; separate antennas could add, typically, 60 db more of isolation.

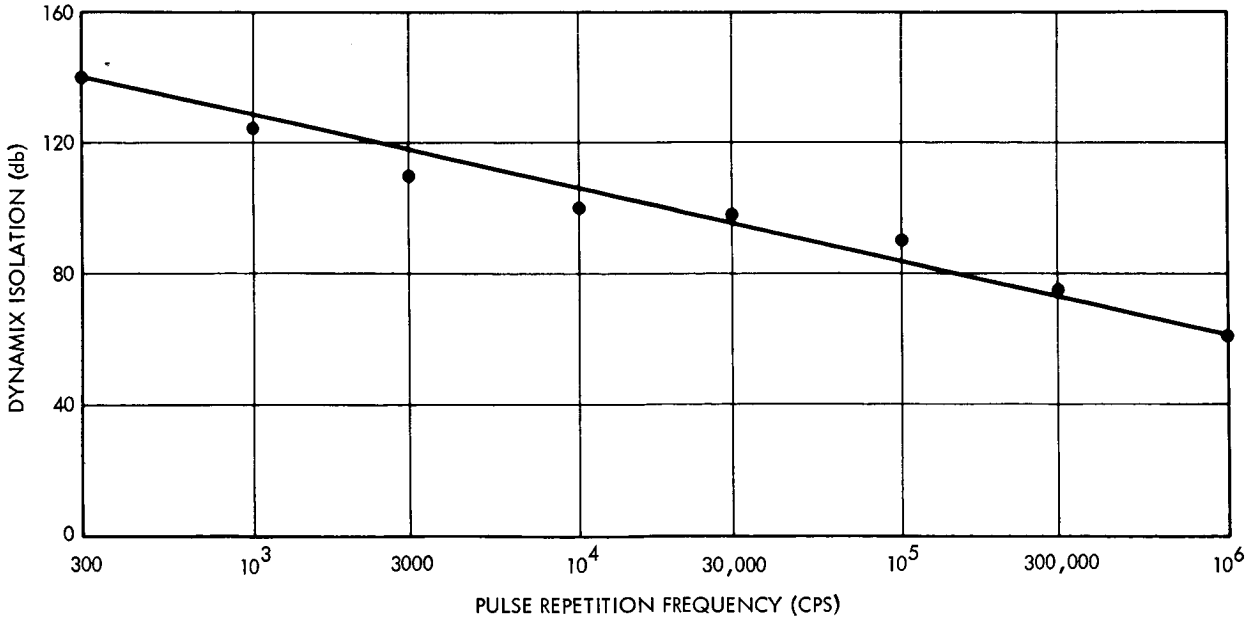

Figure 4-11. Altimeter Dynamic Isolation versus Pulse Repetition Frequency

5. EVALUATION OF THE EXTENDED RANGE ALTIMETER WITH A SIMULATED LUNAR RETURN

5.1 INTRODUCTION

This section contains a description of the analysis and subsequent development of a lunar-return signal simulator used to evaluate the extended range altimeter (ERA) in a representative lunar signal environment. The section continues with a description of the associated tests to which the ERA was subjected. Finally, plotted test results are presented to form the basis for the ERA system evaluation.

5.2 NOISE ANALYSIS

This analysis was conducted to ascertain the nature of the lunar-return signal from which the ERA would determine range or altitude. To avoid confusion in the discussions regarding system noise or noise contamination, the noise of the lunar-return signal is termed "terrain return."

The signal to be detected and processed by the ERA is provided by pulses of transmitted energy reflected from the lunar surface. A study of the reflection process from such a surface is therefore in order.

From an orbiting altitude, the lunar terrain viewed by the altimeter antenna will vary from rugged mountains to flat crater floors and maria. Also, since the vehicle will probably descend to a maria or crater floor, this type of surface should be considered for the final approach.

A smooth surface is characterized as one which has small excursions from the mean height compared to the wavelength of the impinging energy; or it has a correlation distance which is large compared to the dimensions of the illuminated surface area. In this case, the reflected transmitted energy possesses a spectral density identical to that of the transmitted pulse but shifted in frequency by an amount proportional to the vertical velocity component of the altimeter vehicle. Of course, the returned or reflected energy is diminished from that of the transmitter by an amount depending upon the distance between the transmitter and reflecting surface. A low reflection surface in which the loss was independent of frequency would simply reduce the reflected energy an additional amount without changing the spectral shape.

On the other hand, a diffuse surface, or one which has excursions from the mean height comparable to or larger than the wavelength of the impinging energy, and which has a correlation distance much smaller than the dimensions of the illuminated area will diffusely reflect the incident energy. Reflection would occur from a large number of independently scattering areas and the amplitude and phases of the returns from the separate scatterers would be statistically independent. Thus, by the central limit theorem, the quadrature components of the total return are Gaussian distributed; and the envelope of the total return is Rayleigh distributed. Furthermore, if the Gaussian distributed return is stationary (time invariant), then definition of the return is completed by specification of the power spectral density. Thus, if a Gaussian function can be generated with the proper power spectral density, then a good laboratory simulation can be achieved.

Two equivalent approaches may be taken to determine the correct power spectral density. From a study of the mission dynamics, antenna beamwidth, etc., the power spectral density could be determined directly. The second approach would be to determine the correlation function of the return and obtain the power spectral density via the Fourier Transform. The choice of an approach would depend upon the dominant factor determining the power spectral density. The differential doppler to scatterers within the illuminated area would be the dominant factor in determining the return spectrum spreading for a wide antenna beamwidth. A narrow antenna beamwidth and a moderate-to-large horizontal velocity would cause return fluctuations largely due to successive illumination of surface scattering elements. In the limit of a narrow pencil beam, this effect could mask the doppler spreading at low altitudes.

If differential doppler is the dominant factor in the spectrum spreading, direct determination of the power spectral density would be most fruitful. On the other hand, if successive scatterer illumination is the dominant factor, determination of the power spectral density from the correlation function of the return would be more straightforward.

The 100-n mi orbital case has been chosen to illustrate the interaction of the spectrum spreading factors. Assuming the following,

Orbital velocity	$V = 5260$ ft/sec
Antenna beamwidth	$\theta = 1/15$ radian
Transmitted frequency	$f_o = 10^{10}$ cps

then the spectrum spreading is given by

$$\text{bandwidth} = 2\,\frac{2V \sin(\frac{\theta}{2}) f_o}{C}$$

$$= \frac{4(5260)(1/30)10^{10}}{10^9}$$

$$\approx 7,000 \text{ cps.}$$

To indicate the influence of successive scatterer illumination on the bandwidth, the following procedure was followed. The diameter of the illuminated surface area is given by:

$$D = (\text{beamwidth}) \times (\text{altitude})$$

$$= 1/15 \times 6 \times 10^5$$

$$= 4 \times 10^4 \text{ ft.}$$

The correlation time of the return should be of the order of the time necessary to travel this distance, or

$$\text{correlation time} \approx \frac{D}{V} = \frac{4 \times 10^4}{5260} = 7.6 \text{ sec,}$$

and the resultant bandwidth should be no larger than ten times the reciprocal of the correlation time, or

$$\text{bandwidth} < \frac{10}{7.6} = 1.3 \text{ cps.}$$

Thus, the spectrum spreading due to successive scatterer illumination is negligible for the orbital case and differential doppler is the dominant factor in determining the spectral shape.

The return power spectral density will be influenced by the projection of the antenna pattern on the terrain as well as the angle dependence of the cross section per unit area of the surface (σ_o). Therefore, specification of an exact power spectral density would be speculative without detailed information on the antenna to be used and the scattering characteristics of the lunar surface. For these reasons, as well as for ease of simulation, only the bandwidth of the simulated return has been specified and not the exact power spectral density. If the performance of the altimeter proves to be a strong function of the simulated return bandwidth, further sophistication in the shaping of the spectrum may be advisable.

Fortunately, Gaussian terrain return can be simulated by narrowband thermal noise. Additionally, an adjustable filter bandwidth will satisfy the requirement for simulation of latter portions of the mission in which the spacecraft velocity, and hence the return bandwidth, decreases.

In addition to the return signal bandwidth (which may be calculated from the differential doppler over the illuminated area, or the correlation time of the return) the total return power must be specified for the simulation. The return power may be calculated from*

$$\frac{P_r}{P_t} = \frac{k_t k_r \lambda^2}{16 \pi^2} \frac{G_r \bar{\sigma}_o}{h^2} \qquad (5\text{-}1)$$

where

P_r = received power

P_t = transmitted power

λ = radar wavelength (3 cm)

G_r = receiving antenna gain (35.6 db)

$\bar{\sigma}_o$ = terrain scattering coefficient averaged over illuminated area (taken as -6 db)

h = altitude

k_t, k_r = transmitting and receiving efficiencies (product taken as -6 db).

* "Study of Lunar Landing Performance Study Interim Report No. 1," Section 4.4.3, dated 21 June 1963 and prepared under Contract NAS 8-5205.

Substituting these quantities into Equation (5-1)

$$\frac{P_r}{P_t} = -20 \log h - 29 \text{ db, with h in meters,}$$
$$= -20 \log h - 97 \text{ db, with h in nmi .}$$

For an orbital altitude of 100 n mi = 1.853×10^5 m, (108 db)

$$\frac{P_r}{P_t} = -137 \text{ db}$$

Thus, the total power in the simulated terrain return is estimated to be 137 db below the transmitted power for the 100-nmi orbital case, and (20 log h + 29 db) for the general case; and the bandwidth is estimated to be 7000 cps in the orbital case and 1.33 V_h cps (where V_h is horizontal velocity in fps) in the general case.

5.3 NOISE GENERATOR DEVELOPMENT

Generation of the terrain-return signal composed of narrowband noise is accomplished by selecting spectral portions of a white-noise source in the low frequency domain by passive filtering techniques. The selected bandwidth of noise is then superimposed upon an 80-kc CW carrier and subsequently hetrodyned in two additional steps to a 200-mc center. At this point, the PRF gated transmitter operating at an X-band frequency minus 200 mc is mixed with the 200-mc noise signal in a balanced modulator which suppresses the X-band carrier. The two sidebands remaining are then presented to a selective filter which passes only one of them for processing by the ERA receiver.

A block diagram of the noise generation process is shown in Figure 5-1.

The white-noise source is a General Radio Model GR 1390B which uses a gas discharge tube to generate noise of uniform spectral content. Spectral filtering is accomplished in a Krohn-Hite 330 M bandpass filter which provides noise outputs in a 400-cps band centered at 1 kc and in a 5-kc band centered at 10 kc. Selection of either wide- or narrowband noise is accomplished by switching the GR noise source into the appropriate filter bank.

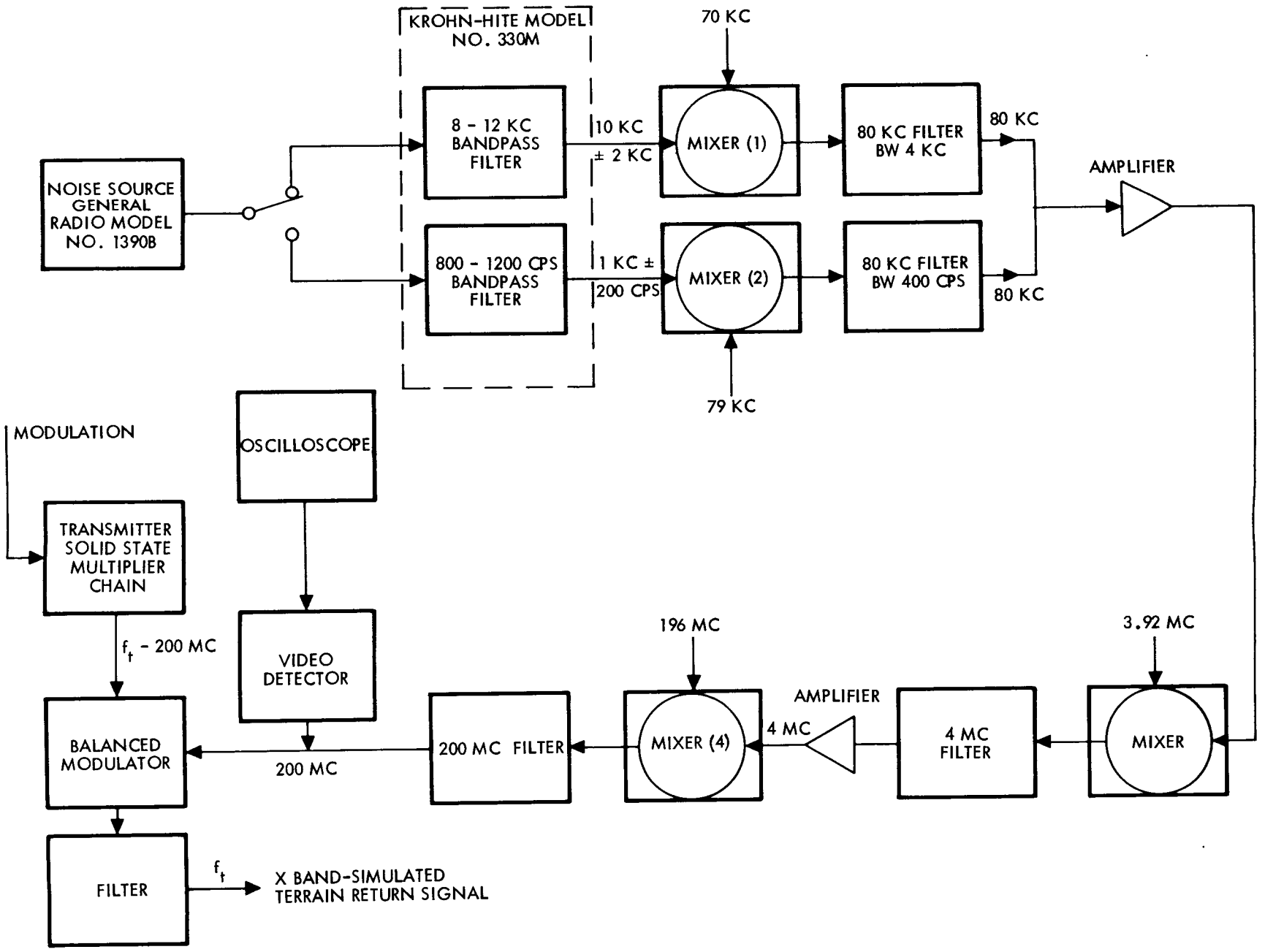

Figure 5-1. Block Diagram of Terrain Return Noise Generator

Mixers 1 and 2 up-convert the 10-kc or 1-kc centered noise spectra to 80 kc by mixing with 70-kc and 79-kc signals, respectively. The reference carriers and the associated lower sidebands are removed by selective filtering at the mixer outputs. The bandwidth of the filters is 5 kc for the wideband noise and 400 cps for the narrowband noise.

The noise centered at 80 kc is then upconverted to a 4-Mc center frequency by mixing with 3.92 Mc., and then upconverted to 200 Mc by mixing with a 196 Mc signal. Filtering at the 4-Mc frequency is accommodated with a 28-kc bandwidth filter; and with a 4-Mc bandwidth filter at the 200-Mc frequency, thus avoiding any additional restriction of the noise spectra. Intermediate amplifiers raise the signal to the required levels for subsequent processing.

Final conversion of the 200-Mc noise signal to X-band is performed in a balanced modulator by mixing the signal with a PRF gated signal of $(f_t - 200)$ Mc obtained from a solid state multiplier chain. The $(f_t - 200)$ Mc carrier frequency is suppressed by the balanced modulator by about 20 to 30 db. The upper sideband is extracted while other sidebands are suppressed in a four section Chebishev type waveguide filter connected to the output of the balanced modulator. Again, the bandwidth of the balanced modulator and filter is very large compared to the noise bandwidth. The balanced modulator output signal obtained is the noise to simulate a terrain return signal centered at X-band.

A photograph of the 400-cps and 5-kc noise spectra, taken at the output of the 200-mc mixer of the simulator, is shown in Figure 5-2.

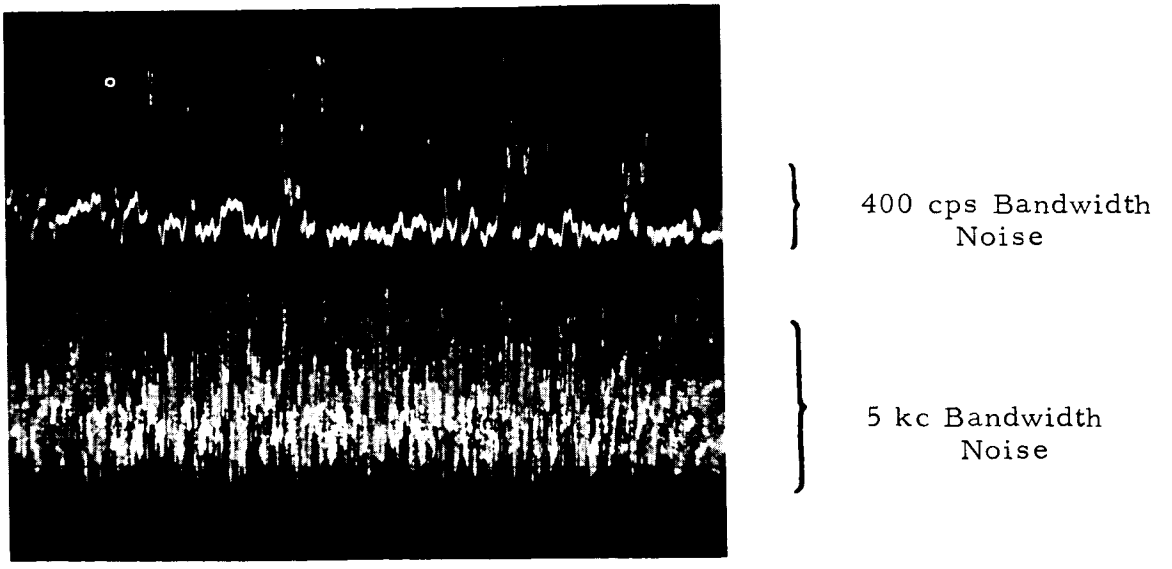

Figure 5-2. Noise Detected at the 200-Mc Mixer of the Terrain Return Simulator

Figure 5-3, taken at the output of the 500-kc IF amplifier, shows the 500-cps modulated noise signal just prior to IF limiting. The top sweep in the photograph of Figure 5-3 shows noise with a 5-kc bandwidth, and the bottom sweep shows it with a 400-cps bandwidth. At first

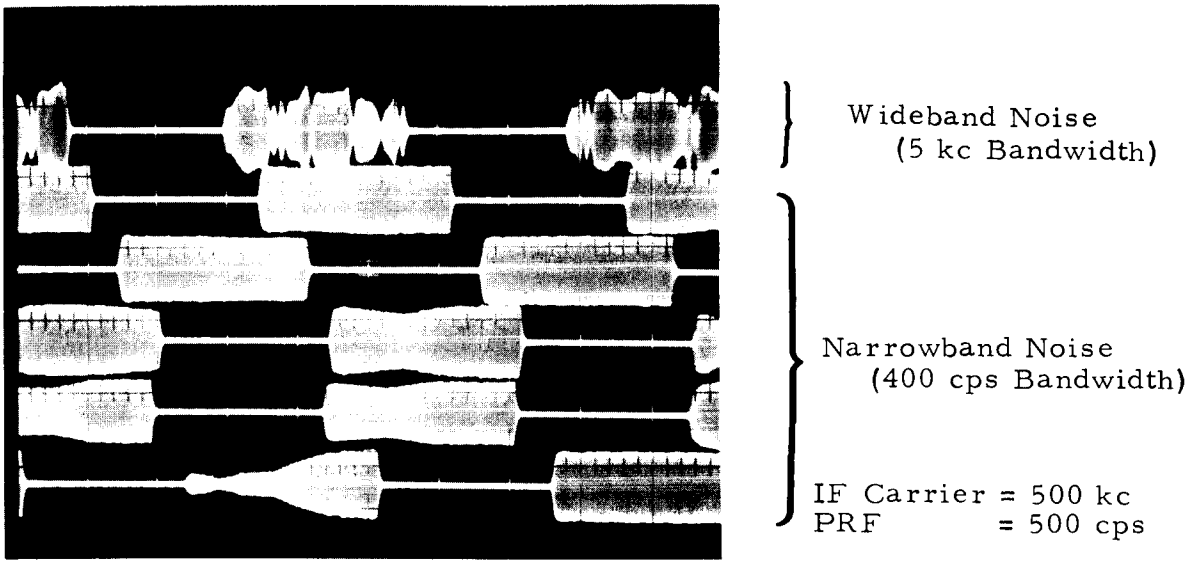

Figure 5-3. Terrain Return Signal Observed at the 500-kc IF Amplifier Output

glance, Figure 5-3 suggests that the lower sweeps do not demonstrate a commensurate amount of narrowband noise modulation relative to the wideband trace (top sweep). This is an illusion because the 500-cps PRF rate nearly matches the 400-cps noise bandwidth, a phenomenon which would be more apparent if the sweep rate of the scope were lowered for the narrowband noise display.

It may be noted that the wideband noise of 5-kc width does not match the estimated 7-kc width from the noise analysis presented earlier. This discrepancy occurred because the original estimate of a 5-kc width was corrected to the present 7-kc figure after the tests had been conducted using 5-kc width simulation. The only adjustment required in the data is one of velocity. Since the bandwidth is directly proportional to velocity, the 5-kc width employed for testing implies that the equivalent velocity is $\frac{5}{7}$ times the assumed orbital velocity of 5260 ft/sec, or 3760 ft/sec.

5.4 ALTIMETER SYSTEM TESTS

A block diagram, Figure 5-4, shows the equipment configuration employed to test the altimeter performance using simulated terrain-return signals. Three independent variables were available for control of the test stimuli; namely, the terrain return bandwidths of 5 kc or 400 cps corresponding to orbital velocity of 3760 ft/sec and to lunar touchdown, respectively, the magnitude of the terrain return power, and the altimeter range or altitude.

The instrumentation includes the altimeter receiver whose input stimulus may be either from the terrain return simulator or from an uncontaminated X-band signal source for calibration purposes, etc. Signal power level control is provided by precision variable attenuators.

The ERA receiver signal is converted to 65 Mc by mixing the X-band test signal with the output of the first LO chain and then amplified and filtered before connection to the 500-kc mixer. Bandwidth restriction to 5 kc is provided by the second IF which is composed of four stages of amplification and a limiter. An IF takeoff in the early stages is converted to 38 kc by the third mixer and a 462-kc third LO which is used for AFC of the signal generators after frequency discrimination and integration. A second output of the 500 kc IF is a 30-cps dither signal which is phase detected with respect to a 30-cps reference oscillator; and subsequently is integrated to provide a control voltage for the PRF generator. The receiver AGC provides control over input level variations of 80 db.

PRF dither is provided by the 30-cps reference oscillator. The dithered PRF signal is provided in two phase opposed outputs; one for gating the first LO and the other for gating the transmitter after an adjustable time delay. The time delay simulates range or altitude effects.

Figures 5-5 through 5-8 illustrate the deviation from the mean PRF for different combinations of terrain return power level, spectral spreading and PRF dither percentage. The line connection of the data points is an artifice to aid in demonstrating the data. The mean PRF for each of the curves was, nominally, 19 KC.

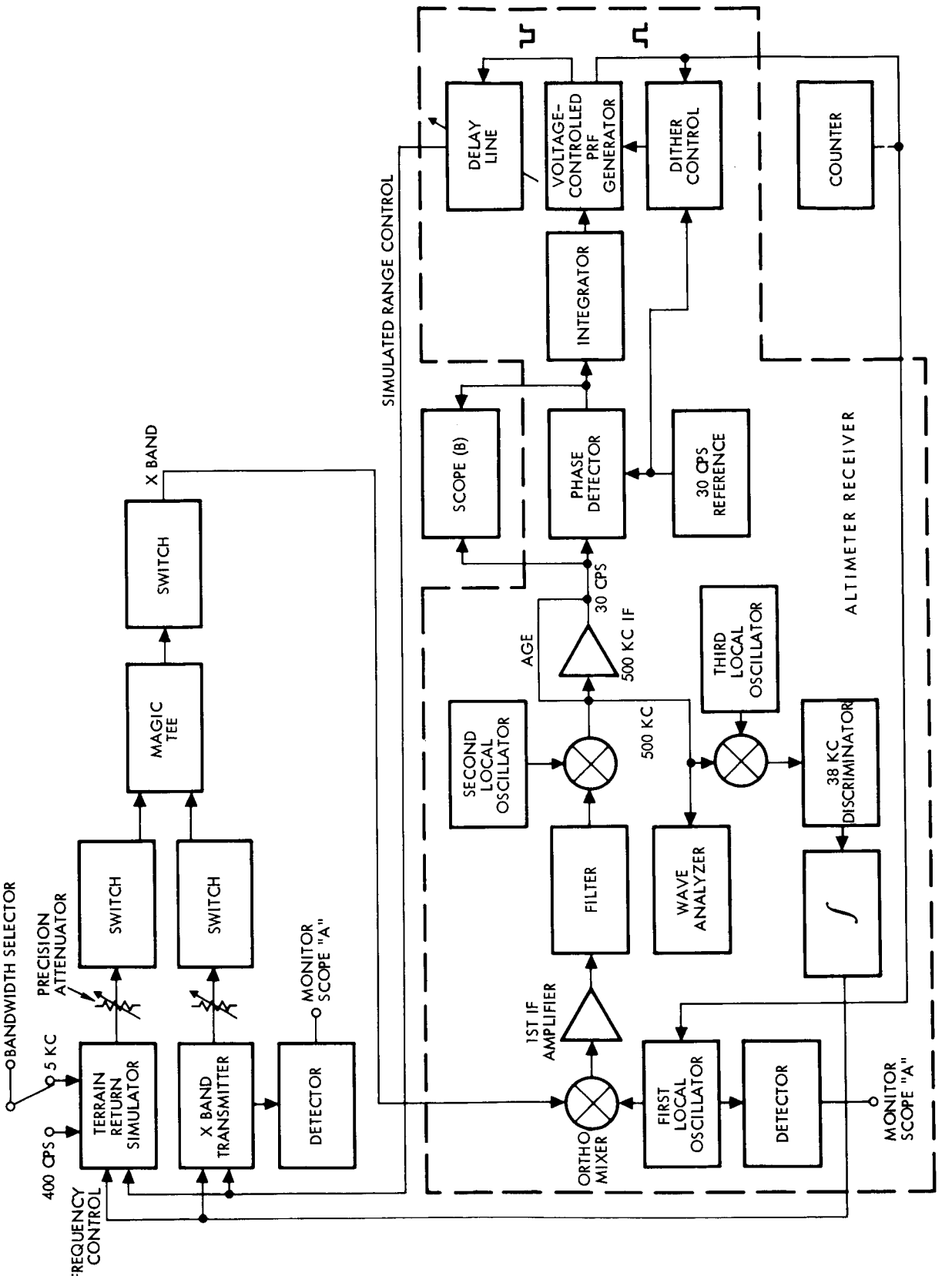

Figure 5-4. Simplified Block Diagram, Altimeter Test Configuration

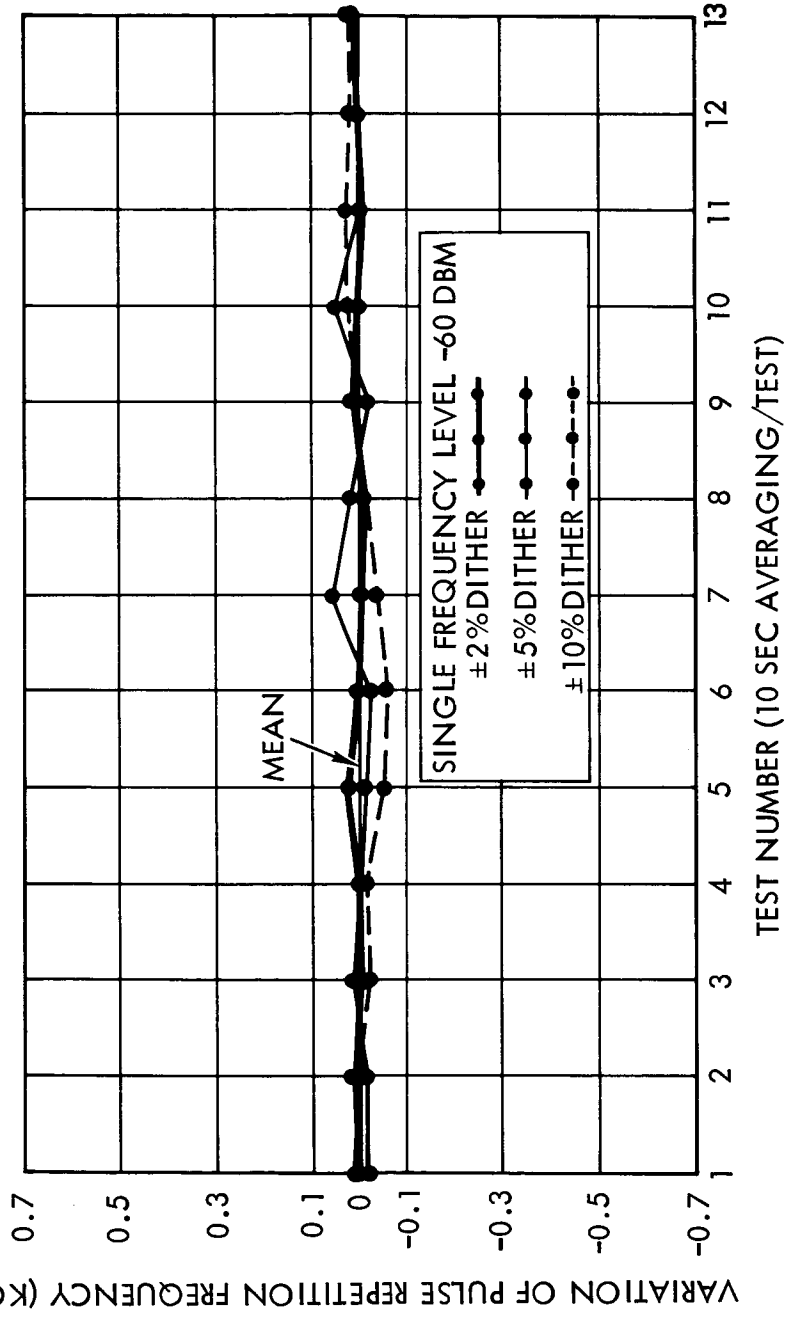

Figure 5-5. PRF Readings versus Dither for a High-Level, Single-Frequency Received Signal

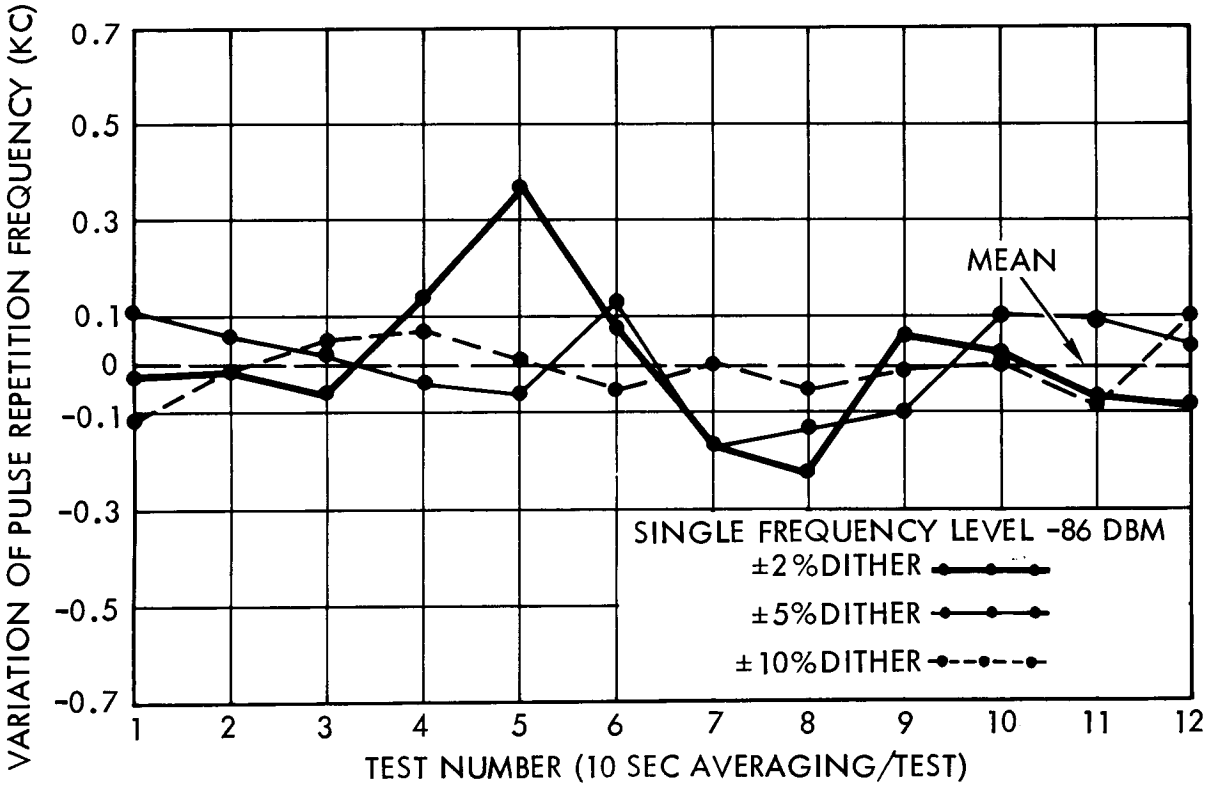

Figure 5-6. PRF Readings versus Dither for a Low-Level, Single-Frequency Received Signal

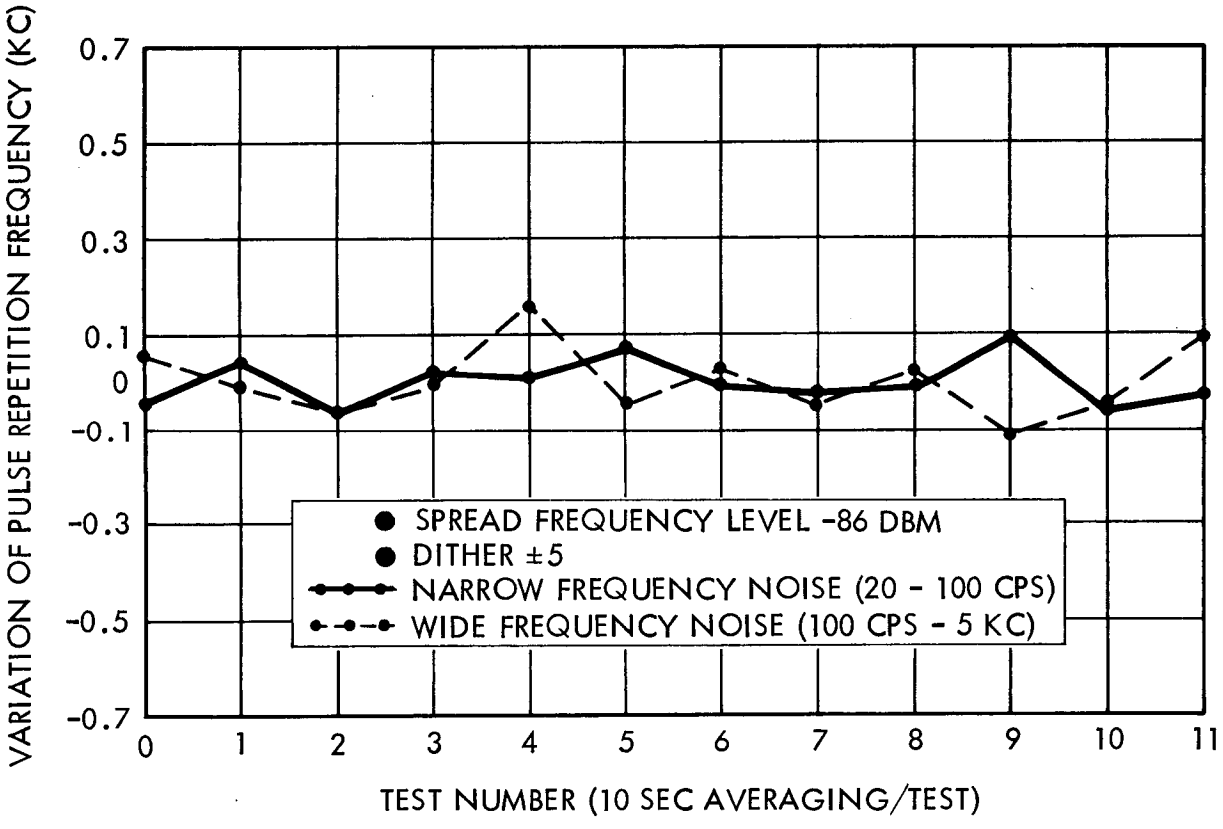

Figure 5-7. PRF Readings versus Spread Frequency Bandwidth

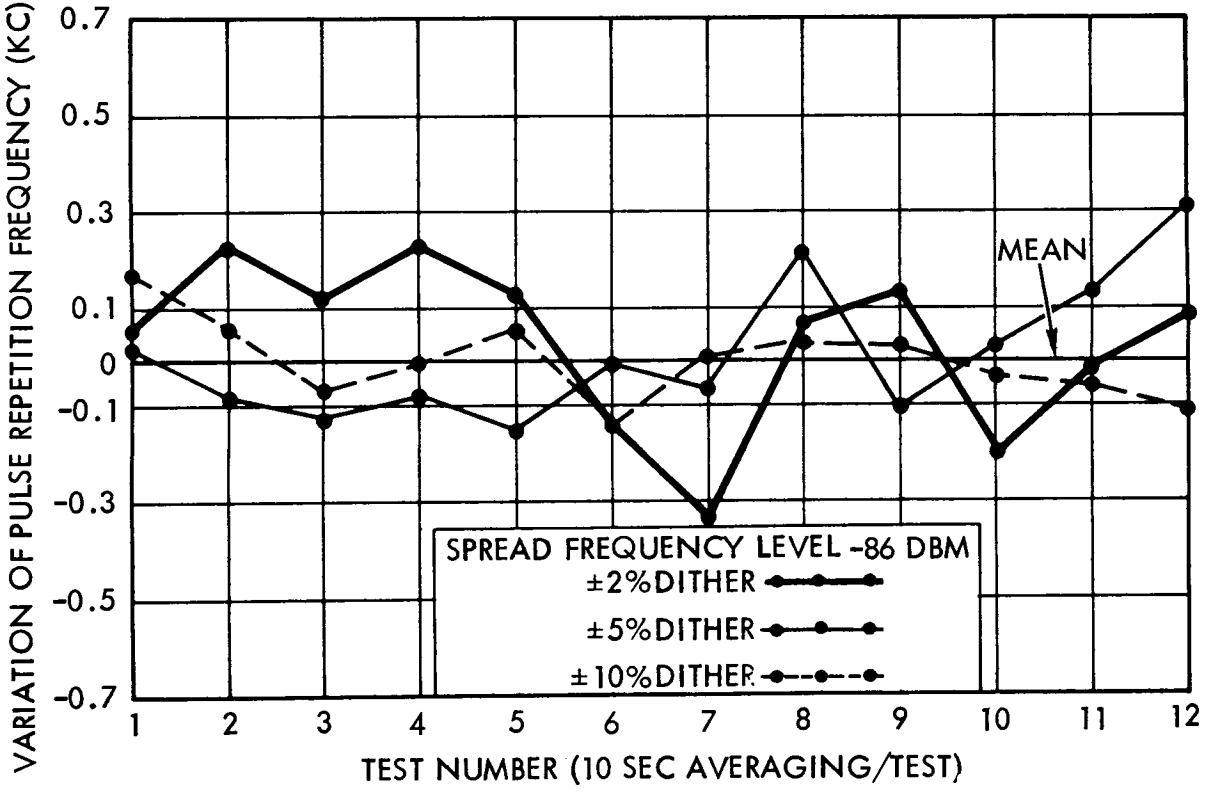

Figure 5-8. PRF Readings versus Dither for a Wide Band Spread Frequency Received Signal

In the absence of spectral spreading, the PRF deviation from the mean reduces as the signal strength increases, which would be expected intuitively. Near the receiver background noise threshold, the ranging performance is noticeably improved for 10 percent dither compared to low (2 percent) dither. This could conceivably be the effect of a finite detection threshold in the PRF control loop. For receiver S/N ratios as large as 28 to 30 db, and with the non-spread spectrum as an input, the data reveals that the deviation from the mean is less than 0.3 percent with any dither percentage tested.

For the tested condition of 5 percent dither, there appears to be little difference between the wide or narrow spread spectrum cases and the non-spread spectrum case at signal powers near the receiver noise threshold. This also is not surprising.

In general, the PRF deviation is least for the non-spread spectrum case and worsens as the spectral width increases. Also, as deduced earlier, the deviation lessens as signal power increases for the non-spread spectrum case, while for spread spectral inputs this tendency is not so pronounced.

Based upon a final analysis of the data, it appears probable that the statistics of the signal and noise were not determined with unqualified accuracy over a 10-sec sampling interval or by a population of 12 samples. Therefore, the curves shown in Figures 5-5 through 5-8 should be evaluated in this light.

It should be noted also that the data presented in Figures 5-5 through 5-8 refers to the deviation of PRF about a mean value, rather than the deviations about a value necessarily representing the correct altitude. It is therefore recommended that this data not be used as a basis for estimating absolute system accuracies, but rather used to indicate the extended range altimeter performance with a spread spectrum received signal relative to its performance with a single frequency received signal.

6. CONCLUSIONS AND RECOMMENDATIONS FOR ADDITIONAL WORK

6.1 CONCLUSIONS

Two major conclusions can be drawn as a result of this study. First, the use of unified sensors does indeed appear feasible and desirable for certain applications; secondly, the PRF-modulation technique continues to be most attractive, especially for applications requiring operation over large variations in range or altitude.

Each of the three unified sensor transmitter-receiver configurations considered appear to offer distinct advantages over completely separate sensors performing the same functions. For review, the unified sensors referred to are a unified long-range altimeter plus beacon tracker, a unified short-range altimeter velocity sensor plus beacon tracker, and a unified short-range altimeter plus interferometer beacon tracker. For each of these unified systems, it was possible to utilize many similar subsystems because dithered PRF modulation, suitable for the requirements of all systems, was used. In addition, receivers were designed to receive signals having the same frequency, and transmitters were designed to generate signals having different but coherently related frequencies corresponding to the two modes of operation. These characteristics permitted a common receiver and much common processing circuitry to be used, as well as common circuitry for most of the transmitters. Only a frequency multiplier section to increase the transmit frequency from UHF to X-band was uncommon to the two transmitters. These design factors contributed appreciably to low size, weight, and power requirements, and high reliability characteristics.

It also appears that antennas for different functions might be combined in the same manner as electronic systems. Significantly, it appears feasible to combine a beacon-tracking radar antenna with an extended-range altimeter antenna to form a single unified antenna, or to combine a beacon tracking radar antenna with a low-range altimeter velocity sensor antenna to form a single unified antenna. If two antennas were combined, however, the resulting unified antenna would be appreciably heavier than either of the single antennas, and the unified antenna could be used for only one function at a time, such as either beacon tracking or

altimetry. Some advantage might exist, however, for a unified electronic transceiver mounted directly to the back of a unified antenna to form a single system capable of either beacon tracking or altimetry.

The feasibility of two separate antenna systems used with a unified transmitter-receiver system would be questionable because such an arrangement would require one electronics package, two antennas, two rotary joints of some type, and RF transmission lines. Conversely, if separate electronics packages were used, each could be mounted directly to the back of their respective antennas so that neither rotary joints nor RF transmission line would be necessary. This would indicate a tradeoff choice of two rotary joints plus transmission line against one additional electronics system. By using advancement in micro-technology over the past 2 years as a gauge, it almost would appear that two electronic systems would be preferable over a single unified one, from a size and weight standpoint, an operational standpoint, and an environmental standpoint, when separate antennas are necessary.

The attractiveness of the PRF modulation technique continues because of its adaptability to each of the three lunar landing sensor functions, its usefulness over very large operating ranges, its capability of being instrumented with narrowband solid-state signal sources, and its satisfactory performance with a spread spectrum return signal. Its adaptability to unified sensors was demonstrated in detail in Section 3. Its ability to perform over larger altitudes was indicated by the operation of the PRF generator and the varactor multiplier signal sources over very wide ranges of PRF's. Its compatibility with a narrowband signal source was also demonstrated in Section 4 by the data describing the modulation waveforms. The only requirement for bandwidth is based upon achieving satisfactory rise times for the modulated signals; and the photographs and data indeed indicate the satisfactory rise times were obtained. Finally, its capability to operate satisfactorily with a spread spectrum return signal was demonstrated in Section 5.

6.2 RECOMMENDATIONS FOR ADDITIONAL WORK

Based upon continuing indications of the desirability of dithered PRF modulation, it would certainly appear advisable to continue the investigation into this ranging technique. Such an investigation program should include the following basic tasks:

- Determine the minimum altitude obtainable with a dithered PRF ranging technique and perform experiments to evaluate the feasibility of ranging down to 10 ft or lower.
- Investigate suitable methods for resolving altitude/slant range ambiguities.
- Investigate the usage of a 90-percent duty cycle for a beacon or transponder tracking system.
- Investigate methods of gating IF amplifiers.

A dithered PRF modulation scheme is believed to afford, potentially, a single altimeter system to accurately measure altitudes varying from tens or hundred of miles down to a few feet. Thus far during the LLS Study, the TRW Systems extended range altimeter feasibility model has been used to measure a simulated range varying from 135 nmi to less than 1 nmi. It is believed that much value would be obtained from an additional study to determine conclusively the absolute minimum altitude to which an extended range altimeter could be used.

With the present dithered PRF altimeter, no means to resolve ambiguities has been established, except the one in which the PRF is swept from a very low value up so that the PRF tracking loop will lock at its unambiguous frequency, i.e., where the round trip phase shift is 180 deg. This technique is not, however, entirely fail-safe because it might be possible to lock at any odd multiple of the correct PRF if, for some reason, it were not affected at the correct frequency, or if it were perhaps affected but subsequently lost.

If a better method to resolve ambiguities were available, greater range-measuring accuracy could be obtained by operating in an ambiguous mode, i.e., operating at an odd multiple of the unambiguous frequency.

Different means for ambiguity resolution appear feasible with high-frequency PRF tracking, but they have neither been thoroughly analyzed nor tested in the laboratory.

The usage of a 90-percent duty cycle should be investigated further to affirm its feasibility for a system operating with a cooperative target. A 90-percent duty cycle modulation scheme would permit the dithered PRF ranging principle to be utilized while not necessitating the full 3-db power loss incurred with a 50-percent duty cycle modulation. Of course, when operating with a transponder, a radar system would not require a time-shared transmitter and receiver to achieve isolation, this being obtained by frequency separation.

The final task would involve an investigation of techniques for gating IF amplifiers. It appears theoretically that if a satisfactory technique for IF gating could be developed, it would permit the thermal noise of a 50-percent duty cycle system to be decreased by 3 db and of a 90-percent duty cycle system to be decreased by a somewhat lesser amount. Also, a satisfactory IF-gating technique would permit appreciably more transmitter-receiver isolation to be achieved either for improved performance or for decreasing circuit complexity. Improved performance would result from the higher receiver-transmitter isolation available, and decreased circuit complexity would result from negating the necessity for dual antennas. For some missions, IF amplifier gating alone might be sufficient for switching the receiver "Off" thereby negating the requirement for either an RF switch or for switching the local oscillator.

7. NEW CONCEPTS

No new concepts have been developed or first reduced to practice during the period of performance of the subject contract.

Appendix A. ANTENNA DISCUSSION AND PERFORMANCE ANALYSIS

A.1 INTRODUCTION

In this appendix, the applicable antenna types are discussed in detail and their comparative performance factors are derived.

A.2 CONICAL SCAN ANTENNA

Conical scan can be implemented electromechanically by a motor-driven, displaced feed-parabolic reflector system, or electronically by a cluster of four apertures whose relative phases are varied by an electronically controlled RF phase shifter located in each of the 4-array feed lines. Conceptually, an electronic conical scan can also be implemented by means of magnetic field modulation of a ferrite device at a feed aperture. However, although electronic beam tilt by this method has been demonstrated, very little has been published with respect to aperture efficiency, side lobes, or beam crossover level rotational symmetry. It is expected that these performance factors leave much to be desired. In addition, since the ferrite devices present a reactive circuit to the feed aperture (aperture blocking or multimoding), have a permeability that is temperature sensitive, and must have at least one portion that is unshielded and radiating, the application of this technique in a thermally extreme environment is not recommended.

The obvious advantage of a conical scan angle tracker is that it has a single signal arm, thereby requiring a minimum amount of signal processing circuitry. The general disadvantage is susceptibility to scintillation effects. For the lunar landing mission, scintillation effects result from multipath during beacon tracking at low elevation angles and engine exhaust during powered descent. At X-band, exhaust scintillations would be more likely to occur with solid propellants; however, present manned descent vehicles utilize liquid propellants. A potential disadvantage of a conical scan angle tracker, utilizing a dithered PRF ranging technique, is the possibility of the scan modulation interferring with the long range, low PRF data. The scan rate must be much less than the lowest PRF rate of 100 to 200 cps, especially when the error signal is delivered with a box car generator. However, because of the low angle rates during angle track, 0 to 8 deg/sec, a low scan rate should be permissible.

A.2.1 Feed-Reflector Conical Scan

The state of the art of lubricants capable of withstanding evaporation in a space vacuum is sufficiently advanced so that it is considered feasible to use a synchronous motor to implement a conically scan antenna for a lunar landing mission.

A disadvantage of using any reflector antenna as part of a dual VHF/X-band antenna is the necessity of situating the circular-polarized (CP), crossed half-wave VHF elements in front of the reflector. Since the reflector behaves as a backing ground plane of varying distance from the VHF radiators, design problems are anticipated in tuning the half-wave elements and shaping the element patterns. An added packaging problem is that of physical interference of the conical scan assembly and its support structure with the 400 mc dipoles.

Minimum interference would be effected with a rear feed (feeder waveguide through the reflector vertex) where the motor assembly is situated behind the reflector. An added advantage to the rear feed would be improved control of the motor temperature as well as a greater length of transmission line separation between the heat of the motor and the focused lunar or sun radiation at the focal point. Disadvantages of the rear feed result from additional mechanical complexity of the extended transmission line, approximately 8 inches for a 24 inch reflector, and the probable loss of adaptability to circular polarization since a rear feed is difficult to adapt to efficient CP reflector illumination.

Because of the effects of the support structure and scanning assembly on the feed-aperture illumination control for a scanning feed, the gain, sidelobe, and beamwidth performance factors are more realistically based on past practical experience rather than on any idealized concepts. On this basis, then, for a wavelength $\lambda = 1/10$ ft, a reflector diameter $D = 2\,\text{ft} = 20\lambda$, focal length $f = D/3 = 8$ in., and an estimated correspondence between aperture efficiency, n, beamwidth factor, K, and a first sidelove level, L, of n = 50 percent, K = 72 deg, and L = 20 to -25 db, the conical scan performance estimates are:

$$\text{Gain} = G = n\frac{4\pi A}{\chi^2} = n(20\pi)^2 = 33 \text{ db}$$

$$3 \text{ db beamwidth} = B = \frac{K\lambda}{D} = \frac{72}{20} = 3.6 \text{ deg}$$

The error angle slope is a function of the antenna beamwidth and crossover level (or beam tilt) and can be conveniently derived if the conical scanning beam is assumed to have a circular symmetric shape and its field can be expressed in the Gaussian form,

$$E(\theta, \phi) = e^{-a^2\left(\theta^2 + \theta_0^2 - 2\theta_0\theta\cos\phi\right)} \qquad \text{(A-1)}$$

where

$a^2 = 1.388/B^2$ for a one-way, beacon-tracking, voltage pattern

θ = target offset angle from boresight

θ_0 = beam tilt angle

ϕ = conical scan angle with respect to the target azimuth angle

For conical scan, error angle slope is the change in carrier modulation with target angle offset from boresight. The usual expression for an amplitude modulated wave is,

$$A(t) = \left[(A_0 + Af_s(t)\right] = A_0\left[(1 + mf_s(t)\right]$$

where

A_0 = carrier, or beam crossover level

A = modulation level

$f_s(t)$ = modulation, or scan frequency

$m = A/A_0$ = modulation index

Then,

$$E(t, \theta, \phi) = \left[e^{-a^2\theta_0^2} + E(\theta,\phi) f_s(t)\right] = e^{-a^2\theta_0^2}\left[1 + m(\theta, \phi)f_s(t)\right] \qquad \text{(A-2)}$$

where

$$m(\theta, \phi) = \frac{E(\theta, \phi)}{e^{-a^2\theta_0^2}}$$

The maximum modulation occurs at $\phi = 0, \pi$ (target in the plane of beam offset). Also, as the target angle off boresight gets small ($\theta \rightarrow \theta_0$), the scan rate harmonics can be assumed to approach 0 with all the modulation going into the fundamental scan rate, f_s. Since the modulation is proportional to the pattern voltage difference of Equation (A-1) at the $\theta = 0$ and π positions, Equation (A-2) can be written as:

$$E(t, \theta) = e^{-a^2\theta_0^2} \left[1 + m(\theta) \cos 2\pi f_s t \right] \qquad \text{(A-3)}$$

where

$$m(\theta) = \frac{E(\theta)}{e^{-a^2\theta_0^2}} = \frac{e^{-a^2\theta^2}}{2} \left(e^{2a^2\theta\theta_0} - e^{-2a^2\theta\theta_0} \right)$$

The error angle slope about boresight is:

$$K = \frac{dm}{d\theta} \text{ (at } \theta = 0) = 2a^2\theta_0 = \frac{2.776}{B^2} \theta_0 \frac{mv}{mr} \text{ per v at crossover} \qquad \text{(A-4)}$$

where

B, θ_0 are in radians.

Equation (A-4) defines the error angle slope with respect to a normalized crossover level. This error slope is convenient for comparison with the error slopes of other antenna types and is the appropriate expression for use when the antenna gain is referred to the crossover gain during angle track. Since the crossover gain decreases and the error slope increases as the beam tilt is increased, a tradeoff choice is necessary. Where the beam tilt RF design problem is not a limiting factor, the choice of crossover level relates to minimizing angle track errors due to receiver noise.

The usual expression for angle track error is:

$$\sigma_\theta = \frac{\sigma\phi}{K} = \frac{1}{Ks/n\sqrt{2}} \qquad \text{(A-5)}$$

where

K = error angle slope

s/n = voltage signal to noise ratio

By Equation (A-5), it is apparent that angle track errors can be minimized by maximizing the product of error angle slope and the square root of the crossover gain. Defining the product as the sensitivity S, then

$$S = K\sqrt{G(\theta_0)} = K\, e^{-a^2\theta_0^2}\sqrt{G_{max}} = 2a^2\theta_0\, e^{-a^2\theta_0^2}\sqrt{G_{max}} = S_0\sqrt{G_{max}} \qquad \text{(A-6)}$$

where

$$S_0 = S/\sqrt{G_{max}} = \text{normalized sensitivity}$$

For a constant G_{max} and beamwidth B, integration of Equation (A-6) and equating the resulting expression to 0 gives:

$$S = S_{max} \text{ and } S_0 = S_{0\,max} \text{ at } \theta_0 = 0.6B$$

Table A-I lists some calculated values of S_0, K, and crossover gain loss as a function of beam tilt θ_0. Since beam tilt design complexity for a conical scan angle tracker increases with increasing beam tilt, a crossover level between 2 and 3 db would probably be used. Since a 3-db crossover provides a nearer to maximum S, a 3-db crossover will be assumed for comparative purposes. For a 3.6-deg beamwidth, and a 3-db crossover level, Equation (A-4) gives the error angle slope as

$$K = 22.15\,\frac{mv}{mr} \text{ per v at crossover}$$

Table A-I. Reflector Type Conical Scan Beacon Tracker Error Angle Slope, Crossover Gain Loss, and Sensitivity Versus Beam Tilt

Beam Tilt in Beamwidths B	Angle Slope K	Normalized Sensitivity, S_o	Crossover Gain Loss
0.3 B	0.83/B	0.732/B	1.1 db
0.4 B	1.11/B	0.888/B	2 db
0.5 B	1.39/B	0.982/B	3 db
0.6 B	1.665/B	1.01/B	4.3 db
0.7 B	1.94/B	0.984/B	5.9 db

Angle track errors, that are systematic and independent of receiver noise levels, will occur at the antenna front end due to RF amplitude errors or asymmetries which appear after the antenna has been boresight aligned. These errors may be due to beam tilt, insertion loss, or gain variations over the scan cycle resulting from environmental effects, or they may be due to changes of net received signal strength over the scan cycle due to multipath effects. If there is a net amplitude ratio error, A, between the 0 and π scan position, the voltage pattern difference by Equation (A-1) becomes:

$$\Delta(\theta) = e^{-a^2(\theta_0-\theta)^2} - A\, e^{-a^2(\theta_0+\theta)^2} \qquad \text{(A-7)}$$

By Equation (A-7), $\Delta(\theta)$ will track to zero modulation for a target at an error angle, θ, off boresight where:

$$A = e^{4a^2\theta\theta_0}$$

The front end systematic error angle slope about boresight is:

$$K_s = \frac{dA}{d\theta}\ (\text{at } \theta = 0) = 4a^2\theta_0 = \frac{5.552}{B^2}\,\theta_0\ \frac{V}{\text{rad}}\ \text{per v} \qquad \text{(A-8)}$$

For

$$\theta_0 = B/2$$

$$B = 3.6 \text{ degrees} = 0.0627 \text{ rad}$$

$$K_s = 44.2 \text{ V/rad per v}$$

and the db error voltage per mr error angle will be:

$$20 \log (1 - K_s \, d\theta) = 20 \log (0.956) = 0.4 \text{ db}$$

A.2.2 Array Cluster-Conical Scan

The advantage of the array cluster-conical scan over the feed-relector conical scan is that the former presents a more compact package and presents a lesser problem of radiation interference between the X-band receiver and the VHF transmitter. The VHF transmitter might consist of cavity backed half-wave slots mounted flush with the face of the array and located along the centerlines separating the four 1 foot by 1 foot arrays, assuming a 2-foot square antenna package. The use of electronic conical beam scanning, electronically controlled X-band phase shifters, in place of the synchronous motor conical scan has both advantages and disadvantages. The thermal dissipation and mechanical problems of the motor scan assembly are replaced by a complex electronic drive and thermally sensitive phase shifting elements, one for each of the four arrays, whose operating temperature must be closely controlled to avoid angle track errors.

Each of the four X-band arrays is a resonant, normal beam array. Beam tilt and conical scan are each implemented by varying the relative phase between each of the four equal normal beams. By means of a triple hybrid complex, signals from the four phased arrays can be combined at a single output port and effect a composite beam pattern of the generalized form

$$E(\theta, \phi) = \frac{f(\theta, \phi)}{2} \left[e^{j\varphi 1} + e^{j\varphi 2} + e^{j\varphi 3} + e^{j\varphi 4} \right] \qquad \text{(A-9)}$$

where θ, ϕ are the usual spherical space coordinates.

$f(\theta, \phi)$ = normalized beam pattern of each array

= $f(\theta)$ for a circular systematic beam pattern

$\varphi_1, \varphi_2, \varphi_3, \varphi_4$ = the relative phases between the four arrays and are functions of θ_0, θ, and ϕ and the separation, d, between array phase centers.

The 1/2 factor relates to voltage drops through the combining hybrids. Any analysis of Equation (A-9) can be simplified by considering the linear case where $\phi = 0$. For a circular symmetric single array normalized beam pattern, $f(\theta)$, the net tilted beam pattern in the plane θ, $\phi = 0$ is, since $\varphi_1 = \varphi_2 = -\varphi_3 = -\varphi_4$:

$$E(\theta, 0) = \frac{f(\theta)}{2}\left[2\, e^{j\varphi} + 2\, e^{-j\varphi}\right] = 2f(\theta) \cos \varphi = 2f(\theta) \cos \frac{\pi d}{\lambda}(\sin \theta - \sin \theta_0) \qquad \text{(A-10)}$$

where

$\pi d/\lambda \sin \theta_0$ = the + or - phase required per phase shifter, referenced to the array cluster center, to obtain a beam tilt θ_0 (total phase difference = $2\pi d/\lambda \sin \theta_0$)

$\pi d/\lambda \sin \theta$ = phase variation between arrays, referenced to the array cluster center, for a target at an elevation angle θ. (θ = 0 degrees along boresight.)

d = separation between array phase centers

Equation (A-10) defines the tilted beam pattern in the angle track mode. During the search mode, the phase bias is removed and the beam pattern is a maximum along boresight, ($\theta_0 = 0$). Its generalized form is then:

$$E(\theta) = 2f(\theta) \cos \frac{\pi d}{\lambda} \sin \theta \qquad \text{(A-11)}$$

Like Equation (A-3) for the feed-reflector conical scan, the near boresight sinusoidal amplitude modulated pattern is, from Equation (A-10),

$$E(t, \theta) = E(0)\left[1 + m(\theta) \cos 2\pi f_s t\right] \qquad \text{(A-12)}$$

where

$$m(\theta) = \frac{E(\theta)}{E(0)} = 1/2 \frac{f(\theta)}{f(0)} \frac{\left[\cos \frac{\pi d}{\lambda} (\sin \theta - \sin \theta_0) - \cos \frac{\pi d}{\lambda} (-\sin \theta - \sin \theta_0)\right]}{\cos \left(\frac{\pi d}{\lambda} \sin \theta_0\right)}$$

The normalized error angle slope about boresight is, since $f(\theta) = \max$ at $\theta = 0$,

$$K = \frac{dm}{d\theta} (\text{at } \theta = 0) = \frac{\pi d}{\lambda} \tan \left(\frac{\pi d}{\lambda} \sin \theta_0\right) \frac{mv}{mr} \text{ per v at boresight} \qquad \text{(A-13)}$$

By Equation (A-13), it is seen that the error angle slope of an array cluster conical scan is formed from phase variations between displaced phase centers and a bias phase ($\pi d/\lambda \sin \theta_0$), in contrast to the error curves formed by amplitude variations between tilted beams as in a rotating feed con-scan. It is similar to a phase monopulse comparator except that it incorporates phase shifters and a single output port in place of the three output ports of a normal phase monopulse array. During the search mode, when the phase bias is equal to zero, the antenna performance and beam shape is that of the sum arm of a phase monopulse array. Since the 20 to 25 db sidelobe specification is primarily a search mode requirement, the pattern of Equation (A-11) must provide 20 db or lower sidelobes. Since Equation (A-10) describes the pattern of the difference arm of a phase monopulse array, and since it is known that for a reasonably good error angle shape the difference pattern of a phase monopulse array must have high sidelobes when the sum pattern has low sidelobes, the sidelobes of Equation (A-10) will be higher than those of Equation (A-11). For the lunar landing mission, these conditions appear to be acceptable, however further analysis of sidelobe multipath effects during angle track could possibly indicate a potential problem area. Appendix B reviews the relative dependence of the effective phase center spacing d between array aperture on the sum arm sidelobe specifications for a phase monopulse angle tracker. This same dependence exists for the search mode sidelobe specification and the angle track mode effective phase center spacing, d of an array cluster conical scan. On the basis of the analysis in the appendix, an

effective phase center spacing of d = 0.75 times the 10λ geometrical spacing is assumed (d = 7.5λ) for a 20 to 25 db sidelobe specification in the search mode.

Since boresight gain decreases with beamtilt, it is appropriate to summarize the gain-beam tilt dependence before making a beam tilt choice.

The angle track mode gain function, $G(\theta)$, can be determined by squaring Equation (A-10) and is found to be:

$$G(\theta) = G_o 4f^2(\theta) \cos^2 \frac{\pi d}{\lambda} (\sin \theta - \sin \theta_0) \qquad \text{(A-14)}$$

where

G_o = gain of each single array

$f(\theta) = 1$ at $\theta = 0$

The crossover gain, at $\theta = 0$, is

$$G(0) = G_o 4 \cos^2 \frac{\pi d}{\lambda} \sin \theta_0 \qquad \text{(A-15)}$$

The maximum gain point is at $\theta = \theta_0$ where

$$G(\theta_0) = G_{max} = G_o 4f^2(\theta_0) \qquad \text{(A-16)}$$

From Equation (A-14), the search mode gain at $\theta_o = 0$ and $\theta = 0$ is:

$$G_s = 4G_o \qquad \text{(A-17)}$$

It is not practical in this case to determine the beam tilt angle in the same manner previously used in Equation (A-6), because the normalized error angle slope always increases faster than the square root of the boresight gain decreases with increasing beam title θ_0. Consequently, the calculated sensitivity continues to increase until zero boresight gain occurs. Therefore, the choice of beam tilt will be such as to provide an error angle slope equivalent to the field reflector conical scan. On this basis, setting d = 7.5λ in the expression for the error angle slope, Equation (A-13), gives,

$$K = 7.5\pi \tan (7.5\pi \sin \theta_0) = 22.15 \frac{mv}{mr} \text{ per v}$$

resulting in,

principal plane bias phase $= 7.5\pi \sin \theta_0 = 43.2$ deg

conical scan beam tilt $\theta_0 = 1.83$ deg

minimum phase difference (at azimuth angles $\phi = 0, 180, \pm 90$) $= 86.4$ deg

maximum phase difference (at $\phi = \pm 45$ deg, ± 137 deg) $= 122$ deg

The corresponding gains are:

- For the search mode, and an operative efficiency n = 63 percent

$$G_s = 4G_o = n\, 1600\pi = 35 \text{ db (from Equation (A-17)}$$

- For the angle track mode at crossover gain

$$G(0) = 4G_o \cos^2 43.2 \text{ deg} = 32.2 \text{ db (from Equation (A-15)}$$

- For the angle track mode, the maximum gain at θ_0, for $f^2(\theta_0) \cong -0.5$ db

$$G_{max} = G(1.83 \text{ deg}) = 34.5 \text{ db (from Equation (A-16)}$$

Systematic RF angle track errors can occur due to both RF phase errors and amplitude errors. The errors may be due to environmentally induced phase shifter errors, environmental changes in multiple reflection effects between the phase shifter triple hybrid array complex, or multipath effects. For a net amplitude ratio error, A, and phase shift error, ϵ, Equation (A-10) gives the normalized voltage pattern difference as:

$$\Delta(\theta) = \cos \frac{\pi d}{\lambda} (\sin \theta - \sin \theta_0) - A \cos \left[\frac{\pi d}{\lambda} (-\sin \theta - \sin \theta_0) + \epsilon \right] \quad \text{(A-18)}$$

For a phase error only case, $\Delta(\theta)$ will track to a null off boresight and a target error angle, θ, will occur according to the following expression.

Because phase shift control for the array cluster sequential lobing is appreciably less complex than for conical scan, this type does warrant consideration. The performance characteristics of the sequential lobing 4-array cluster, however, are essentially those discussed for the conical scan 4-array cluster. The principal difference is in the error angle slope K. Since the step modulation lobing rate harmonics do not approach zero near boresight, the modulation equation [Equation (A-3)] that relates to the pattern voltage difference becomes:

$$E(t,\theta) = E(0)\left[1 + m(\theta)\sum A_m \cos(2\pi m f_s t)\right] \qquad \text{(A-21)}$$

where $m(\theta)$ is given by Equation (A-12)

For the case of the target in the plane of either the up-down or left-right lobing pairs, the modulation waveform may be approximated by a 50 percent duty factor square wave. Since only the lobing rate fundamental is available to the narrow band angle track servo, Equation (A-21) can be rewritten as:

$$E(t,\theta) = E(0)\left[1 + m(\theta)\frac{2}{\pi}\cos(2\pi f_s t)\right] \qquad \text{(A-22)}$$

Defining the lobing modulation factor as $m_\ell(\theta) = \frac{2}{\pi} m(\theta)$, the effective modulation and error angle slope ($dm\ell/d\theta$) is seen to be 4 db less than its conical scan counterpart. (Needless to say, for a larger beam tilt and a lower crossover gain, the error slope can be increased.) From Equation (A-13) the normalized error angle slope about boresight for sequential lobing can be found to be:

$$K = \frac{dm\ell}{d\theta} \text{ (at } \theta = 0) = \frac{2d}{\lambda}\tan\left(\frac{\pi d}{\lambda}\sin\theta_0\right) \qquad \text{(A-23)}$$

For a 7.5λ effective phase center spacing and a 1.83 deg beam tilt, as was the case with the conical scan array cluster, the angle track and search mode gains are the same. The error angle slope and phase shifter requirements are found to be:

$K = 15 \tan 43.2 \text{ deg} = 14.1 \frac{mv}{mr}$ per v and the up-down or left-right phase difference = 86.4 deg

Is is to be noted that whereas the sequential lober requires only 3-phase shift values per phase shifter (0 degrees, -86.4, or -43.2 degrees) the conical scan cluster requires that each phase shifter provide phase shift values ranging from at least 0 degrees to -122 degrees. Most likely a fairly simple digital device could be used to control the phase shifters. The calibration and control module complexity as well as the accompanying greater phase errors of the conical scan certainly appear to offset the advantage of its greater angle error slope.

The sequential lober RF systematic phase and amplitude angle error slopes that relate to antenna front end angle track errors are the same as for the conical scanner (Equations A-19 and A-20), since their error angles are in effect the angular shift of equal amplitude crossover levels and are not a function of the type of modulation.

The final type of sequential lobing is the reflector-4 feed antenna type where four simultaneous beams (up-down and left-right) are alternately switched to a single output port by a triple position switch. The RF switching can be electronically implemented by either diodes, ferrite devices or by electromechanical switches. This type of lobing antenna has the packaging and gain disadvantages of the rotating feed-reflector antenna type, a comparativity low error angle slope due to sequential lobing step modulation, and active switching devices requiring high isolation to minimize systematic angle track errors due to environmental variations. The isolation requirements can be derived by referring to the feed-reflector systematic angle error slope, Equation (A-8). For a crossover level and beamwidth that are the same as those of the conical scan feed-reflector antenna, $K_s = 0.0442$ v/mr. Since leakage phase can be erratic, the worst case of in-phase leakage from beam two when switching to beam one, and out-of-phase leakage from beam 1 when switching to beam 2 must be considered. This leakage results in an amplitude unbalance and a corresponding error angle, $\Delta\theta$, of the form

$$\frac{S_1 - L_2}{S_2 + L_1} = 1 - K_s \Delta\theta \qquad \text{(A-24)}$$

where

S = signal level through the indicated switch

L = leakage level through the indicated switch

At crossover $S_1 = S_2 = S$ and for the case of $L_1 = L_2 = L$, Equation (A-24) simplifies to:

$$\frac{S}{L} = \frac{2 - K_s \Delta\theta}{K_s \Delta\theta} = 33 \text{ db for } \Delta\theta = 1 \text{ mr} \qquad \text{(A-25)}$$

Such high isolation levels are fairly difficult to design in an RF electronic switch, and close thermal control would probably be necessary to maintain these isolation levels.

Since this type sequential lobing antenna has few advantages and most of the disadvantages of the other antenna types, it will not be considered any further.

A. 4 AMPLITUDE MONOPULSE ANTENNA

Amplitude monopulse angle tracking is normally implemented by using a 4 feed-reflector antenna providing four tilted beams from which are derived a sum beam for search and range tracking, and two difference beams (up-down and left-right) for angle track. The 4 feed-reflector antenna may have a direct or cassegrain arrangement. The cassegrain type, with the feeds near the reflector vertex and illuminating a hyperbolic subreflector, affords the most compact package and is favored when circular polarization (CP) is required because of the extra length and weight characteristics of CP feeds. The disadvantages entail the necessity of packaging the VHF transmitter dipoles in front of the reflector for the dual frequency system; a bulky package due to a complex feed cluster (especially for CP and/or when maximizing gain and angle error slope while satisfying sidelobe specifications); and the requirements for three signal ports rather than one as required for a conical scanner or sequential lober. The advantages of an amplitude monopulse are its adaptability to CP, a large angle error slope, and an accumulated backlog of antenna design experience since this type of monopulse has, to date, been used most commonly.

A comparative evaluation of amplitude monopulse performance parameters requires a consideration of the following:

(1) A sidelobe increase due to aperture blocking effects of the cassegrain subreflector, the VHF half-wave elements and the support structure for each. A cassegrain dual reflector antenna will be assumed used because it provides a minimum package depth and improved feed cluster design control for optimizing aperture illumination and implementing CP radiation.

(2) When multiple beams originate from a common aperture, the radiation pattern (which determines the sidelobe level and the beamwidth) and the crossover levels cannot be specified independently. This is a consequence of the orthogonality principal which is based on conservation of energy relations. On a practical implementation basis, if the feeds are made large enough to provide the proper illumination control toward lowering sidelobes and minimizing spillover gain loss, the feeds are then too large and cannot be placed close enough to provide satisfactory crossover levels. And if the feeds are made small enough to provide the desired crossover levels, illumination control is lost and the consequences are an increase in sidelobe levels and gain loss due to spillover. If dielectric rod feeds are used with the objective of providing illumination control through rod length and crossover level control through a closer allowable spacing because of the decreased feed lateral dimensions, the consequence is a loss of illumination control because of the strong coupling between the parallel running rods.

(3) The choice between linear or circularly polarized radiation is also a choice between the utilization of a near optimum performance four-horn triple-mode feed for linear polarization or a limited performance basic four-horn feed (four square or circular horns, one per quadrant of a square grid) for circular polarization since the rectangular triple mode horn dimensions (about 1/2 λ by 3/2 λ for proper aperture illumination) would not be adaptable to circular polarization. The four-horn triple mode feed provides a means for separate control of the sum and different beam aperture distributions, thereby approaching the optimum performance case as limited by the orthogonality principal.

An analytical discussion of the performance restraints imposed by Paragraphs (2) and (3) is given in Appendix C. With regard to Paragraph (1) the minimum cassegrain aperture blockage diameter d is: $d = \sqrt{2\lambda F}$.

For an F/D = 1/3, focal length F = 6.67λ and d = 3.65λ, aperture blockage for a d = 3.65λ and D = 20λ will raise a -25 db sidelobe to approximately -19 db. The VHF elements and the various support structures

$$\epsilon = \frac{\pi d}{\lambda}(\sin\theta - \sin\theta_0 + \sin\theta + \sin\theta_0) = \frac{2\pi d}{\lambda}\sin\theta, \text{ or } \theta = \sin^{-1}\frac{\epsilon\lambda}{2\pi d}$$

Thus the systematic phase error angle slope about boresight is:

$$Ksp = \frac{d\epsilon}{d\theta}\ (\text{at } \theta = 0) = \frac{2\pi d}{\lambda} \tag{A-19}$$

For example, for an effective d = 7.5λ, Ksp = 15π = 2.7 deg/mr. Thus the allowable phase error per mr of apparent angle error is 2.7 degrees.

For the amplitude error only case, $\Delta(\theta) = 0$ at

$$A = \cos\frac{\pi d}{\lambda}(\sin\theta - \sin\theta_0)/\cos\frac{\pi d}{\lambda}(-\sin\theta - \sin\theta_0)$$

And the systematic amplitude error angle slope about boresight is:

$$Ksa = \frac{dA}{d\theta}\ (\text{at } \theta = 0) = \frac{2\pi d}{\lambda}\tan\left(\frac{\pi d}{\lambda}\sin\theta_0\right) \tag{A-20}$$

Again for d = 7.5λ and θ_0 = 1.83 deg, K_{sa} = 44.3 v/rad per v, and the allowable amplitude error per mr of angle error is:

$$20\log(1 - K_{sa}d\theta) = 0.4 \text{ db}$$

A.3 SEQUENTIAL LOBING ANTENNA

Sequential lobing can be implemented by a motor driven nutating displaced-feed parabolic reflector system; electronically by a 4-array cluster with the same arrangement as conical scan array cluster except that beam tilt would only in the $\phi = 0, \pi$ and $\phi = \pi/2, -\pi/2$ planes; or by electronically switching between separate feeds in a four feed antenna system.

A general disadvantage of all sequential lobing angle trackers is that they provide less modulation power to the narrow band angle tracking receiver when tracking in the vicinity of the boresight axis. In addition, since a nutating motor drive is more complex to implement than a conical scan motor drive, this type of sequential lobing warrants no further consideration.

might be expected to raise the sidelobes an additional 2 db. Consequently a near cosine taper providing an unobstructed aperture design sidelobe level in the order of -28 db would be necessary to satisfy the -20 db sidelobe specification.

Two performance parameters of two horn cluster cases will be considered; that for circular polarization where separable sum and difference beam illumination control is not attainable, and that for linear polarization where separable illumination control is available.

A.4.1 CP Horn Cluster

As reviewed in Appendix C, where separable illumination control is not obtainable, the performance penalty must be either poor sum beam aperture illumination (and a consequent poor sum beam gain and increased sum beam sidelobes) or a poor difference beam aperture illumination (and a consequent poor difference beam gain and a decreased normalized error angle slope). Since aperture blockage effects have already degraded the sum beam sidelobes, the choice would favor stressing the sum beam performance.

With a sum arm near cosine taper providing in the order of -28 db sidelobes, and allowing for some stray blockage losses, a sum arm aperture efficiency of n = 50 percent is estimated.

In this case

$$\text{Sum Beam Gain} = G\sum = n\left(\frac{\pi D}{\lambda}\right)^2 = n\,400\pi^2 = 33 \text{ db}$$

As discussed in Appendix C, a sum arm cosine illumination is obtained by two in-phase horns where each horn provides a uniform illumination and is displaced from the other to provide a -4 db seam crossover. In this case orthogonality is also satisfied and no additional gain loss will occur due to coupling between beams. (Orthogonality is exactly satisfied for the sin u/u pattern of a rectangular aperture and can be assumed to be sufficiently satisfied for the J_1 (u)/u bessel function pattern of a circular aperture.) The resultant difference arm illumination will be sin $\pi/2$ x (x = $\pm$1 at the aperture edges) and a large spillover gain loss will occur in the difference beam. As discussed in Appendix G, Equations (G-5) and (G-7), where two

crossover beams are assumed to obtain the sum beam and the normalized error angle slope, a correction factor, $\sqrt{P}$, is necessary where spillover losses are grossly different.

The normalized error angle slope about boresight is conveniently obtained by expressing the crossover beams in Gaussian form, giving:

$$\sum(\theta) = e^{-a^2(\theta_0-\theta)^2} + e^{-a^2(\theta_0+\theta)^2} \tag{A-26}$$

$$\sum(0) = 2\, e^{-a^2\theta_0^2} = \text{normalization N} \tag{A-27}$$

$$\Delta(\theta) = \frac{1}{N}\left[e^{-a^2(\theta_0-\theta)^2} - e^{-a^2(\theta_0+\theta)^2}\right] = \frac{1}{2}\, e^{-a^2\theta^2}\left(e^{+2a^2\theta\theta_0} - e^{-2a^2\theta\theta_0}\right) \tag{A-28}$$

The normalized error slope, for equal spillover losses, is then, by Equation (G-5) of Appendix G:

$$K = \frac{d\Delta(\theta)}{d\theta} \text{ (at } \theta = 0) = 2a^2\theta_0 = \frac{2.776}{B^2}\,\theta_0 \frac{mv}{mr} \text{ per v of } \sum \tag{A-29}$$

And where the spillover losses are grossly different, by Equations (G-5) and (G-7) of Appendix G:

$$K = \sqrt{P}\,\frac{2.776}{B^2}\,\theta_0\,\frac{mv}{mr} \text{ per v of } \sum \tag{A-30}$$

For the present case of an optimum sum arm illumination for maximizing sum beam gain and minimizing sum beam sidelobes, the consequent near $\sin \pi x/2$ difference arm illumination will result in a difference beam spillover gain loss of about 2 db. In this case, $P = 0.794$. For a 4 db crossover level, $\theta_0 = 0.576B$, and for a near uniform illumination on a circular aperture, a beam width to aperture diameter dependence of $B = 1.1\lambda/d$ is estimated. Equation (A-30) is then:

$$K = 1.152d/\lambda\,\frac{mv}{mr} \text{ per v of } \sum \tag{A-31}$$

and by Equation (A-31), for $d = 20\lambda$, the normalized error angle slope $K = 23.04$.

A.4.2 Linear Polarization Four Horn Triple Mode Feed

With separate illumination control, the large spillover gain loss in the difference beam can be eliminated without a consequent degradation of sum beam gain loss. The sum beam gain, being limited by the sidelobe specifications, is estimated at 33 db similar to the gain of the CP horn cluster feed. The difference beam aperture illumination can now be approximated by the no spillover full sine illumination, as defined by Equation (C-11) of Appendix C. The resulting difference beam pattern (Equation C-9), Appendix C also satisfies orthogonality so no gain loss will result due to coupling between beams. Combining terms in Equation (A-9), the beam pattern can be expressed as:

$$\Delta_n(\theta) = \frac{\Delta(\theta)}{N} = \frac{1}{N}\left[\frac{\cos(u+\pi)}{1-(u+\pi)^2(2/\pi)^2} - \frac{\cos(u-\pi)}{1-(u-\pi)^2(2/)^2}\right] \quad \text{(A-32)}$$

where

$$u = \frac{\pi d}{\lambda}\sin\theta$$

N = normalization factor for maximum of $\Delta_n(\theta) = 1$

Equation (A-32) expresses a rectangular aperture difference beam pattern as the difference between two beams whose crossover level (at u = 0) is -9.5 db. At this low crossover level, a Gaussian beam pattern approximation for a circular aperture, similar to Equations (A-26), (A-27), and (A-28), is not adequate towards deriving the error angle slope. A better approximation is to use Equation (A-32) with a modified aperture diameter d. In addition, since the sum and difference patterns are obtained from combinations of different and separately controlled beams, the error angle slope normalization is different from the steps outlined by Equations (A-26) through (A-31) for the CP horn cluster case.

Combining terms in Equation (G-5) of Appendix C, the cosine illumination normalized sum beam pattern can be expressed as:

$$\sum(\theta) = \frac{\cos u}{1-\left(\frac{2u}{\pi}\right)^2} \quad \text{(A-33)}$$

Since the beam pattern of Equation (A-33) is the same as the patterns of the two beams of Equation (A-32) (except for different beam tilt angles) the gain of each of the three beams will be equal for equal or negligable spill-over losses. Consequently, the gain ratio between the difference and sum beams is $(G\Delta/G\sum = N^2$ where N is the difference beam normalizing factor in Equation (A-32).

From Equations (G-2), (Appendix G) and (A-32), the normalized error angle slope is then:

$$K = \sqrt{\frac{G\Delta}{G\sum}} \frac{d\Delta_n(\theta)}{d(\theta)} = N \frac{d}{d\theta} \frac{\Delta(\theta)}{N} = \frac{d}{d\theta} \Delta(\theta) \frac{mv}{mr} \text{ per } v\sum$$

where $\Delta(\theta)$ is given by Equation (A-32).

Differentiating

$$K = \frac{d}{d\theta} \Delta(\theta) \quad (\text{at } \theta = 0) = 1.78 \frac{d_e}{\lambda} \tag{A-34}$$

where $d_e = k\,d$ = rectangular aperture width equivalent to a circular aperture of diameter d. The proportionality constant, k, may be estimated by equating beamwidths for a rectangular aperture cosine distribution and a circular aperture near cosine distribution. On this basis

$$BW = 1.2 \frac{\lambda}{d_e} = 1.33 \frac{\lambda}{d} \text{ and } k = \frac{d_e}{d} = 0.9$$

and the normalized error angle slope is:

$$K = 1.61 \frac{d}{\lambda} \frac{mv}{mr} \text{ per } v\sum \tag{A-35}$$

and for $d = 20\lambda$, $K = 32.2$. Comparison of the error angle slopes for the CP and linear polarized horn feeds shows an estimated increased error angle slope sensitivity of 2.9 db for the linear polarization case where separate aperture illumination control can be more realistically implemented.

A.4.3 Systematic Angle Track Errors

Systematic angle track errors will occur in the case of difference beam precomparator RF amplitude unbalances. For the CP feed case, Equation (A-7) and (A-8) apply and the systematic error angle slope is:

$$K_s = \frac{5.552}{B^2}\,\theta_0\,\frac{\text{unit}}{\text{rad}} \qquad \text{(A-36)}$$

For $\theta_0 = 0.576B$, and $B = 1.1\,\lambda/d = 1.1/20 = 0.055$ rad, $K_s = 58.2$ unit/rad and the db error voltage allowance per mr error angle, $d\theta$, is:

$$20 \log (1 - k_s d\theta) = 20 \log (0.942) = 0.5 \text{ db}$$

For the linear polarized feed case, and a net amplitude error, A, between precomparator inputs, the voltage pattern difference is:

$$\Delta(\theta) = \frac{\cos (u + \pi)}{1 - (u+\pi)^2\left(\frac{2}{\pi}\right)^2} - A\,\frac{\cos (u - \pi)}{1 - (u - \pi)^2\left(\frac{2}{\pi}\right)^2} \qquad \text{(A-37)}$$

By Equation (A-37), $\Delta(\theta)$ will track to zero modulation for a target at an error angle θ off boresight where (for $\Delta(\theta) = 0$):

$$A = \frac{1 - (u - \pi)^2\left(\frac{2}{\pi}\right)^2}{1 - (u + \pi)^2\left(\frac{2}{\pi}\right)^2} \qquad \text{(A-38)}$$

where

$$u = \frac{\pi d}{\lambda} \sin \theta$$

To avoid the lengthy differential term obtained by differentiating $A(k_s = dA/d\theta)$, an alternate is to set θ equal to 1 mr error and then derive A by Equation (A-38). In this case, for $\theta = 10^{-3}$:

$$A = \frac{1 - 4\left(\frac{d}{\lambda}\,10^{-3} - 1\right)}{1 - 4\left(\frac{d}{\lambda}\,10^{-3} + 1\right)} = 0.907 \text{ for an effective diameter } d = 0.9 \times 20\,\lambda = 18\,\lambda$$

and the db error voltage allowance per error angle is $20 \log A = 0.8$ db.

A.5 PHASE MONOPULSE ANTENNA

Phase monopulse angle tracking is implemented by a displaced phase-center, 4-array cluster forming a square aperture, where each array is resonant fed and provides a normal beam. A phase summation of these four beams provides the sum beam; and an up-down and left-right phase subtraction provides the two difference beams. The advantages of the phase monopulse array are minimum package depth, the absence of any aperture obstructions (VHF transmitter consists of flush-mounted cavity-backed slots), the absence of any lossy or environmentally sensitive active RF elements, and good aperture illumination control for attaining the design objectives. The disadvantages are lack of separate sum and difference beam aperture illumination control, and the poor adaptability to circular polarization. Because illumination control is not separable, error angle slope performance must be traded off for sum beam sidelobe performance.

The normal beam resonant slot resonant feeder line design does not allow a circular polarized slot element since a resonant feeder line must be loaded by either pure series or pure shunt elements (and spaced by multiples of a half-guide wavelength), while a c-p slot element presents both shunt and series loading. The alternative of 45-degree polarizing plates on the radiating surface of the array will inevitably result in a gain and sidelobe degradation, as well as an increased frequency sensitivity, due to some slots being blocked or near blocked (slot spacings must be constant) and due to some loss of aperture illumination control by the polarizing plate transmission line. A performance evaluation of the phase monopulse array will be limited to the linear polarization case since a practical evaluation of the c-p case with polarizing plates would require hardware implementation and experimental evaluation.

Appendix B summarizes the general phase monopulse array design procedure with respect to arriving at a tradeoff performance evaluation with respect to sum beam gain and error angle slope for a given sum beam sidelobe specification. Table B-1 in Appendix B reviews the tradeoff performances. Assuming a sum beam sidelobe specification of 20 db or lower and allowing for about 2 db sidelobe increase due to a narrow center strip

used by the VHF slot radiators, a near cosine aperture illumination is assumed providing a 20- to 23-db sum beam first sidelobe. By Table B-1, the sum beam gain is down 1 db from the optimum gain uniform illumination and the effective phase center spacing is 0.73 times the geometrical center-to-center spacing between arrays. Although the theoretical efficiency of the uniform illumination aperture is 100 percent, 80 percent efficiency (-1 db) is a more practical estimate to allow for waveguide losses, finite array edge effects, and small VSWR losses. On this basis, the cosine illumination efficiency is estimated as n = 63 percent (-2 db).

The sum beam gain is then, for d = 20 λ

$$G_{\Sigma} = n4\frac{\pi A}{\lambda^2} = 1008\pi = 35 \text{ db}$$

By Equation (B-3) of Appendix B, the normalized error angle slope is, for D = 0.73 d/2 = 0.365 d:

$$K = \frac{\pi D}{\lambda} = 1.147\ d/\lambda \frac{mv}{mr} \text{ per } V\Sigma \qquad \text{(A-39)}$$

or, alternately, by the more absolute method of deriving and differentiating the normalized difference beam pattern (Equations B-16 and B-17 of Appendix B), the normalized error angle slope is:

$$K = 1.142\ d/\lambda \frac{mv}{mr} \text{ per } v\Sigma \qquad \text{(A-40)}$$

Using Equation (A-40) for d = 20 λ, K = 22.84.

Systematic angle track errors will occur in the case of difference beam precomparator RF phase unbalances. For a net phase error, $e^{j\psi}$, between difference arm precomparator inputs, the difference pattern will be of the form

$$\Delta(\theta) = E(\theta)(e^{ju} - e^{j\psi}\, e^{-ju}) \qquad \text{(A-41)}$$

where

$E(\theta)$ = beam pattern of each subarray

$u = \frac{\pi D}{\lambda} \sin\theta$

D = effective phase center spacing

By Equation (A-41), $\Delta(\theta)$ will track to zero modulation for a target at an error angle, θ, off boresight, where

$$\psi = 2u = \frac{2\pi D}{\lambda} \sin \theta$$

and the systematic error angle slope about boresight is:

$$K_s = \frac{d\psi}{d\theta} \text{ (about } \theta = 0) = \frac{2\pi D}{\lambda} = \frac{360D}{\lambda} \frac{\text{deg}}{\text{rad}} \qquad \text{(A-42)}$$

For D = 0.73 d/2, and D = 20 λ, K_s = 2.63 deg/mr and the precomparator RF error allowance per mr error angle is 2.63 degrees.

A.6 INTERFEROMETER ANTENNA

The interferometer type of angle track antenna may take a variety of forms. The type that presents some operational advantages for a beacon-track lunar landing mission is the wide angle, high resolution, all electronic search and angle track planar interferometer. High resolution, in conjunction with wide angle coverage, requires ambiguity resolution. Appendix D illustrates the interferometer planar layout and provides an analysis of a basic three element planar interferometer with either two additional receiving elements (displaced by 0.577 λ) or two frequency reception (displaced by 284 Mc at λ = 1/10 foot) for ambiguity resolution. The search coverage is limited primarily by the beamwidth limitations of the interferometer elements. For a ±60 degree coverage in elevation a gain decrease of 3 to 5 db is anticipated.

The all electronic search and angle track planar interferometer, by eliminating the mechanical gimbaling, has the advantages of inertialess search, and minimum weight and power consumption. By the use of the multiplicative technique, where separate mixers are used for each element and RF phase differences are converted to IF phase differences, the lossy and environmentally sensitive RF phase shifters are eliminated. Another advantage is adaptability to circular polarization.

Since the interferometer element must have a broad beamwidth for the required wide angle coverage, low gain is a major disadvantage of the electronic search and track interferometer. Utilization of such an antenna type for an LLS mission would be limited to some combination of increased beacon transmit power, increased beacon directivity, and decreased range requirements.

Table A-II summarizes the performance parameters of the five-element and three-element-two frequency wide angle search and track planar interferometer. For comparison, the performance parameters of a simple, nonambiguous, three-element planar interferometer are also included. For angle track, the low gain of the interferometer is partially compensated by the high error angle slope (6 db or more at θ = 60 degrees, and 12 db or more at θ = 0 degree, above the error angle slope of the other angle track antenna types).

The systematic error angle slope, K_s, is the same as the null tracking error angle slope, K. For the multiplicative interferometer, the phase error allowance (RF + IF phase errors up to the IF phase comparator) per mr systematic error angle is then 7.2 degrees cos θ, where θ is the look angle off normal.

Table A-II. Planar Interferometer Performance Review

Type	Low Resolution Simple 3 Element	High Resolution 5 Element	High Resolution 3 Element, 2 Frequency
Baseline at 9.84 Gc (λ = 1/10 ft)	1.46 λ by 1.46 λ (1.75 by 1.75 in.)	20 λ by 20 λ (2 by 2 ft)	20 λ by 20 λ Δ_f = 284 Mc
Ambiguity element spacing	None	0.577 λ (0.68 in.)	None
Nonambiguous angular coverage in elevation and horizontal	θ = ±20 deg	θ = ±60 deg	θ = ±60 deg
Number of resolved ambiguities	None	34	34
Error angle slope K, in degrees/mr	0.526 cos θ ($2\pi d/\lambda$ cos θ)	7.2 cos θ ($2\pi d/\lambda$ cos θ)	7.2 cos θ ($2\pi d/\lambda$ cos θ)
Minimum phase error tolerance, ambiguity element resolution	None	10.4 deg	10.4 deg
Gain at θ = 0 deg	14 db	8 db*	8 db*
Gain at θ max	11 db	3 to 5 db*	3 to 5 db*

*Element beam width designed for a search coverage of 120 deg in elevation (θ_{el} = ±60 deg) and 60 deg in horizontal (θ_h = ±30 deg)

A.7 MULTIBEAM PARABOLIC REFLECTOR FOR ALTIMETER/VELOCITY SENSOR

The advantages of the parabolic reflector antenna are design and fabrication simplicity, and a frequency insensitive beam tilt. What may at first appear to be a weight advantage will, most likely, be a weight disadvantage when suitable structural precautions are added to provide feed and reflector curvature stability towards minimizing beam tilt changes under the spaceborne temperature extremes. Figure 3- (Section 3.3.4) illustrates the multibeam dual reflector packaging concept. Table A-III (Appendix A) provides a qualitative comparison with the multibeam array antenna types. It is anticipated that the -30-db cross-talk, sidelobe specification will be very difficult to attain with the multibeam reflector. With suitable feed tapering, a -30-db sidelobe can be attained in the diametric direction, if the other receiving beam is not in position. However, the addition of the second feed will inevitably increase this cross-talk sidelobe level. The effect can be described from either a transmitting or receiving viewpoint. As a transmitter, with feed No. 1 transmitting, some of the transmit power will be intercepted by feed No. 2. Feed No. 2 will both scatter and reradiate approximately one half of this intercepted energy. The reradiated portion is a function of feed No. 2 loading and VSWR and is zero for the matched case. However, the scattered power is independent of loading and will tend to be focused off the reflector in the same direction as would the ordinary radiation from feed No. 2. The result is a cross-talk lobe that did not exist in the absence of feed No. 2. By reciprocity, the same cross-talk sidelobe will occur when the antenna is receiving.

It is unlikely that a -30-db cross-talk specification can be satisfied under conditions of reasonable aperture efficiency (where the feeds are illuminating approximately the same full aperture area and are therefore interacting with each other) and sufficiently rigid structural supports (which also result in scattering sidelobes). A -25-db cross-talk lobe would be estimated as a more likely lower limit. A quantitative performance evaluation of the multibeam parabolic reflector will be reviewed after the multibeam array is discussed.

A.8 MULTIBEAM RESONANT PLANAR ARRAY

Appendix F presents the design concepts of the three most applicable types of altimeter/velocity sensor multibeam array antennas. Beam accuracy requirements dictate that the slot radiator excitation phase be essentially invariant with waveguide wavelength changes due to frequency drifts, environmental temperature changes, and the normal limitations on waveguide dimensional accuracy. This can only be practically attained by resonant feeding where the slot elements are always excited by the 0 or π phase of the standing wave field in the feeder waveguide. With resonant feeding, the beam tilt angle is a function of the geometrical spacing between adjacent radiators with π phase difference. Since a beam maximum occurs in those radiation directions where the free space phase difference between elements is π deg (π excitation $\pm\pi$ free space phase = 0 or 2π) a minimum of two beams will occur. Appendix F reviews the applicable four beam and two beam types. Since all types have a single input part, the two or four beam array is used as a transmitter antenna and the receiver antenna is either a two beam array (with RF phased tilt angles) or a single normal beam resonant array (with mechanical tilt angle). Where the two beam array is used as a single beam receiver (one mixer for each beam), a 3-db receiver gain loss occurs. Where the two beam array is used as a two beam receiver (one mixer for two beams), this 3-db gain loss may be viewed as the same as the 3-db loss incurred when combining two signals through a hybrid junction into a single mixer input. The two beam arrays reviewed in Appendix F are the beam switching types where, with time sharing, a total of four beams (two transmit and two receive beams) can be made to perform the function of either six or eight beams (three or four transmit and three or four receive beams). Figure 3- (Section 3.3.4) illustrates this time sharing concept. The advantage gained is, for the same package area, a narrower two way beamwidth than the four beam transmitter array-four separate receiver arrays antenna type.

Table A-III gives a qualitative comparison of the multibeam reflector and the two multibeam array types.

Table A-III. Altimeter/Velocity Sensor Antenna Types

	Multibeam, Dual Reflector	Multibeam Transmit Array, Single Beam Receivers	Two-Beam Switching Arrays
Two-way gain (extended ground reflector and same radiating area)	Reference G_0	Less than G_0	Less than G_0*
Two-way beam width (same radiating area)	Reference BW_o	Similar to BW_o in one plane, greater than BW_o in other plane	Less than BW_o in one plane, similar to BW_o in other plane
Cross-talk and other sidelobes	Limited control, can have feed coupling cross-talk problem	Controllable	Limited control due to switch leakage
R-T Isolation	Difficult to predict dependent on feeds and structural protrusions, 50-60 db estimate	60-70 db	60-70 db
Beam Accuracy	Boresight alignment beam angle correction feature can be environmentally sensitive	Beam angle correction feature, environmentally insensitive	Only second order beam angle correction features, environmentally insensitive
Packaging	Awkward, potentially heavy package, deep, needs rigid feed-dish support structure	Compact area, shallow, rigid, needs minimum support structure	Compact area, shallow, rigid, needs minimum support structure
Beam Angle Limitations	Any angle, but favors small angles to avoid BW, gain and sidelobe degradation	Angles must be 13 deg or greater in one plane and 20 deg or greater in other plane	Same 12 and 20 deg limitations

*Assuming a maximum 6 db time sharing loss

A.9 QUANTITATIVE EVALUATION OF MULTIBEAM ANTENNA TYPES

Figure 3-10 (Section 3.3.4) illustrates the packaging concept of the three antenna types. For the packaging dimensions shown, the resultant radiating area is approximately 4 square feet for each antenna type. The wavelength is $\lambda = 1/10$ foot. The performance parameters to be derived are the transmit and receive gains and the two way beamwidths. A three beam velocity sensor, VS, is assumed.

A.9.1 Multibeam Reflector, Velocity Sensor Beams

Assume a reflector diameter D = 2 ft, f/D $\approx$ 1/3, f $\approx$ 0.67 ft; and a beam tilt $\approx$ 15 degrees fore-aft and $\approx$10 degrees laterally. After cutting and packaging, fore-aft dimension D_1 = 2 ft and lateral dimension D_2 = 1.3 ft. Due to obstructing septum on the 10-degree lateral beam tilt, the effective lateral dimension is D_2 = 1.15 ft.

Due to the effective long f/D_2 ratio, and due to the limited 10 degree beam tilt in the lateral direction, beam broadening is small for the lateral beam tilt. In this case the lateral beamwidth, for a 22- to 25-db sidelobe is estimated as:

$$B_1 = 73^o \frac{\lambda}{D_2} = \frac{73}{11.5} = 6.35 \text{ deg}$$

Due to the shorter f/D_1 ratio and the larger (15 deg) beam tilt in the fore-aft direction, beam broadening is increased and the sidelobe level rises rapidly. In this case, the fore-aft beamwidth, for an 18-db sidelobe is estimated as:

$$B_f = 84 \text{ deg} \frac{\lambda}{D_1} = \frac{84}{20} = 4.2 \text{ deg}$$

Since the aperture is not of circular cross section, the transmitter and receiver gain is more conveniently estimated by the relation:

$$G = L \frac{4\pi}{B_1 B_f} \qquad \text{(A-43)}$$

where L = loss factor due to spillover loss, power in sidelobes, and scattered power due to feed and support structure obstructions. For L estimated at -2.5 db and beamwidth, B, in degrees

$$\text{Receiver and transmitter gain } G = \frac{23,200}{B_1 B_f} = 870 = 29.4 \text{ db}$$

Since three beams are transmitted, the transmit gain is referenced to $P_T/3$ in the range equation, where P_T = total solid state source power.

For a diffuse ground reflector and a Gaussian-like power pattern, the integral of the transmit and receive power pattern product over the infinite terrain target gives an effective two-way beamwidth of the form (see Appendix H):

$$B_2 = \frac{B_t B_r}{\sqrt{B_t^2 + B_r^2}} \qquad \text{(A-44)}$$

where B_t and B_r are, respectively, the transmit and receive one-way beamwidths.

For the multibeam reflector, $B_t = B_r = B$ and Equation (A-44) simplifies to:

$$B_2 = 0.707B \qquad \text{(A-45)}$$

The two-way beamwidths are then:

Lateral beamwidth: $B_{2\ell} = 0.707(6.35 \text{ deg}) = 4.5 \text{ deg}$

Fore-aft beamwidth: $B_{2f} = 0.707(4.2 \text{ deg}) = 3 \text{ deg}$

A.9.2 Multibeam Reflector, Altimeter Beam

Where the altimeter beam is oriented for zero beam tilt, its extimated performance factors are:

One-way lateral beamwidth: $B_l = 73 \frac{\lambda}{D_l} = 6.35 \text{ deg}$

One-way fore-aft beamwidth: $B_f = 73 \frac{\lambda}{D_2} = 3.65 \text{ deg}$

Two-way lateral beamwidth: $B_{2l} = 0.707\ (6.35 \text{ deg}) = 4.5 \text{ deg}$

Two-way fore-aft beamwidth $B_{2f} = 0.707(3.65 \text{ deg}) = 2.6 \text{ deg}$

For loss factor L = 2 db $\quad$ Gain $= \frac{26,000}{B_l B_f} = 1124 = 30.5 \text{ db}$

A.9.3 Four Beam Transmitter Array, Single Beam Receivers

Unless the altimeter beam is time shared with one of the VS beams, the altimeter transmitter array is interlaced with the VS transmitter array (providing two beams due to the wide element spacing) and the altimeter also has a single beam receiver. The no time sharing case is assumed.

Total radiating aperture:	2 by 2 ft
VS transmitter aperture:	2 by 2/3 ft
Each receiver aperture:	1 by 2/3 ft
Altimeter transmitter aperture:	2 by 2/3 ft
Receiver aperture:	1 by 2/3 ft

For a 20-db sidelobe specification, the VS and altimeter transmitter beamwidths and gains (efficiency n = 0.7) are estimated to be:

Lateral beamwidth: $B_l = 60 \text{ deg } \lambda / \frac{20}{3} \lambda = 9 \text{ deg}$

Fore-aft beamwidth: $B_f = 60 \text{ deg } \lambda / 20 \lambda = 3 \text{ deg}$

Gain: $G_t = n 4 \frac{\pi A}{\lambda^2} = n \, 1600 \, \pi / 3 = 30.7 \text{ db}$

Since one of four beams transmits unused power the effective VS gain, referenced to $P_{T/3}$ in the range equation, where P_T = total solid state source power, is

Effective VS gain: $G_{te} = 30.7 - 1.2 = 29.5$ db

Since one of two beams transmits unused power, the effective altimeter gain, referenced to P_T in the range equation, is:

Effective altimeter gain: $G_{te} = 30.7 - 3 = 27.7$ db

For a 30-db VS cross-talk sidelobe specification, where a Taylor or Dolpn illumination taper is assumed, the VS receiver beamwidth and gains (efficiency n = 0.63) are estimated at:

Lateral beamwidth: $B_l = 60 \text{ deg } \lambda / \frac{20\lambda}{3} = 9.0 \text{ deg}$

Fore-aft beamwidth: $B_f = 66 \text{ deg } \lambda / 10\lambda = 6.6 \text{ deg}$

Gain: $G_r = n \, 4\pi \, A/\lambda^2 = n \, 800 \, \pi / 3 = 27.2 \text{ db}$

The altimeter receiver need satisfy a sidelobe specification only of the order of 20 db. The estimated performance, for n = 0.7, is:

Lateral beamwidth: $B_l = 60 \text{ deg } \lambda \Big/ \frac{20\lambda}{3} = 9 \text{ deg}$

Fore-aft beamwidth: $B_f = 60 \text{ deg } \lambda / 10\,\lambda = 6 \text{ deg}$

Gain: $G_r = n\, 4 \frac{\pi A}{\lambda^2} = n\, 800\, \pi/3 = 27.7 \text{ db}$

By equation (A-44) the two way VS and altimeter beamwidths are:

VS lateral and fore-aft beamwidths: $B_{21} = 6.65$ deg,

$B_{21} = 2.73$ deg

Altimeter lateral and fore-aft beamwidths: $B_{21} = 6.35$ deg,

$B_{21} = 2.69$ deg

A.9.4 Two Beam Switching Arrays — Time Shared VS and Altimeter Beams

In this case the cross-talk limitations are due to a combination of switching leakage and receiver array sidelobe design. Since a -31-db switch leakage and a -30-db receiver sidelobe could, in the worst case, add to a -25-db cross-talk sidelobe, a practical limitation on cross-talk level will be estimated at -25 db.

For a total radiating aperture of 2 by 2 feet, each two beam transmit and receiver aperture is 2 by 1 foot. Due to the resonant array and low leakage switching bandwidth limitations, the time shared VS and altimeter RF frequencies are assumed to be essentially equal. Both transmit and receive arrays require design for -30-db sidelobe levels to give a -25 db (with a -31 db switch leakage specification) cross-talk specification. The transmit and receive arrays will therefore be equal in performance. The estimated performance factors are:

Lateral beamwidth: $B_l = 66 \text{ deg } \lambda / 10\,\lambda = 6.6 \text{ deg}$

Fore-aft beamwidth: $B_f = 66 \text{ deg } \lambda / 20\,\lambda = 3.3 \text{ deg}$

By Equation A-45, the two way beamwidths are:

Lateral: $B_{2l} = 0.707\ (6.6\ \text{deg}) = 4.66\ \text{deg}$

Fore-aft: $B_{2f} = 0.707\ (3.3\ \text{deg}) = 2.33\ \text{deg}$

The gain for $n = 0.63$, is:

$$G = n\,\frac{4\pi A}{\lambda^2} = n\ 800\ \pi = 32\ \text{db}$$

Since only one of two beams are used on both transmit and receive arrays, the effective gain is (transmit gain referenced to P_T):

$$G_e = 32 - 3 = 29\ \text{db}$$

For comparison with the other antenna types that are referenced to $P_T/3$, and assuming a 6 db time sharing loss:

$$P_T\ G_{te}\ G_{re} \times \frac{1}{4} = \frac{P_T}{3}\ G_{te}\ G_{re} \times \frac{3}{4} = \frac{P_T}{3}\ G_{te}\ G_{re} - 1.2\ \text{db}$$

and the time shared effective gain is

$$G_{se} = 29 - 0.6 = 28.4\ \text{db}$$

Appendix B. PHASE MONOPULSE ERROR ANGLE SLOPE – SIDELOBE CONSIDERATIONS

A low sum beam sidelobe specification requires a cosine type of amplitude illumination taper over the full array aperture. This amplitude weighting toward the center of the aperture effectively moves the phase centers of each subarray closer together, thereby decreasing the error angle slope. A guideline towards relating sum beam sidelobes to effective phase center spacing and to error angle slope is derived in this section.

The phase monopulse sum and difference voltage patterns are obtained by a phase summation of the subarray normal beams $[E(\theta)]$ of the form

$$E_{\Delta}(\theta) = \frac{E(\theta)}{N}\left(e^{ju} - e^{-ju}\right) = \frac{2E(\theta)}{N} \sin u \qquad \text{(B-1)}$$

$$E_{\Sigma}(\theta) = \frac{E(\theta)}{N}\left(e^{ju} + e^{-ju}\right) = \frac{2E(\theta)}{N} \cos u \qquad \text{(B-2)}$$

where

$$u = \frac{\pi D}{\lambda} \sin \theta$$

θ = elevation angle off boresight

D = effective spacing between subarray phase centers

N = sum beam normalization factor

= $2E(0)$ at $\theta = 0$

The normalized error angle slope, by Equation (G-5) of Appendix G, is

$$K = \frac{dE_{\Delta}(\theta)}{d\theta} \text{ (at } \theta = 0) = \frac{\pi D}{\lambda} \frac{mv}{mr} \text{ per } V\Sigma \qquad \text{(B-3)}$$

By Equation (B-3), and when the sum and difference patterns are expressed by Equations (B-1) and (B-2), it is seen that the error angle slope about boresight is independent of the beam shape, $E(\theta)$, since $E(\theta)$ is a maximum at $\theta = 0$. However, D, $E(\theta)$,and the array gain are all functions of the aperture illumination. The dependence of D on aperture illumination can

be formulated by expressing the sum and difference patterns in terms of the array individual element summations. For the linear array case or for the principal plane rectangular array case with separable aperture illuminations $[f(x, y) = f(x)f(y)]$, the patterns are

$$E_\Sigma(\theta) = \left[K_N e^{j(2N-1)u} + \cdots K_2 e^{j3u} + K_1 e^{ju} + K_{-1} e^{-ju} + K_{-2} e^{-j3u} + \cdots K_{-N} e^{-j(2N-1)u}\right] \quad \text{(B-4)}$$

$$E_\Delta(\theta) = \left[K_N e^{j(2N-1)u} \cdots K_2 e^{j3u} + K_1 e^{ju} - K_{-1} e^{-ju} - K_{-2} e^{-j3u} \cdots - K_{-N} e^{-j(2N-1)u}\right] \quad \text{(B-5)}$$

where

$2N$ = total number of elements on a side

d = spacing between elements

$2Nd$ = total aperture length

L = Nd = subarray aperture length

$u = \frac{\pi d}{\lambda} \sin \theta$

Since the amplitude illumination over the full aperture is always symmetrical along each side, $K_N = K_{-N}$ and Equations (B-4) and (B-5) simplify to

$$E_\Sigma(\theta) = 2 \sum_{n=1}^{N} K_n \cos (2n - 1)u \quad \text{(B-6)}$$

$$E_\Delta(\theta) = 2 \sum_{n=1}^{N} K_n \sin (2n - 1)u \quad \text{(B-7)}$$

Derivation of the error angle slope requires normalization of Equations (B-6) and (B-7). At $\theta = 0$, $u = 0$ and from Equation (B-6)

$$E_\Sigma(0) = 2 \sum_{n=1}^{N} K_n$$

The normalized sum and difference patterns are then

$$E_{\Sigma}(\theta) = \frac{1}{\Sigma K_n} \sum_{n=1}^{N} K_n \cos (2n - 1)u \tag{B-8}$$

$$E_{\Delta}(\theta) = \frac{1}{\Sigma K_n} \sum_{n=1}^{N} K_n \sin (2n - 1)u \tag{B-9}$$

and the normalized error angle slope is

$$K = \frac{dE_{\Delta}(\theta)}{d\theta} (\text{at } \theta = 0) = \frac{\pi d}{\lambda} \frac{\sum_{n=1}^{N} K_n(2n - 1)}{\Sigma K_n} \tag{B-10}$$

Equating Equations (B-9) and (B-3), it is seen that the effective phase center spacing is

$$D = d \frac{\sum_{n=1}^{N} K_n(2n - 1)}{\sum_{n=1}^{N} K_n} = d\left(\frac{2\Sigma K_n n}{\Sigma K_n} - 1\right) \tag{B-11}$$

The series summation of Equation (B-11) can be solved in closed form for the simple cases of symmetrical illumination (uniform or half sine, etc.) over each subarray. In this case, $K_1 = K_N$, $K_2 = K_{N-1}$, etc., and

$$\sum_{n=1}^{N} K_n = 2 \sum_{n=1}^{N/2} K_n \text{ and } \sum_{n=1}^{N} K_n n = \sum_{n=1}^{N/2} K_n(N + 1) = N \sum_{n=1}^{N/2} K_n + \sum_{n=1}^{N/2} K_n$$

Substituting these equalities into Equation (B-11), it is found that,

$$D = dN = L = \text{subarray width} = 1/2 \text{ full array width.}$$

Since these illumination types result in high sum beam sidelobes, solutions to Equation (B-11) are desired where the illumination tapers off from the full array center and therefore is not symmetrical over the subarray. In this case it is convenient to approximate Equation (B-11) by a continuous aperture integral of the normalized form

$$D = 2L \frac{\int_0^1 f(x)x\,dx}{\int_0^1 f(x)\,dx} \qquad \text{(B-12)}$$

where the integral is from the full array center to the array edge (or from the inside to the outside of a subarray), and,

$f(x)$ = amplitude distribution or amplitude weighting

= K_n of Equation (B-11)

x = moment arm length or phase displacement of each incremental element

dx = $(2n - 1)$ of Equation (B-11)

$2L$ = full aperture length

Table B-I lists the sum beam gains relative to a uniform illumination gain, the sum beam first sidelobe levels, and the effective phase center spacings [by Equation (B-12)] for the more common aperture illuminations $f(x)$.

Table B-I. Phase Monopulse Phase Center Separation, Sum Beam Gain and First Sidelobe, Versus Aperture Illumination

Sum Arm Aperture Illumination $\int_{-1}^{1} f(x)e^{jux}\,dx$	Phase Center Separation, D, Aperture Length = 2L	Sum Beam, First Sidelobe	Sum Beam, Gain
Uniform $f(x) = 1$	L	-13.5 db	G_o reference
Near cosine on a pedestal $f(x) = 1 - x^2/2$	0.9L	-17.1 db	G_o - 0.2 db
$f(x) = 1 - x^2$	0.75L	-20.6 db	G_o - 0.9 db
Cosine $f(x) = \cos \frac{\pi x}{2}$	0.73L	-23.0 db	G_o - 1 db
Ramp $f(x) = 1 - \lvert x \rvert$	0.67L	-26.4 db	G_o - 1.3 db

Equation (B-11) [with Equation (B-3)] is an abbreviated technique toward determining and comparing normalized error angle slopes of various aperture distributions. On a more exact basis, the radiation patterns (for the same sum and difference arm radiated power) need to be determined and the difference pattern, $\frac{\Delta(\theta)}{N}$, [where N is the normalization factor determined by $\frac{\Sigma(\theta)\max}{N} = 1$] differentiated toward obtaining the error angle slope.

As a correlating example, for the case of the cosine aperture illumination

$$\Sigma(\theta) = \int_{-1}^{1} \cos \frac{\pi x}{2} e^{jux} = \frac{\sin\left(u + \frac{\pi}{2}\right)}{\left(u + \frac{\pi}{2}\right)} + \frac{\sin\left(u - \frac{\pi}{2}\right)}{\left(u - \frac{\pi}{2}\right)} \qquad \text{(B-13)}$$

$$\frac{\Sigma(\theta)}{N} = \frac{\pi}{4}\left[\frac{\sin\left(u + \frac{\pi}{2}\right)}{\left(u + \frac{\pi}{2}\right)} + \frac{\sin\left(u - \frac{\pi}{2}\right)}{\left(u - \frac{\pi}{2}\right)}\right] \qquad \text{(B-14)}$$

where

$$u = \frac{\pi d}{\lambda} \sin\theta$$

and,

$$\Delta(\theta) = \int_{o}^{1} \cos \frac{\pi x}{2} e^{jux} - \int_{-1}^{o} \cos \frac{\pi x}{2} e^{jux} \qquad \text{(B-15)}$$

giving

$$\frac{\Delta(\theta)}{N} = \frac{\pi}{4}\left[\frac{1 - \cos\left(u + \frac{\pi}{2}\right)}{\left(u + \frac{\pi}{2}\right)} + \frac{1 - \cos\left(u - \frac{\pi}{2}\right)}{\left(u - \frac{\pi}{2}\right)}\right] \qquad \text{(B-16)}$$

And the cosine illumination normalized error angle slope is

$$\frac{d}{d\theta}\frac{[\Delta(\theta)]}{N} \text{ (at } \theta = 0) = 1.142 \frac{d}{\lambda} \frac{mv}{mr} \text{ per } V\Sigma \qquad \text{(B-17)}$$

In comparison, by Table B-I and Equation (B-3), the cosine illumination normalized error angle slope is

$$K = \frac{\pi D}{\lambda} = \frac{\pi}{\lambda} \times 0.73 \frac{d}{2} = 1.147 \frac{d}{\lambda}.$$

Appendix C. AMPLITUDE MONOPULSE PERFORMANCE CONSIDERATIONS

For mathematical convenience, a square aperture is assumed whose distribution is separable into a product of two functions $f(x, y) = f(x)\ f(y)$. The integrals of the aperture distributions are therefore also separable and consideration can be limited to single integrals providing the normalized principal plane patterns of the form:

$$\phi = 0 \text{ deg plane: } E(\theta) = 1/2 \int_{-1}^{1} f(x)\ e^{jux} dx \qquad \text{(C-1)}$$

$$\phi = 90 \text{ deg plane: } E(\theta) = 1/2 \int_{-1}^{1} f(y)\ e^{juy} dy \qquad \text{(C-2)}$$

where

$$u = \frac{\pi d}{\lambda} \sin \theta$$

d = aperture dimension

$f(x), f(y)$ = aperture distributions over, respectively, the x and y directions.

For a uniform aperture distribution in the x direction, $f(x) = 1$, and by Equation (C-1):

$$E(\theta) = 1/2 \int_{-1}^{1} e^{jux} dx = \frac{\sin u}{u} \qquad \text{(C-3)}$$

When a cosine type of aperture distribution is required from two in-phase horns of a feed-reflector monopulse antenna to satisfy a sum arm side lobe specification, Equation (C-1) becomes:

$$\Sigma(\theta) = 1/2 \int_{-1}^{1} \cos \frac{\pi x}{2}\, e^{jux} dx = 1/4 \int_{-1}^{1} \left(e^{j \frac{\pi x}{2}} + e^{-j \frac{\pi x}{2}} \right) e^{jux} dx$$

$$= 1/4 \int_{-1}^{1} \left[e^{j \left(u + \frac{\pi}{2} \right) x} + e^{j \left(u - \frac{\pi}{2} \right) x} \right] dx \qquad \text{(C-4)}$$

Integration of Equation (C-4) yields

$$\Sigma(\theta) = 1/2 \frac{\sin\left(u + \frac{\pi}{2}\right)}{u + \frac{\pi}{2}} + 1/2 \frac{\sin\left(u - \frac{\pi}{2}\right)}{u - \frac{\pi}{2}} \quad \text{(sum arm cosine illumination)} \qquad \text{(C-5)}$$

From Equations (C-3), (C-4), and (C-5), it is seen that the cosine aperture illumination from the sum arm in-phase horns provides a beam pattern equivalent to the summation of two crossover beams, where each beam is due to a uniform illumination with, respectively, a $+\frac{\pi}{2}x$ and a $-\frac{\pi}{2x}$ progressive phase tilt across the aperture. In effect, each horn requires a near uniform illumination and is offset to provide a $\frac{\pi}{2}$ maximum phase variation across the aperture. This results in the desired cosine aperture distribution for the sum arm.

The difference pattern is the difference of these two beams and is

$$\Delta(\theta) = 1/2 \frac{\sin\left(u + \frac{\pi}{2}\right)}{u + \frac{\pi}{2}} - 1/2 \frac{\sin\left(u - \frac{\pi}{2}\right)}{u - \frac{\pi}{2}} \qquad \text{(C-6)}$$

and the corresponding difference pattern integral is:

$$\Delta(\theta) = 1/4 \int_{-1}^{1} \left[e^{j\left(u + \frac{\pi}{2}\right)x} - e^{j\left(u - \frac{\pi}{2}\right)x}\right] dx = 1/2 \int_{-1}^{1} \sin\frac{\pi x}{2}\, e^{jux} dx \qquad \text{(C-7)}$$

where

$\sin\frac{\pi x}{2}$ = out-of-phase-horns aperture illumination.

The theoretical feasibility of attaining Equation (C-6) is based on satisfaction of the orthogonality principle. By this principle, coupling between beams will not occur (and gain and side lobes will not degrade) if, for a uniform aperture illumination, the beams are spaced at multiples of π radians. By Equation (C-5) or (C-6) it is seen that the $\frac{\pi}{2}$ and $\frac{-\pi}{2}$ beam spacing (total spacing = π) satisfies this criteria. The corresponding

required crossover level is:

$$\text{at } \theta = 0: \quad \frac{\sin\left(u + \frac{\pi}{2}\right)}{u + \frac{\pi}{2}} = \frac{\sin\frac{\pi}{2}}{\frac{\pi}{2}} = \frac{2}{\pi} = 4 \text{ db}$$

The practicality of this type of aperture illumination for a feed-reflector monopulse is based on the spillover gain loss occurring from the difference arm aperture illumination. The resultant $\sin\frac{\pi x}{2}$ illumination provides an amplitude maximum at the aperture edges ($x = \pm 1$). The practical consequence is a gross spillover and gain loss. By the definition of difference beam error angle slope (Equation G-2 of Appendix G):

$$K = \sqrt{\frac{G_\Delta}{G_\Sigma}} \; \frac{dE_\Delta(\theta)}{d\theta} \quad \text{at } \theta = 0 \tag{C-8}$$

where

E_Δ is normalized so E_Δ max = 1

it is seen that low difference arm gain results in a degradation of error angle slope.

By a continuation of this process of relating aperture distributions, and resultant beam patterns and beam tilt, it can be shown that two-horn efforts to increase the difference pattern gain by decreasing spillover loss will result in poor sum pattern side lobe and gain performance either through poor sum arm aperture illumination or coupling between beams because the orthogonality principle is not satisfied under resultant beam-tilt conditions.

A technique toward resolving this difficulty is that of separable control of the sum and difference arm aperture illuminations. The triple-mode horn technique is a method toward separable control. By this method, a triple mode is used in the azimuth plane (two cosine modes for sum arm and one full sine mode for difference arm) to reduce difference arm illumination spillover loss while providing a near-optimum sum illumination. In the elevation plane, four narrow-height horns are used in

place of two. The two inside horns are coupled to the elevation sum arm to provide an illumination comparable to that of Equation (C-4). All four horns are used for the elevation difference arm. An examination of the beaming toward satisfying orthogonality and the aperture distribution toward low spillover gain loss can be done in simple terms for the elevation case. If two more horns are added to the top and bottom of the two-horn case of Equation (C-4), with each of the four horns providing $\frac{\sin u}{u}$ patterns as per Equation (C-5), the resultant difference arm pattern is (for beam 1 + beam 2) - (beam 3 + beam 4).

$$2\Delta(\theta) = \frac{\sin\left(u + \frac{3\pi}{2}\right)}{\left(u + \frac{3\pi}{2}\right)} + \frac{\sin\left(u + \frac{\pi}{2}\right)}{u + \frac{\pi}{2}} - \frac{\sin\left(u - \frac{\pi}{2}\right)}{u - \frac{\pi}{2}} - \frac{\sin\left(u - \frac{3\pi}{2}\right)}{\left(u - \frac{3\pi}{2}\right)} \qquad \text{(C-9)}$$

Expressing Equation (C-9) as the difference of two beams:

$$\Delta(\theta) = \Sigma_1(\theta) - \Sigma_2(\theta) \qquad \text{(C-10)}$$

and relating Equations (C-9) and (C-10) to Equations (C-4) and (C-5), it is seen that the corresponding difference arm integral is:

$$\Delta(\theta) = 1/4 \int_{-1}^{1} \left[e^{j\left(u + \frac{3\pi}{2}\right)x} + e^{j\left(u + \frac{\pi}{2}\right)x} - e^{j\left(u - \frac{3\pi}{2}\right)x} - e^{j\left(u - \frac{\pi}{2}\right)x} \right] dx$$

$$= 1/4 \int_{-1}^{1} \left(e^{\frac{\pi x}{2}} + e^{-\frac{\pi}{2}x} \right) \left(e^{\pi x} - e^{-\pi x} \right) e^{jux} dx$$

$$= 1/2 \int_{-1}^{1} \cos\frac{\pi}{2}x \sin \pi x \, e^{jux} dx \qquad \text{(C-11)}$$

where

$\cos\left(\frac{\pi}{2}x\right)\sin(\pi x)$ = difference arm aperture distribution.

By Equation (C-9), since all beams are separated by multiples of π radians, orthogonality is satisfied. And by Equation (C-11), the aperture distribution is seen to be zero at the aperture edges, thereby avoiding spillover gain loss in the difference beam.

Appendix D. WIDE-ANGLE, HIGH-RESOLUTION PLANAR INTERFEROMETER

Figure D-1 defines the coordinate system and the physical arrangement of an electronic search and angle track planar interferometer.

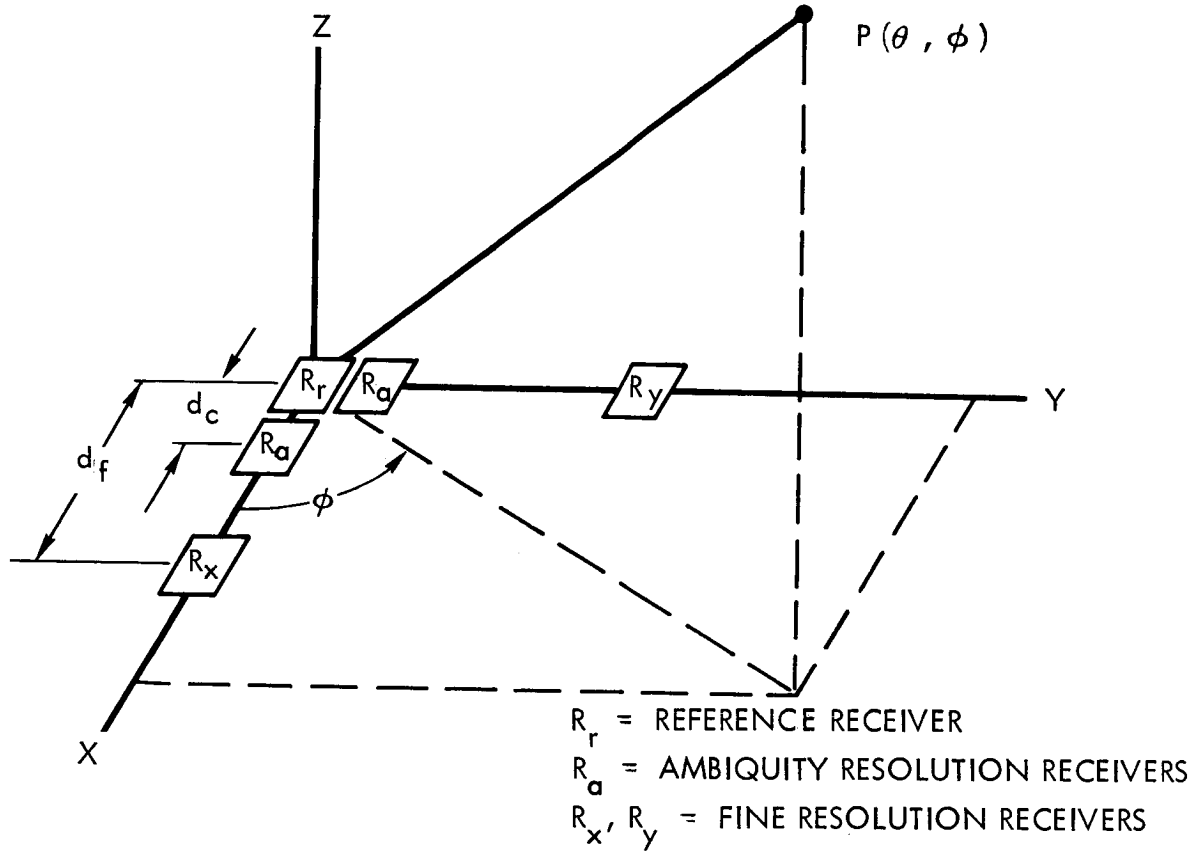

Figure D-1. Planar Interferometer Coordinate System

The phase, φ, of the radiation from a far field point $P(\theta,\phi)$, at R_x and R_y, when referenced to R_r, is

$$\varphi_x = \frac{2\pi d_x}{\lambda} \sin\theta \cos\phi \text{ at } R_x \qquad \text{(D-1)}$$

and

$$\varphi_y = \frac{2\pi d_y}{\lambda} \sin\theta \sin\phi \text{ at } R_y \qquad \text{(D-2)}$$

where d_x and d_y each refer to either d_c or d_f in Figure D-1.

Where $d = d_x = d_y$, the elevation angle, θ, is obtained by

$$\varphi = \sqrt{\varphi_x^2 + \varphi_y^2} = \frac{2\pi d}{\lambda} \sin\theta \qquad \text{(D-3)}$$

or

$$\theta = \sin^{-1}\left(\frac{\varphi\lambda}{2\pi d}\right)$$

The azimuth angle, ϕ, is obtained by Equations (D-1) and (D-3), or (D-2) and (D-3), or by

$$\frac{\varphi_y}{\varphi_x} = \tan\phi \qquad \text{(D-4)}$$

The error angle due to phase errors $\Delta\varphi_x$ and $\Delta\varphi_y$ at a look angle θ is:

$$\Delta a = \sqrt{(\Delta\theta)^2 + (\Delta\phi)^2 \sin^2\theta} \qquad \text{(D-5)}$$

where

$$\Delta\varphi_x = \frac{2\pi d}{\lambda}(\cos\theta \cos\phi\Delta\theta - \sin\theta \sin\phi\Delta\phi)$$

$$\Delta\varphi_y = \frac{2\pi d}{\lambda}(\cos\theta \sin\phi\Delta\theta + \sin\theta \cos\phi\Delta\phi)$$

By Equation (D-5), it can be seen that the error angle, Δa, is a maximum for a given phase error, $\Delta\varphi_x$ and $\Delta\varphi_y$, where the phase errors result in an elevation error angle only. In this case, $\Delta\phi = 0$, and by Equation (D-5):

$$\Delta a = \Delta\theta = \frac{\sqrt{\Delta\varphi_x^2 + \Delta\varphi_y^2}}{k} = \frac{\Delta\varphi}{k} \qquad \text{(D-6)}$$

where the resolution factor $k = \frac{2\pi d}{\lambda} \cos\theta$.

Since Equation (D-6) applies to the linear as well as the worst-error case planar interferometer and since the maximum number of ambiguities occur in the x-z or y-z planes, ambiguity resolution analysis can be simplified by considering only the linear case, $\varphi = 0^{\circ}$ or 90° in Equations (D-1) and (D-2).

A minimum complexity ambiguity-resolving linear interferometer utilizes three elements. By Figure D-1, the fine and coarse-phase differences, referenced to R_r, are

$$\varphi_f = \frac{2\pi d_f}{\lambda} \sin\theta \tag{D-7}$$

$$\varphi_c = \frac{2\pi d_c}{\lambda} \sin\theta \tag{D-8}$$

For a maximum search angle of $\pm\theta_o$, the first coarse ambiguity occurs at a coarse element spacing, d_c, where:

$$\pi = \frac{2\pi d_c}{\lambda} \sin\theta_o \tag{D-9}$$

or

$$d_c = \frac{\lambda}{2 \sin\theta_o}$$

From Equation (D-7), the fine interferometer resolution factor is:

$$k_f(\theta) = \frac{\Delta\varphi_f}{\Delta\theta_f} = \frac{2\pi d_f}{\lambda} \cos\theta \tag{D-10}$$

From Equation (D-8), under Equation (D-9) constraint, the coarse interferometer resolution factor is:

$$k_c(\theta) = \frac{\Delta\varphi_c}{\Delta\theta_c} = \frac{2\pi d_c}{\lambda} \cos\theta = \frac{\pi \cos\theta}{\sin\theta_o} \tag{D-11}$$

The fine element spacing, d_f, is limited by the accuracy of the coarse interferometer, $\Delta\theta_c$, toward resolving each adjacent phase ambiguity of the fine interferometer. The limits on d_f can be obtained by equating coarse-angle error to the fine-angle change when the fine interferometer phase changes by 2π with increasing θ.

Then, from Equations (D-10) and (D-11):

$$\Delta\theta_c = \frac{\Delta\varphi_c}{k_c(\theta)} = \Delta\theta_f = \frac{\Delta\varphi_f}{k_f(\theta)} = \frac{2\pi}{k_f(\theta)}$$

And the coarse interferometer phase error allowance for ambiguity resolution is:

$$\Delta\varphi_c = \frac{2\pi k_c(\theta)}{k_f(\theta)} = \frac{\pi\lambda}{d_f \sin\theta_o} \qquad \text{(D-12)}$$

By Equation (D-10), the fine interferometer phase error allowance for an angular accuracy $\Delta\theta_f$ is:

$$\Delta\varphi_f = \Delta\theta_f \frac{2\pi d_f}{\lambda} \cos\theta \qquad \text{(D-13)}$$

Comparison of Equations (D-12) and (D-13) shows there is a practical limit to a three-element, linear interferometer resolution accuracy (or five-element planar interferometer) since increasing d_f increases the error allowance on $\Delta\varphi_f$ but decreases the error allowance on $\Delta\varphi_c$. The maximum practical spacing, d_f max, would be chosen for $\Delta\varphi_c = \Delta\varphi_f$ at $\theta = \theta_o$. Then, by Equations (D-12) and (D-13)

$$\frac{d_f \max}{\lambda} = 1 \Big/ \sqrt{2\,\Delta\theta_f \sin\theta_o \cos\theta_o} \qquad \text{(D-14)}$$

An alternative technique toward ambiguity resolution is a dual-frequency interferometer where a second X-band frequency, displaced by Δ_f, is used in place of the third element displaced by d_c. In the case where $f_2 = f_1 - \Delta_f$, a phase ambiguity at a maximum look angle $\pm\theta_o$, occurs when

$$\pi = \frac{2\pi d}{c}\left(f_1 - f_2\right)\sin\theta_o = \frac{2\pi d}{c}\Delta f \sin\theta_o = \frac{2\pi d}{\lambda_1}\left(\frac{\Delta_f}{f_1}\right)\sin\theta_o \quad \text{(D-15)}$$

and

$$\left(\frac{\Delta_f}{f_1}\right) d = \frac{\lambda_1}{2\sin\theta_o} \quad \text{(D-16)}$$

By relating Equations (D-15) and (D-16) to Equations (D-7), (D-8), and (D-9), it is seen that

$$d_c = \left(\frac{\Delta_f}{f_1}\right) d \quad \text{(D-17)}$$

$$\varphi_f = \frac{2\pi d}{\lambda_1}\sin\theta \quad \text{(D-18)}$$

$$\varphi_c = \frac{2\pi d}{\lambda_1}\left(\frac{\Delta_f}{f_1}\right)\sin\theta \quad \text{(D-19)}$$

And the dual frequency interferometer performance equation equivalence of Equations (D-10), (D-11), (D-12), (D-13), and (D-14) of the three-element, single-frequency interferometer is:

Angle Resolution: $$k_f(\theta) = \frac{\Delta\varphi_f}{\Delta\theta_f} = \frac{2\pi d}{\lambda_1}\cos\theta \quad \text{(D-20)}$$

Ambiguity Resolution: $$k_c(\theta) = \frac{\Delta\varphi_c}{\Delta\theta_c} = \frac{2\pi d}{\lambda_1}\left(\frac{\Delta_f}{f_1}\right)\cos\theta = \frac{\pi\cos\theta}{\sin\theta_o} \quad \text{(D-21)}$$

Ambiguity resolution phase-error allowance:

$$\Delta\varphi_c = 2\pi \frac{k_c(\theta)}{k_f(\theta)} = \frac{\pi\lambda_1}{d \sin \theta_o} \tag{D-22}$$

Phase error allowance for an angular accuracy $\Delta\theta_f$:

$$\Delta\varphi_f = \Delta\theta_f \frac{2\pi d}{\lambda_1} \cos\theta \tag{D-23}$$

Maximum practical element spacing for an angular accuracy $\Delta\theta_f$ ($\Delta\varphi_c = \Delta\varphi_f$ at $\theta = \theta_o$)

$$\frac{d_{max}}{\lambda_1} = 1 \Big/ \sqrt{2\Delta\theta_f \sin\theta_o \cos\theta_o} \tag{D-24}$$

Appendix E. ALTIMETER/VELOCITY SENSOR BEAM ORIENTATION CONSIDERATIONS

Figure E-1 defines the multibeam planar array spherical coordinate system with respect to the beam tilt angles and the corresponding Velocity Sensor velocity vector angles. The beam tilt angles are expressed in the usual elevation angle, θ, and azimuth angle, ϕ, coordinates. For the horizontal (or heading) velocity (V_H) referenced along the +x axis (ϕ=0), the drift velocity (V_D) referenced along the +y axis (ϕ=90°), and the vertical (V_V) velocity (decreasing altitude) referenced along the +Z axis, (θ=0°) the doppler frequency equations are, for the general case of four beams oriented at θ_n, ϕ_n (one in each of the four quadrants):

$$f_{sb} = \frac{2}{\lambda}(-V_H \cos\phi_2 \sin\theta_2 + V_V \cos\theta_2 + V_D \sin\phi_2 \sin\theta_2) \quad \text{(E-1)}$$

$$f_{pb} = \frac{2}{\lambda}(-V_H \cos\phi_3 \sin\theta_3 + V_V \cos\theta_3 - V_D \sin\phi_3 \sin\theta_3) \quad \text{(E-2)}$$

$$f_{sf} = \frac{2}{\lambda}(V_H \cos\phi_1 \sin\theta_1 + V_V \cos\theta_1 + V_D \sin\phi_1 \sin\theta_1) \quad \text{(E-3)}$$

$$f_{pf} = \frac{2}{\lambda}(V_H \cos\phi_4 \sin\theta_4 + V_V \cos\theta_4 - V_D \sin\phi_4 \sin\theta_4) \quad \text{(E-4)}$$

where:

f_{sb} = doppler due to starboard back beam (quadrant 2)

f_{pb} = doppler due to port back beam (quadrant 3)

f_{sf} = doppler due to starboard forward beam (quadrant 1)

f_{pf} = doppler due to port forward beam (quadrant 4)

Since there are three unknowns, V_H, V_D and V_V, only three doppler equations are required so three beams are usually used instead of four. The choice of beam angles is a function of the vehicle flight path and of the multibeam constraints of the antenna type. An additional constraint is that of the altimeter beam where a combined Altimeter/Velocity Sensor antenna is required. The altimeter beam may be one of the velocity sensor beams (with time sharing) or a separate beam to avoid time sharing.

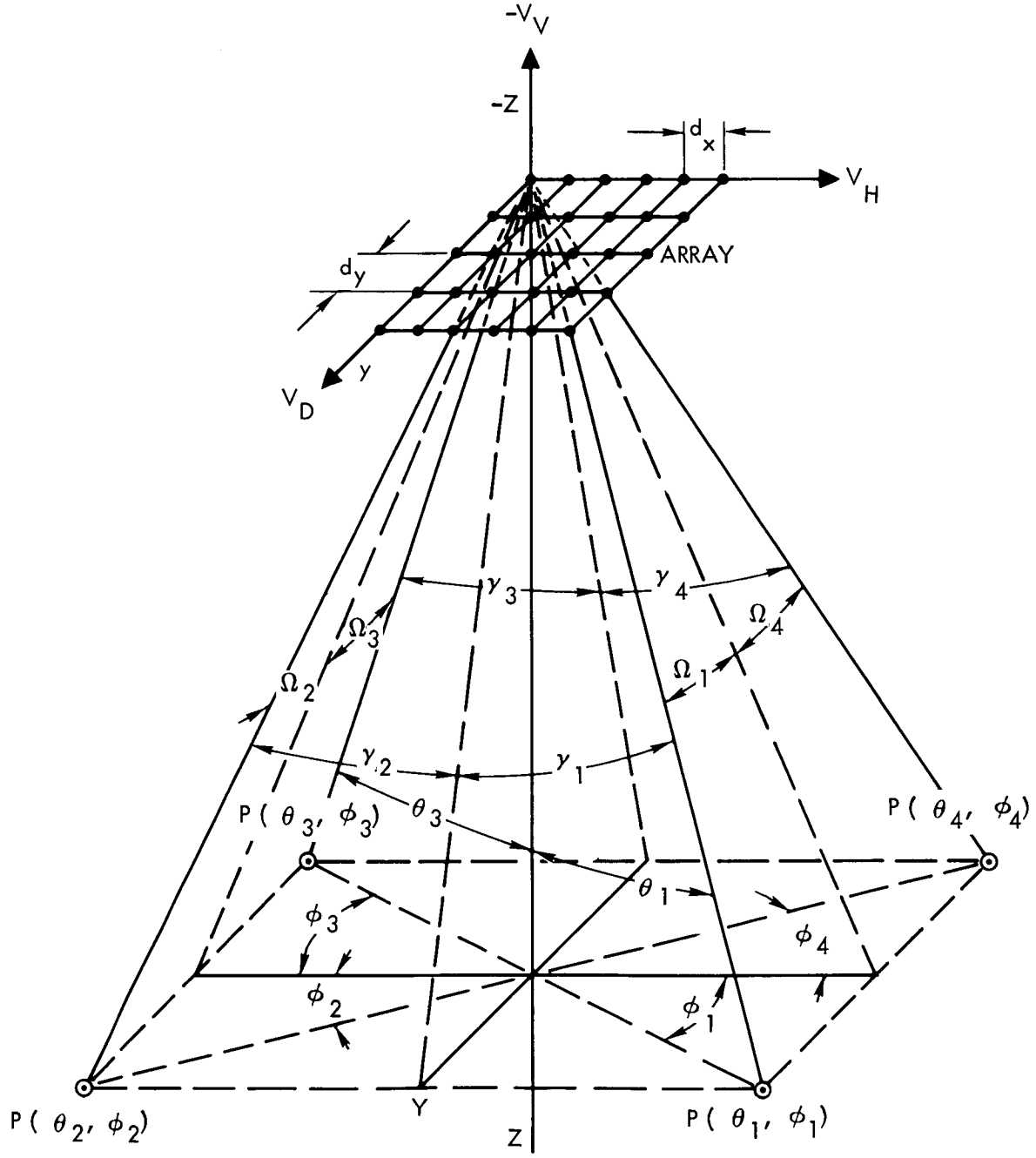

$$\text{SIN}(\gamma) = \text{COS}(\phi)\,\text{SIN}(\theta)$$
$$\text{SIN}(\Omega) = \text{SIN}(\phi)\,\text{SIN}(\theta)$$

Figure E-1. Velocity Sensor — Multibeam Array Beam Coordinates

In either case, a minimum package requires the altimeter beam to be formed by the same aperture area. The flight path for the general lunar landing mission may be a direct radial descent where V_V is much greater than V_D or V_H or, at the other extreme of a Hohmann trajectory orbital descent, where, at the higher altitudes, V_H is much greater than V_D or V_V and, at the lower altitudes (below 1000 ft), V_V is greater than V_H or V_D. In the Hohmann descent, two latched antenna positions are necessary. Since the Hohmann trajectory orbital descent presents the more complicated descent case, the beam orientations for this descent will be discussed. At the higher altitudes where V_H is predominant, it is naturally desired to minimize errors in measurement of V_H V_H errors will occur mainly due to pitch angle errors which result in fore-aft error angles, $\cos \Delta\phi \sin \Delta\theta$. However, if V_H is obtained by differencing two symmetrically located beams, one looking forward and one looking backward, then doppler errors due to pitch errors will tend to cancel. For example, for an up-pitch error, differencing the forward beam, $f_f + \Delta f$, and the rear beam, $-f_f + \Delta f$ (doppler less negative), results in a difference = $f_f + \Delta f - (-f_f + \Delta f) = 2 f_f$. Individual pitch errors, Δf, will decrease as beam tilt, θ, increases. However as θ increases, sensitivity decreases and ground bias errors increase. For separate altimeter/VS beams, where a choice can be made with respect altimeter beam orientation, a normal beam alitmeter or a slant range altimeter beam appears to be somewhat arbitary since each has some advantage. A normal beam has maximum signal return and minimum doppler and doppler spread. A slant range beam provides a doppler comparable to the velocity sensor slant range beam which may provide a signal processing advantage. In addition, for an FM-CW altimeter, the higher ranging frequency from the slant range beam may possibly provide an improvement in signal to noise ratio due to a decreased AM noise background. At the low altitudes however, a normal or near normal beam is necessary for a reliable near touchdown measurement. Since V_V is dominant at altitudes below the 1000-ft final position, beam symmetry with respect to the diametric f_{sb} and f_{pf} beams, in conjunction with doppler summing (since both dopplers are now positive) is desired to minimize errors due to pitch changes.

From these considerations, where a symmetrical fore-aft and port-starboard beaming orientation is assumed desirable for both high and low altitude operation, then: $\phi_1 = \phi_2 = \phi_3 = \phi_4$, $\theta_1 = \theta_2 = \theta_3 = \theta_4$. For the three beam case (f_{sb}, f_{pb}, f_{pf}), Equations (E-1), (E-2), and (E-4) provide:

$$V_H = \frac{\lambda}{4 \cos \phi \sin \theta} (f_{pf} - f_{pb}) = \frac{\lambda}{4 \sin \gamma} (f_{pf} - f_{pb}) \qquad \text{(E-5)}$$

$$V_D = \frac{\lambda}{4 \sin \phi \sin \theta} (f_{sb} - f_{pb}) = \frac{\lambda}{4 \sin \Omega} (f_{sb} - f_{pb}) \qquad \text{(E-6)}$$

$$V_V = \frac{\lambda}{4 \cos \theta} (f_{sb} + f_{pf}) \qquad \text{(E-7)}$$

For equations (E-5), (E-6), and (E-7) to apply at altitudes both above and below the 1000-ft final position, the following restraints are imposed on the common package altimeter beam:

(1) Separate altimeter beam: beam normal at low altitude so beam is also normal at high altitudes.

(2) Altimeter beam time shared with one of the velocity sensor beams: A slant range beam (about 15 to 22 deg off normal) at both high and low altitudes.

Since condition (2) for the altimeter beam is not desirable at the low altitudes, an alternate beam orientation below 1000 ft is to be considered. By Figure E-1, and Equations (E-1), (E-2), (E-3), and (E-4):

$$\sin \gamma_n = \cos \phi_n \sin \theta_n \qquad \text{(E-8)}$$

where

γ_n = fore-aft beam tilt angle

and

$$\sin \Omega_n = \sin \phi_n \sin \theta_n \qquad \text{(E-9)}$$

where

and

Ω_n = port-starboard beam tilt angle

n refers to quadrants 1, 2, 3, and 4.

Assuming beam symmetry at the high altitudes, then $\gamma_1 = \gamma_2 = \gamma_3 = \gamma_4 = \gamma$, and $\Omega_1 = \Omega_2 = \Omega_3 = \Omega_4 = \Omega$. If, in the low altitude latch position, γ_2 and γ_3 are made equal to zero, the low altitude doppler equations are, for the same three beam case as for Equations (E-5), (E-6), and (E-7),

$$f_s = \frac{2}{\lambda} (V_V \cos \Omega + V_D \sin \Omega) \qquad \text{(E-10)}$$

$$f_p = \frac{2}{\lambda} (V_V \cos \Omega - V_D \sin \Omega) \qquad \text{(E-11)}$$

$$f_{pf} = \frac{2}{\lambda} (V_H \sin 2\gamma + V_V \cos \Omega - V_D \sin \Omega) \qquad \text{(E-12)}$$

Since the backbeams have been moved forward to the y drift axis, $f_{sb} = f_s$ and $f_{pb} = f_p$ and:

$$V_H = \frac{\lambda}{4 \sin 2\gamma} (f_{pf} - f_p) \qquad \text{(E-13)}$$

$$V_D = \frac{\lambda}{4 \sin \Omega} (f_s - f_p) \qquad \text{(E-14)}$$

$$V_V = \frac{\lambda}{4 \cos \Omega} (f_s + f_p) \qquad \text{(E-15)}$$

By Equation (E-15) it is seen that errors in V_V due to pitch errors in the yz plane (plane of f_s and f_p) tend to cancel since as f_s increases, f_p decreases. Also, errors in V_V due to pitch errors in the xz plane are negligible since the horizontal velocities, H_V, (along x axis) do not contribute to f_s or f_p. By Equation (E-14) the same minimum effect of pitch errors on V_D errors also occurs. V_H errors will be greatest for pitch changes in the xz plane since in this plane changes in f_p are negligible compared to changes in f_{pf}, so Equation (E-13) is not self compensating.

Where Equations (E-13), (E-14), and (E-15) apply below 1000 ft and Equations (E-5), (E-6), and (E-7) apply above 1000 ft, the following restraints are imposed on the common package altimeter beam:

(1) Separate altimeter beam: beam normal at low altitudes so beam is a slant range beam at high altitudes (about 15 to 22 deg off normal).

(2) Altimeter beam time shared with one of the velocity sensor beams: A slant range beam at high altitudes (about 15 to 22 deg off normal) and a smaller angle slant range beam at low altitudes (about 10 deg).

Appendix F. MULTIBEAM RESONANT PLANAR ARRAY DESIGN ANALYSIS

Figure F-1 defines the multibeam planar array xy coordinate system with respect to the spherical coordinate beam tilt angles.

The general planar array beam pattern in a direction θ, ϕ, for (MXN) elements with a constant phase difference between elements, is,

$$E(\theta, \phi) = \psi(\theta, \phi) \sum_{m=o}^{M-1} \sum_{n=o}^{N-1} A_{mn} e^{jm(kd_x u_x - \gamma_x) + jn(kd_y u_y - \gamma_y)} \qquad (F-1)$$

For the usual case where the aperture illumination is separable into a product of two functions ($\Sigma A_{mn} = \Sigma A_m \Sigma A_n$):

$$E(\theta,\phi) = \psi(\theta,\phi) \sum_{m=o}^{M-1} A_m e^{jm(kd_x u_x - \gamma_x)} \sum_{n=o}^{N-1} A_n e^{jn(kd_y u_y - \gamma_y)} \qquad (F-2)$$

where:

$\psi(\theta,\phi)$ = element pattern.

A_m, A_n = element excitation amplitude in, respectivity, the x and y directions.

$k = 2\pi/\lambda$, λ = wavelength.

d_x, d_y = element spacing in, respectively, the x and y directions.

$u_x = \sin\theta \cos\phi = \sin\gamma$.

$u_y = \sin\theta \sin\phi = \sin\Omega$.

γ_x, γ_y = constant phase difference between elements in, respectively, the x and y directions.

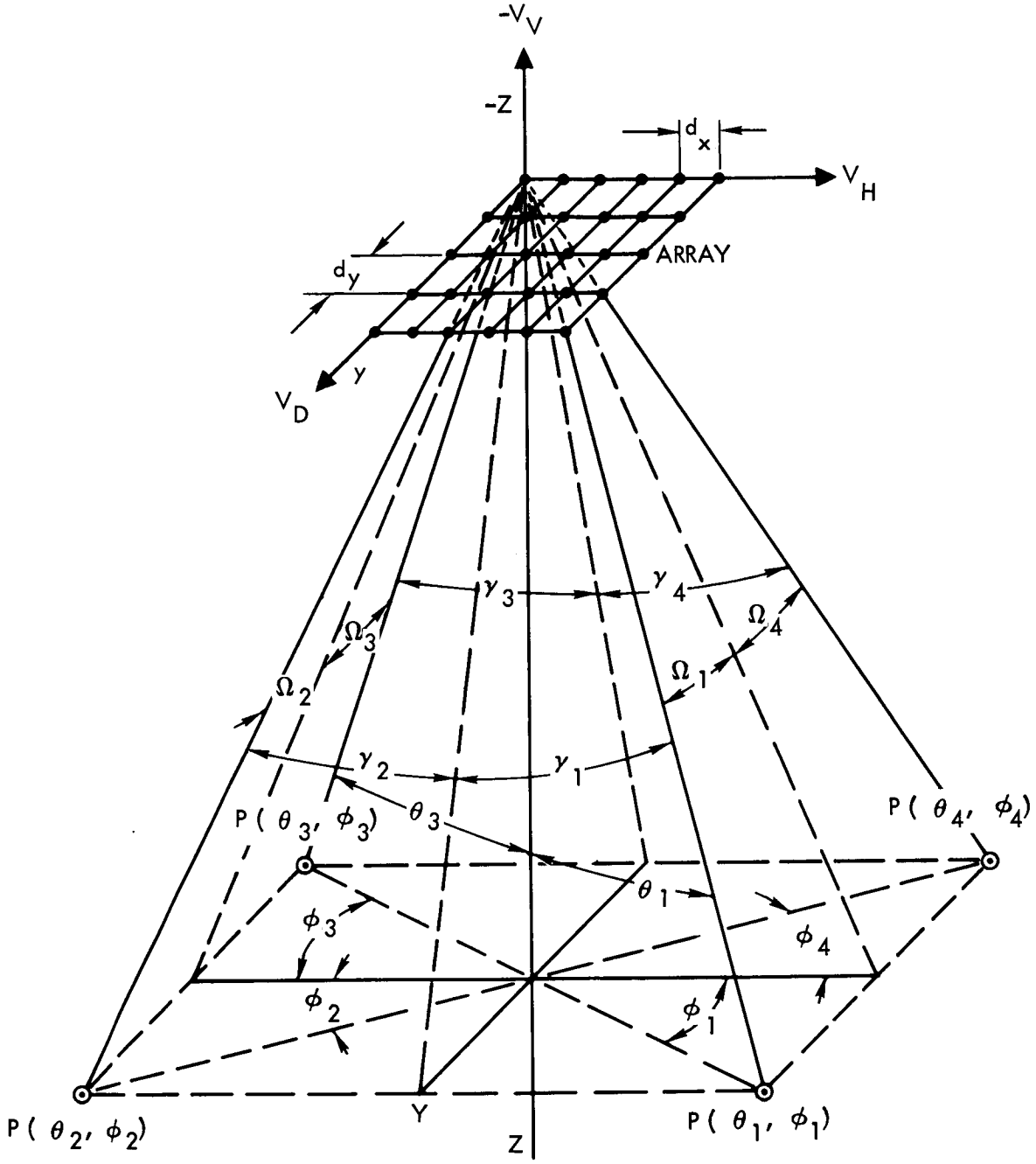

$$\text{SIN}(\gamma) = \text{COS}(\phi)\,\text{SIN}(\theta)$$
$$\text{SIN}(\Omega) = \text{SIN}(\phi)\,\text{SIN}(\theta)$$

Figure F-1. Velocity Sensor – Multibeam Array Beam Coordinate

By Equation (F-2) it is seen that beam maximum will occur whenever the vectors in both series summation terms are all simultaneously in phase. In this case:

$$E(\theta,\phi) = \sum_{m=o}^{M-1} \max \sum_{n=o}^{N-1} \max = \max\,(\theta, \phi) \qquad \text{(F-3)}$$

at θ,ϕ, where, for a sufficiently large spacing, d_x and d_y:

$$\frac{2\pi d_x}{\lambda} \sin\theta \cos\phi - \gamma_x = 2\pi k, \; k = 0, \pm 1 \text{ etc.} \qquad \text{(F-4)}$$

$$\frac{2\pi d_y}{\lambda} \sin\theta \sin\phi - \gamma_y = 2\pi L, \; L = 0, \pm 1 \text{ etc.} \qquad \text{(F-5)}$$

or

$$\frac{2\pi d_x}{\lambda} \sin\theta \cos\phi = \gamma_x + 2\pi k, \; k = 0, \pm 1 \text{ etc.} \qquad \text{(F-6)}$$

$$\frac{2\pi d_y}{\lambda} \sin\theta \sin\phi = \gamma_y + 2\pi L, \; L = 0, \pm 1 \text{ etc.} \qquad \text{(F-7)}$$

Single Port-Four Beam Resonant Array

In this case $\gamma_x = \pi$, and $\gamma_y = \pi$ and from Equations 6 and 7:

$$\frac{2\pi d_x}{\lambda} \sin\theta \cos\phi = \pi + 2\pi k, \; k = 0, \pm 1 \text{ etc.} \qquad \text{(F-8)}$$

and

$$\frac{2\pi d_y}{\lambda} \sin\theta \sin\phi = \pi + 2\pi L, \; L = 0, \pm 1 \text{ etc.} \qquad \text{(F-9)}$$

Four beams will occur, one in each quadrant, for the following combinations: $k = 0$, $L = 0$; $k = -1$, $L = 0$; $k = 0$, $L = -1$; and $k = -1$, $L = -1$.

In each case, except for a positive or negative sign indicating the quadrant of occurrence, the beam angles θ, ϕ, at which Equations (F-8) and (F-9) are simultaneously satisfied are determined by:

$$\sin\theta \sin\phi = \frac{\lambda}{2d_y} \tag{F-10}$$

$$\sin\theta \cos\phi = \frac{\lambda}{2d_x} \tag{F-11}$$

Referring to Figure F-1 and Equations (E-5) through (E-16) of Appendix E, it is seen that Equations (F-10) and (F-11) relate directly to the heading and drift angles, γ and Ω. Therefore, for mathematical convenience Equations (F-10) and (F-11) will be expressed in terms of γ and Ω thereby avoiding solving Equations (F-10) and (F-11) for θ and ϕ. On this basis:

$$\text{for heading angle } \gamma: \quad \sin\gamma = \frac{\lambda}{2d_x} \tag{F-12}$$

$$\text{for drift angle } \Omega: \quad \sin\Omega = \frac{\lambda}{2d_y} \tag{F-13}$$

Since most velocity sensor beam orientations use a γ angle of about 15 to 20 deg and a Ω angle of about 10 deg, Equations (F-12) and (F-13) indicate that d_x and d_y must be, respectively, about 1.5 and 2.5λ. However, by Equations (F-8) and (F-9) it is seen that additional beams will be formed for these spacings since (F-8) and (F-9) will then also be satisfied for, respectively, k = 1, -2 and L = 2, -2, -3. Constraints on d_x and d_y must then be established. It is also found that, to approach a small Ω, the element pattern in the sin θ sin ϕ direction must be made directive toward nulling out the additional main lobes that will occur due to the large d_y. An added constraint is that d_x and d_y must be spaced by integers of a half guide wavelength ($n\lambda_g/2$) for resonant line feeding.

On this basis:

$$d_x < 1.5\lambda \text{ and } d_x = \frac{\lambda_g}{2} = \text{or } \lambda_g \text{ since } \lambda_g \geq \lambda$$

giving, from Equation (F-12):

$$\sin \gamma = \frac{\lambda}{n\lambda_g} \tag{F-14}$$

where:

$$n = 1 \text{ or } 2$$

and the minimum heading angle (γ) is, for $d_x < 1.5\ \lambda$:

$$\sin \gamma > 1/3 \tag{F-15}$$

By Equation (F-15), $\gamma_{min} > 19.5$ deg.

If the elements, d_y, are paired ($\frac{\lambda_g}{2}$ apart) and fed in phase, then the element pattern is

$$\psi(\theta,\phi) = e^{j\frac{\pi\lambda_g}{\lambda} \sin\theta \sin\phi} + e^{j\frac{-\pi\lambda_g}{\lambda} \sin\theta \sin\phi} = 2 \cos\left(\frac{\pi\lambda_g}{\lambda} \sin\theta \sin\phi\right) \tag{F-16}$$

By Equation (F-9), if d_y is spaced just under 2.5λ, additional main lobes can occur at L = 1, -2. For $d_y = 1.5\lambda_g$ (and $< 2.5\lambda$), then by Equation (F-9), these lobes will occur at θ, $\phi = \pm 3\pi$

or at:

$$\sin\theta \sin\phi = \frac{\lambda}{\lambda_g}$$

But by Equation (F-16) it is seen that $\psi(\theta, \phi) = 0$ at $\sin\theta \sin\phi = \lambda/\lambda_g$. Consequently, the directive paired slot element will cancel the additional wide spacing lobes of $d_y < 2.5\lambda$ and $= 1.5\lambda_g$.

In summary for the drift angle Ω:,

$$d_y < 2.5\lambda \text{ and } d_y = 1.5\lambda_g,$$

giving, from Equation (F-13):

$$\sin \Omega = \frac{\lambda}{2d_y} = \frac{\lambda}{3\lambda_g} \qquad \text{(F-17)}$$

The minimum drift angle Ω, for $d_y < 2.5\lambda$, is

$$\sin \Omega_{min} > 1/5 \qquad \text{(F-18)}$$

By Equation (F-18), $\Omega_{min} > 11.5$ deg.

Single Port – Two Beam Switching Resonant Array

Two types are applicable: Type I, where two beams are switched from forward-starboard and rear-port to forward-port and rear-starboard, and, Type II, where two beams are switched from forward-starboard and forward-port to rear-starboard and rear-port.

Type I

This type can be conveniently analyzed in terms of a composite of two identical arrays, each fed separately, and interlaced in the X direction, ($d_x/2$ displacement) and displaced by distance, $d_y/2$, in the y direction. The beam pattern, $E(\theta, \phi)$ of Equation (F-2) is thereby modified to the form,

$$E(\theta, \phi, S) = \frac{E(\theta, \phi)}{2}\left[\left(1 + e^{j(S + k\, u_x\, d_x/2 + k\, u_y\, d_y/2}\right)\right]$$
$$= \frac{E(\theta, \phi)}{2}\left[1 = e^{j(S + P)}\right] = E(\theta, \phi)\, A\, (S, P) \qquad \text{(F-19)}$$

where

$S = 0$ or π for beam switching.

At the beam maxima, by Equations (F-12) and (F-13):

$$u_x = \sin \gamma = \frac{\lambda}{2d_x} \text{ in quadrants 1 and 4} \qquad \text{(F-20)}$$

$$u_x = \sin(-\gamma) = -\frac{\lambda}{2d_x} \text{ in quadrants 2 and 3} \qquad \text{(F-21)}$$

$$u_y = \sin \Omega = \frac{\lambda}{2d_y} \text{ in quadrants 1 and 2} \qquad \text{(F-22)}$$

$$u_y = \sin(-\Omega) = -\frac{\lambda}{2d_y} \text{ in quadrants 3 and 4} \qquad \text{(F-23)}$$

Therefore, depending on the quadrant, the phase factor, P, of Equation (F-19) is:

$$P = \frac{k}{2}(u_x d_x + u_y d_y) = \frac{\pi}{\lambda}(\pm\frac{\lambda}{2} \pm \frac{\lambda}{2}) = \frac{\pi}{2}(\pm 1 \pm 1)$$

and depending on the value of S (0 or π) two of the four beams from $E(\theta, \phi)$ will be cancelled.

In summary:

	S = 0	S = π
Quadrant 1, P = π,	A(S, P) = 0	1
Quadrant 2, P = 0,	A(S, P) = 1	0
Quadrant 3, P = $-\pi$,	A(S, P) = 0	1
Quadrant 4, P = 0,	A(S, P) = 1	0

Type II

This type is also conveniently analyzed in terms of a composite of two identical arrays, each fed separately and out of phase by $\pi/2$ or $3/2\pi$, and interlaced in the x direction ($d_x/2$ displacement). In this case there is no displacement in the y direction. The beam pattern, $E(\theta,\phi)$ of Equation (F-2), is thereby modified to the form,

$$E(\theta, \phi, S) = \frac{E(\theta, \phi)}{2}\left[1 + e^{j\pi/2 + S + k u_x d_x/2)}\right]$$
$$= \frac{E(\theta, \phi)}{2}\left[(1 + e^{j\pi/2 + S + P)}\right] = E(\theta, \phi)\ A\ (S, P) \qquad \text{(F-24)}$$

where:

$$S = 0 \text{ or } \pi \text{ for switching}$$

From Equation (F-20) and (F-21):

$$P = \frac{k}{2} u_x d_x = \frac{\pi}{\lambda} (\pm \frac{\lambda}{2}) = \pm \frac{\pi}{2}$$

and the beaming summary is:

		S = 0	S = π
Quadrant 1,	P = +π/2,	A(S, P) = 0	1
Quadrant 2,	P = -π/2,	A(S, P) = 1	0
Quadrant 3,	P = -π/2,	A(S, P) = 1	0
Quadrant 4,	P = +π/2,	A(S, P) = 0	1

The design constraints on the beam switching arrays are the same as those for the fixed four beam array.

Appendix G. ERROR ANGLE SLOPE DEFINITIONS

Where the angle track error angle slope, K, is referred to the gain, G_Δ, of the difference voltage antenna pattern, $E_\Delta(\theta)$

$$K = \frac{dE_\Delta(\theta)}{d\theta} \text{ at } \theta = 0 \text{ in } \frac{mv}{mr} \text{ per V of } \Delta, \qquad (G\text{-}1)$$

where $E_\Delta(\theta)$ is normalized so E_Δ max = 1.

Since, in most angle trackers, the error angle voltage modulates a carrier voltage, it is most convenient (and a mathematical transformation error is less likely to occur) if the error angle slope is referenced to unity carrier voltage (or sum voltage antenna pattern E_Σ) along boresight. In this case only the error angle slope, K, and the carrier gain along boresight need be specified towards determining system sensitivity. On this basis:

$$K = \sqrt{\frac{G_\Delta}{G_\Sigma}} \frac{dE_\Delta(\theta)}{d\theta} \text{ at } \theta = 0 \text{ in } \frac{mv}{mr} \text{ per V of } \Sigma, \qquad (G\text{-}2)$$

where $E_\Delta(\theta)$ is normalized so E_Δ max = 1, and

G_Δ = difference beam gain

G_Σ = sum beam gain along boresight

Both Equations (G-1) and (G-2) are mathematically inconvenient in that normalization of $E_\Delta(\theta)$ requires that the specific difference pattern be derived, and then normalized before K can be obtained. A generalized beam pattern can be assumed (Gaussian for a reflector conical scan or sequential lober), thereby simplifying the analysis when both the carrier and difference voltage patterns can be taken as the resultant of the same two beams, $E(\theta)$ and $E(-\theta)$. In this case

$$E_\Delta(\theta) = \frac{1}{N}\left[E(\theta) - E(-\theta)\right] \qquad (G\text{-}3)$$

where N is the sum beam normalizing factor defined by

$$E_{\Sigma}(\theta) = \frac{1}{N}\left[E(\theta) + E(-\theta)\right] = 1 \text{ at } \theta = 0 \text{ deg}$$

The comparative gains are then

$$\frac{G_{\Delta}}{G_{\Sigma}} = \frac{E_{\Delta}^{2}(\theta_o)}{E_{\Sigma}^{2}(\theta)} = \frac{1}{N^2} \tag{G-4}$$

And Equation (G-2) can be simplified to:

$$K = \frac{dE_{\Delta}(\theta)}{d\theta} \text{ at } \theta = 0 \text{ in } \frac{mv}{mr} \text{ per V of } \Sigma \tag{G-5}$$

where $E_{\Delta}(\theta)$ is normalized as per Equation (G-3). The application of Equation (G-5) for each antenna type warrants further clarification.

For conical scan and sequential lobing

$$E(\theta, t) = \left[1 + m(\theta) f_s(t)\right] = \left[1 + E_{\Delta}(\theta) f_s(t)\right] \tag{G-6}$$

where $f_s(t)$ = scan or lobing rate function which includes the fundamental and harmonics. The term $f_s(t)$ is discussed in more detail in the conical scan and sequential lobing sections.

By Equation (G-3), $N = 2E(0)$ and $m(\theta) = E_{\Delta}(\theta) = \frac{E(\theta) - E(-\theta)}{2E(0)}$

$m(\theta)$ = modulation factor.

For an amplitude monopulse reflector either of three cases may apply (see Appendix C):

a) Approximate case of negligible spillover gain loss in difference beam, full aperture utilization by sum beam, common horns for the sum and difference beams, and a crossover level satisfying the orthogonality criteria. In this case, by Equation (G-3)

$$E_{\Delta}(\theta) = \frac{1}{N}\left[E(\theta) - E(-\theta)\right]$$

where N is the sum beam normalizing factor defined by

$$E_{\Sigma}(\theta) = \frac{1}{N}\left[E(\theta) + E(-\theta)\right] = 1 \text{ at } \theta = 0 \text{ degree.}$$

b) Usual case of common horns but either a large spillover gain loss in the difference beam or a poor aperture utilization by the sum beam. Crossover level is assumed to be 4 db or lower so that gain loss or sidelobe level increase is assumed small due to orthogonality not being satisfied. In this case, Equation (G-3) modifies to

$$E_{\Delta}(\theta) = \frac{\sqrt{P}}{N}\left|E(\theta) - E(-\theta)\right| \qquad \text{(G-7)}$$

where N, as in Equation (G-3), is the sum beam normalizing factor defined by

$$E_{\Sigma}(\theta) = \frac{1}{N}\left[E(\theta) - E(-\theta)\right] = 1 \text{ at } \theta = 0 \text{ degree,}$$

and P is equal to the gain change ratio between the difference and the sum beams due to either difference beam spillover loss or sum beam poor aperture utilization. For example, for a 2 db difference arm spillover gain loss and full aperture utilization by the sum arm, P = 0.63.

c) The case of separable aperture illumination control where different horn combinations or different horn modes are used for the sum and difference beams. Low spillover gain losses and a full aperture utilization is assumed. Orthogonality is also assumed to be approximately satisfied (4 db or lower crossover level). In this case Equations (G-5) or (G-7) are not applicable since the sum and difference patterns originate from a combination of different beams. Therefore, Equation (G-2) must be resorted to.

For a phase monopulse array, Equation (G-5) is directly applicable. However, since beam summation is by phase rather than by amplitude, Equation (G-3) has a different form. This form is discussed further in Appendix B.

Appendix H. RADAR AND SENSITIVITY EQUATIONS

It is convenient to define an antenna sensitivity factor for a final comparative performance summary of the various antenna types evaluated in the previous sections. A sensitivity comparison of a VHF (for the ICW dithered PRF radar) and an X-band beacon interrogation link is also appropriate.

H.1 BEACON TRACKER

The one way radar equation is

$$\text{Received Power } P_r = P_T/4\pi G_T \frac{A_r}{R^2} = \frac{P_T}{(4\pi)^2}\lambda^2 \frac{G_T G_r}{R^2} = \frac{P_T}{4\pi}\frac{A_T G_r}{R^2} \qquad \text{(H-1)}$$

The receiver signal to noise ratio (S/N) is

$$\frac{P_r}{FkTB} \qquad \text{(H-2)}$$

The receiver noise phase error is

$$\sigma_\Phi = \frac{1}{\sqrt{nS/N}} = \sqrt{\frac{N}{nS}} = \sqrt{\frac{FkTB}{nP_r}} \qquad \text{(H-3)}$$

where n = function of receiver type and is ≈ 2.

The noise induced angle track error is

$$\sigma_\theta = \frac{\sigma_\Phi}{K} = \frac{1}{K\sqrt{G_r}}\left(\frac{4\pi R}{\lambda}\sqrt{\frac{FkTB}{nP_T G_T}}\right) \qquad \text{(H-4)}$$

where K = antenna error angle slope in mv/mr per V of sum beam or crossover beam along boresight. From Equation (H-4) the antenna angle track sensitivity can then be defined as

$$S_o = K\sqrt{G_r} \qquad \text{(H-5)}$$

H.2 VHF AND X-BAND INTERROGATION LINK COMPARISON

By Equation (H-2) and the last form of Equation (H-1) the comparative signal to noise ratio of a VHF and an X-band interrogation link is

$$\frac{(S/N)_V}{(S/N)_X} = \frac{P_{TV}A_{TW}G_{rv}F_xB_x}{P_{TX}A_{TX}G_{rx}F_vB_v} \qquad \text{(H-6)}$$

For equal angular coverage by the receiving beacon, the X-band and VHF beacon beamwidths are equal, so $G_{rv} = G_{rx}$. The gimbal mounted transmitter antenna areas on the spacecraft are also approximately equal, so $A_{TV} = A_{TX}$. Equation (H-6) is further simplified by considering two cases: where the doppler shift is known so that equal receiving bandwidths can be used ($B_X = B_v$) and where the receiving bandwidths must allow for the doppler uncertainty.

For the first case

$$\frac{(S/N)_v}{(S/N)_x} = \frac{P_{TV}F_X}{P_{TX}F_V} \text{ (equal receiver bandwidths)} \qquad \text{(H-7)}$$

For the second case, since $B = 2V/\lambda \cos \nu$, where V = spacecraft velocity

$$\frac{(S/N)_v}{(S/N)_x} = \frac{P_{TV}F_X\lambda_V}{P_{TX}F_V\lambda_X} \text{ (doppler uncertainty)} \qquad \text{(H-8)}$$

For a solid-state source, where $\lambda_v/\lambda_x = 32 = 15$ db, the VHF power is in the order of 14 db above the available X-band power ($P_{TV}/P_{TX} = 14$ db). The receiver noise figure at VHF is approximately 5 db lower than X-band receiver noise figure ($F_X/F_V = 5$ db). Therefore by Equations (H-7) and (H-8)

$$\frac{(S/N)_v}{(S/N)_x} = +19 \text{ db (equal receiver bandwidths)}$$

and

$$\frac{(S/N)_v}{(S/N)_x} = +34 \text{ db (doppler uncertainty)}$$

where

$$B_l = \text{lateral (or major axis) two-way beamwidth} = \frac{B_{t1}B_{r1}}{\sqrt{B_{t1}^2 + B_{r1}^2}} \tag{H-11}$$

$$B_f = \text{fore-aft (or minor axis) two-way beamwidth} = \frac{B_{tf}B_{rf}}{\sqrt{B_{tf}^2 + B_{rf}^2}} \tag{H-12}$$

Equation (H-9) is then

$$P_r = \frac{P_T \lambda^2}{(4\pi)^3} \frac{\sigma(\theta)}{R^2} 0.36\pi G_T G_r B_l B_f \tag{H-13}$$

Since all the available echo power is received only if the receiver bandwidth is equal to or greater than the doppler spread, the antenna sensitivity may be defined in terms of echo power sensitivity, which relates to the total available echo power, or a signal to noise sensitivity which assumes a receiver bandwidth matched to the doppler spread.

For the first case, from Equation (H-13)

$$\text{antenna echo power sensitivity: } S_E = G_T G_r B_l B_f \tag{H-14}$$

For the second case, for $f_d = \frac{2V}{\lambda} \cos$

$$\text{receiver bandwidth } BW = \Delta f_d = \frac{2V}{\lambda} B \sin \nu \tag{H-15}$$

where

B = two-way beamwidth associated with the velocity V along the angle ν

Of principal interest is the sensitivity at maximum altitude where the velocity V is mainly a heading velocity (Hohmann Trajectory descent) or a vertical velocity (direct descent). In either case, $B \approx B_f$ in Equation (H-15). The signal to noise ratio is then, by Equations (H-13) and (H-15)

Since the VHF transmission from the spacecraft is at a wide beamwidth, interrogation can more quickly occur but at the probable penalty of increased multipath errors during ranging. However, multipath errors may be decreased by a more directive receiver beacon beamwidth.

H.3 ALTIMETER/VELOCITY SENSOR

The two-way radar equation for the echo power received from the lunar surface is

$$P_r = \frac{P_T \lambda^2}{(4\pi)^3} \frac{\sigma(\theta)}{R^2} G_T G_r \int_\Omega \psi_t(\theta, \phi)\psi_r(\theta, \phi) d\Omega \qquad \text{(H-9)}$$

where the ground reflectivity, $\sigma(\theta)$, is approximately constant over the antenna beamwidth (diffuse scattering) and can be taken outside of the integral. The terms $\psi_t(\theta, \phi)$ and $\psi_r(\theta, \phi)$ are, respectively, the transmit and receive power patterns.

By expressing ψ_t and ψ_r in Gaussian form and assuming a circularly symmetrical pattern with beamwidths (B_t, B_r) much less than a radian, the integral of Equation (H-9) is

$$\int_\Omega \psi_t\psi_r \, d\Omega = 2\pi \int_o^\pi e^{-a\theta^2} \sin\theta \, d\theta = \pi \int_o^\infty e^{-a\theta^2} d(\theta^2)$$

$$= \frac{\pi}{b} = 0.36\pi \frac{B_t^2 B_r^2}{B_r^2 + B_t^2} = 0.36\pi B^2 \qquad \text{(H-10)}$$

where B = effective two-way beamwidth $= B_t B_r / \sqrt{B_t^2 + B_r^2}$.

Where the power patterns are of elliptical rather than circular cross section, by equating circular and elliptical areas (or by a more involved integral solution) the integral of Equation (H-9) is then

$$\int_\Omega \psi_t\psi_r d\Omega = 0.36\pi B_l B_f \qquad \text{(H-11)}$$

$$S/N = \frac{P_r}{FkTBW} = \frac{P_T}{(4\pi)^3} \frac{\sigma(\theta)}{R^2} \frac{\lambda^3 0.36\pi}{FkT2V \sin \nu} G_T G_r B_1 \qquad \text{(H-16)}$$

And, for the second case of receiver bandwidth matched to the doppler spread, from Equation (H-16), the antenna signal to noise sensitivity is,

$$S_N = G_T G_r B_1 \qquad \text{(H-17)}$$